TAMPEREEN TEKNILLINEN YLIOPISTO
TAMPERE UNIVERSITY OF TECHNOLOGY
Julkaisu 768 • Publication 768

Taija Hämäläinen

Modelling of Fibre Orientation and Fibre Flocculation Phenomena in Paper Sheet Forming

Tampere 2008

Tampereen teknillinen yliopisto. Julkaisu 768
Tampere University of Technology. Publication 768

Taija Hämäläinen

Modelling of Fibre Orientation and Fibre Flocculation Phenomena in Paper Sheet Forming

Thesis for the degree of Doctor of Technology to be presented with due permission for public examination and criticism in Konetalo Building, Auditorium K1702, at Tampere University of Technology, on the 25th of November 2008, at 12 noon.

Tampereen teknillinen yliopisto - Tampere University of Technology
Tampere 2008

ISBN 978-952-15-2064-8 (printed)
ISBN 978-952-15-2234-5 (PDF)
ISSN 1459-2045

Abstract

The quality of the paper produced can be characterised by numerous properties, such as roughness of the surface or dimensional stability under printing process, to mention but a few. Typically, the paper sheet properties depend on the whole papermaking process starting from stock preparation, and ending with the finishing units. Different paper grades have, naturally, different quality requirements, but two properties, basis weight and fibre orientation, are essential to all of them, since these properties determine the basic structure of the product.

The basic sheet structure, i.e. the fibre network and the solid material distribution, is determined mainly in the wet end of the paper machine, namely in the headbox and in the forming section. The flocculated state of the suspension in the initial drainage zone, as well as the orientation of fibres, are both inherited to the end product. The wet end processes are controlled by fluid mechanics, and thus, this thesis focuses on the investigation of the local phenomena by means of computational fluid dynamics (CFD). Modelling of fibre suspension flows has traditionally been based on a one-phase flow approach. In many circumstances the suspension can be treated as homogeneous generalised Newtonian flow - or even as pure water - but when the focus is set to the forming of the fibrous structure, a more advanced simulation approach is required.

This thesis is concerned with two essential properties, i.e. fibre orientation and fibre flocculation, which are modelled separately. The orientation is modelled by a Fibre Orientation Propability Distribution (FOPD) model. Unlike previous studies, in this thesis the FOPD simulation has been performed in a two-dimensional headbox slice channel, and includes the free jet. Flocculation is modelled with a completely novel approach in pulp and paper industry, a Fibre Floc Evolution (FFE) model, which is based on a population balance. In the FFE model the fibre suspension has been modelled as turbulent Eulerian two phase flow. The physical nature of flocculation process is taken into account, that is, flocs can coalesce to form bigger flocs, and they can break-up into smaller ones.

The numerical results of the FOPD simulations revealed new phenomena and proved the importance of including the free jet in the simulations, since the state of the orientation inside the slice channel does not characterise the situation in the jet reliably. The FFE model turned out to be a solid basis for the fibre flocculation modelling, since it is capable to predict real floc sizes. The model parameters have been validated with one geometry, the turbulence generator pipe. However, the current FFE model is capable to predict, at least qualitatively correctly, the evolution of the floc size distribution in the slice channel as well. In addition, the floc size evolution in the initial drainage zone of a Fourdrinier type of forming section is presented for three different jet-to-wire speed ratios. Although these results can not directly be used for predicting sheet formation, they provide an interesting insight into flocculation phenomena occuring during the forming process.

Preface

The motivation for this thesis is derived from the aspiration to improve the understanding of the mysterious fibre suspension flows. When an engineer meets a mathematician, and performs the research under his guidance, it means combining two completely different ways of thinking: the equations and the phenomena. I am most indebted to my supervisor Professor Jari Hämäläinen for his continuous encouragement and for the fruitful and vivid discussions. Without his endless patience to translate the ideas into the mathematical form, the visions behind this thesis would have remained only in our thoughts.

This work has been carried out in the Department of Physics in the University of Kuopio. I want to thank my collegues from the Paper Physics Group for the inspiring atmosphere, and the many good laughs we had: even though it was a busy time and our goals were some times even more than ambitious, we were never too serious with our research.

I wish to express my gratitude to Docent Hannu Ahlstedt from Tampere University of Technology for sharing his fluid dynamical knowledge with me. Without his excellent lectures and our discussions during my TUT years, I would not have possessed the tools to address the simulation problems of this thesis.

I appreciate the work done by Juha Salmela from VTT Processes. He provided me the experimental data for the validation of my FFE model. The Academy of Finland (grant no. 110617), Tekes and Metso Paper, Inc. are acknowledged for providing the financial support.

I am very grateful to Associate Professor Mark Martinez from University of British Columbia (UBC) and Docent Anders Dahlkild from Royal Institute of Technology (KTH) for the examination of the manuscript. Their valuable feedback and suggestions were of great use for me when clarifying and improving my thesis.

And once again, I want to thank my husband, Jari, but this time for love, support and lovely moments.

Sorsakoski, October 23$^{\text{th}}$, 2008

Taija Hämäläinen

Contents

Nomenclature

Latin symbols

a	empirical constant in Eq. (3.30)
a_{ij}	anisotropy in the Reynolds Stress Model
A	unit area
A_{cd}	interfacial area density
A_{mn}	collision cross-sectional area of the dispersed particles
b	empirical constant in Eq. (3.30)
B_i	body forces
B_B	birth rate due to break-up of larger particles
B_C	birth rate due to coalescence of smaller particles
c_m	mass concentration of fibres
c_v	volumetric fibre concentration
C	coefficient of the FOPD model in Eq. (3.10)
C_{cd}	dimensionless drag coefficient
C_B	break-up coefficient
C_{CT}	turbulent coalescence coefficient
C_{r2}	constant in the Reynolds Stress Model
C_{r4}	constant in the Reynolds Stress Model
C_{r5}	constant in the Reynolds Stress Model
C_s	constant in the Reynolds Stress Model
C_{s1}	constant in the Reynolds Stress Model
C_{SP}	compaction modulus in Eq. (3.50)
$C_{\varepsilon 1}$	constant in the $k-\varepsilon$ model
$C_{\varepsilon 2}$	constant in the $k-\varepsilon$ model
C_μ	constant in Eq. (3.18)
d_{ave}	mean diameter of spherical particles in Eq. (3.14)
d	diameter of a particle
d_f	floc diameter
D_f	average fibre diameter
D_r	rotational diffusion coefficient
D_t	translational diffusion coefficient
D_B	death rate due to break-up into smaller particles
D_C	death rate due to coalescence with other particles
f_{cd}	drag coefficient
f_{BV}	breakage volume fraction
$F_{d,i}^{SP}$	solids pressure force
g_i	gravitational acceleration
$g\left(V_n; V_m\right)$	specific break-up rate
G_0	reference elasticity modulus in Eq. (3.50)
h_{crit}	critical film thickness
h_{init}	initial film thickness

Latin symbols, cont.

k	turbulent kinetic energy
l_f	length-weighted mean fibre length
L_f	average fibre length
L_x	length-weighted mean floc dimension in flow direction
L_y	length-weighted mean floc dimension in cross direction
n	normal unit vector
N	number density of particles in a certain size group
N_f	crowding factor
N_{cf}	crowding factor (based on volumetric concentration)
N_{mf}	crowding factor (based on mass concentration)
p	pressure
P_k	production of the turbulent kinetic energy
Pr_t	turbulent Prandtl number
$\mathcal{P}_{ij}$	production tensor in Reynolds Stress Model
$\dot{q}$	fluid mass flux through the wire
$Q\left(V_m; V_n\right)$	specific coalescence rate
r	radius of a particle
r_{mn}	equivalent radius in Eq. (3.42)
R	coefficient of the FOPD model in Eq. (3.10)
R_w	wire resistance coefficient
Re_r	relative Reynolds number based on the relative speed between continuous and dispersed phase
$\mathcal{R}_{ij}$	pressure-strain correlation in the Reynolds Stress Model
$\mathcal{R}_{ij,1}$ and $\mathcal{R}_{ij,2}$	different parts of pressure-strain correlation in the Reynolds Stress Model
S_{FOPD}	source term in Eq. (4.1)
S_{ij}	strain rate tensor
S_k	source term in Eq. (3.11)
t	time
t_{mn}	time required for coalescence
u_i	velocity components in cartesian coordinates
$u_i^{'}$	velocity fluctuations in cartesian coordinates
u_t	turbulent eddy velocity of the length scale of a particle
V	volume of particles in certain size group
V_f	floc volume
V_f^*	dimensionless floc volume
x_i	position in cartesian coordinates
z	vertical direction in papermaking applications

Greek symbols

α_k	volume fraction of a fluid in two-fluid model, $(k = c, d)$; or volume fraction of particles in a certain size group, $(k = m, n)$
β	numerical constant in Eq. (3.37)
χ	notation for the exponent in Eq. (3.36)
δ_{ij}	Kronecker delta
ε_c	turbulent kinetic energy dissipation
ϕ	fibre orientation angle in FOPD model
$\dot{\phi}$	time rate of change of the orientation vector of an ellipsoid of revolution
η_{mn}	collision efficiency
λ_d	Kolmogorov length scale
μ	dynamic viscosity of a fluid
μ_t	turbulent (or eddy) viscosity
ν	kinematic viscosity of a fluid
θ	the most propable angle in FOPD model
θ_{mn}^T	turbulent collision rate
ρ	density of a fluid
σ	internal strength of a particle or a floc
σ_k	constant in the $k - \varepsilon$ model
σ_ε	constant in the $k - \varepsilon$ model
τ_{ij}	stress tensor
ω_f	fibre coarseness
Ω_{ij}	vorticity
ξ	dimensionless size of eddies in the inertial subrange of isotropic turbulence
ψ	fibre orientation probability distribution
ζ_{mn}	contact time during collision

Subscripts

a	atmospheric
$birch$	birch pulp
c	continuous phase
d	dispersed phase
i, j, k, l	indexes
m, n	particle size groups
min	minimum
max	maximum
$pine$	pine pulp

Abbreviations

CD	cross direction in papermachine
CFD	Computational Fluid Dynamics
CPU	Central Processing Unit
DNS	Direct Numerical Simulation
Exp.	experimental
FFE	Fibre Floc Evolution
FOPD	Fibre Orientation Probability Distribution
J/W	jet-to-wire velocity ratio
MD	machine direction in papermachine
R&D	Reseach and Development

Chapter 1

Introduction

1.1 Industrial application - forming of the paper sheet

Mottled printing paper surfaces and blurry color pictures, missing dots in printed letters and other defects can arise from problems in the paper quality, not necessarily from a printer. Paper quality can be characterised by numerous properties: roughness and gloss of paper surfaces, density and thickness variations and the resulting printing color absorption, fibrous structure of the paper sheet, to mention but a few. Some of them are controlled mainly by finishing units, gloss and roughness for example, but typically the paper sheet quality properties depend on the whole papermaking process starting from different raw materials and stock preparation phases. One example of the link between base paper properties and print quality is illustrated in Fig. 1.1. Uneven basis weight induces uneven base paper thickness, which, in turn, causes density variations in the ready paper, especially in super-calandered paper grades. Finally, the uneven density may cause uneven printing color absoption and deteriorated print quality.

In addition to typical copying and printing papers, there are several other paper grades such as magazine papers, tissue and cosmetic papers, packing and sack papers etc. All the named paper products are made for different end use purposes, and hence, different quality properties are important for each of them. However, two quality properties, basis weight and fibre orientation, are essential for all the paper grades, since they determine the basic structure of the product.

The basic sheet structure, i.e. the fibre network and solid material distribution, is determined in the wet end of the paper machine, namely in the headbox and in the forming section. The wet end phenomena are controlled by fluid dynamics of suspension in which wood fibres are dispersed in water. In addition, there are several different types of additives, such as chemicals, fines and fillers, in the flowing suspension, which makes the flow phenomena highly complicated. The settling of different components on a wet paper web in the forming section determines the mechanical and visual properties of the ready paper sheet [89]. It has been shown by many researchers (see e.g. [54]) that the problems in the headbox and in the

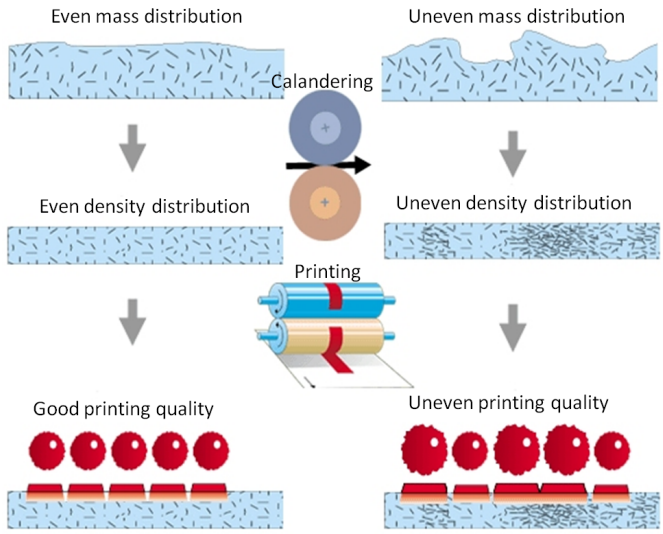

Figure 1.1: Effect of the basis weight variation on the print quality. © KnowPap.

forming section can be inherited in the paper produced. Thus, controlling and understanding the wet end fluid dynamics is essential in order to produce paper of good quality, characterised by even basis weight and controlled fibre orientation.

Flow phenomena determine the fibre orientation distribution in the flowing suspension, and finally in the ready paper sheet as well. Large-scale variations in the basis weight are controlled with automation systems, but small-scale variations, called formation, are controlled by the fluid dynamics, since they result firstly from turbulent fluctuations and concentration variations of the suspension flow in the headbox, and seconly from dewatering and retention variations in the forming section.

The best formation is usually obtained by running the headbox jet with a different speed than the forming section, that is, the jet-to-wire speed ratio is not equal to one. This induces shear to the flowing suspension in the dewatering zone, which, in turn, breaks up the flocs, i.e. small fibre aggregations, and hence, the resulting small scale basis weight is more even. On the other hand, too high shear orients fibres too much in the machine direction (MD) leading to dimensional stability problems like cockling and curling of the ready paper [67]. Nonetheless, the paper web with fibres strongly oriented in MD is stronger than paper with randomly distributed fibres, and thus, machine directional orientation helps in avoiding web breaks and in other runnability issues. As a consequence, there is always a trade off between sheet formation and fibre orientation control.

When papermaking chemicals are added in the suspension, the situation be-

comes even more complex. Chemicals are used to increase retention, i.e., the amount of solid material kept between the forming fabrics. Higher chemical dosage typically gives higher retention, but, on the other hand, may cause undesired flocculation, which increases the small-scale basis weight variation. If retention is low, formation may get better, but large amounts of solids circulating in the wet end is not economical, and high solids content in the white water may also slow down the paper grade changes. Consecuently, the optimization of the papermaking process is not trivial, since formation, orientation, dewatering and the resulting quality properties are interdependent and determined by complex multi-phase flow phenomena occuring in the headbox and in the forming section.

A typical design of a modern headbox is presented in Fig. 1.2. The function of a headbox is primarly to distribute the fibre suspension coming from the stock preparation to an even thin jet of the whole machine width. The large-scale basis weight profile is controlled by adding white water via the dilution devices. The small-scale basis weight variations due to fibre flocculation are minimised by creating turbulence inside the headbox. The initial fibre orientation, i.e., the orientation in the headbox jet, is also dependent on the headbox fluid dynamics as turbulence creates a more random orientation, while acceleration effects create more alignment. Hence, in order to produce paper of good quality, the jet thickness, as well as the flow conditions in the cross-machine direction (CD), must be as equal as possible.

Further, the forming section removes most of the water from the fibre suspension through forming fabrics. The dewatering takes place because there is lower pressure outside the fabrics than in the suspension. In modern gap formers the pressure difference is obtained by vacuum rolls, loadable blades as well as fabric tension and curvature effects, see Fig. 1.3. Dewatering should be as efficient as possible in order to increase solids content as high as possible before the pressing and drying sections, but gentle enough not to deteriorate the z-directional structure and retention. In addition to the dewatering, the jet-to-wire speed ratio affects paper properties, especially the formation and the fibre orientation, as described earlier.

As stated above, the papermaking process is very complicated, and therefore, direct observations of the phenomena are not often possible in the industrial setting. As a consequence, the fundamental knowlegde of fibre suspension flows has been advanced by experiments and theoretical calculations for decades. However, measuring the details of flow phenomena is challenging - and in some situations even impossible - and demands expensive and very careful laboratory setup. Therefore, fibre suspension flows have also been studied by computational fluid dynamics (CFD), which offers practical tools for investigating different mechanims. The next section gives a brief overview of the state-of-the-art concerning modelling of fibre suspension flows in papermaking applications.

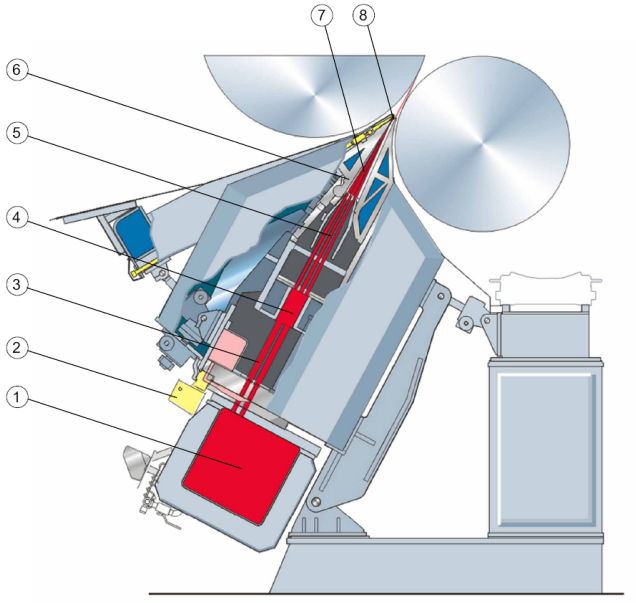

1. Header
2. Dilution control
3. Manifold tube bank
4. Equalizing chamber
5. Turbulence generator
6. Slice channel
7. Vanes
8. Slice bar

Figure 1.2: The structure of a modern headbox. By courtesy of Metso Paper, Inc.

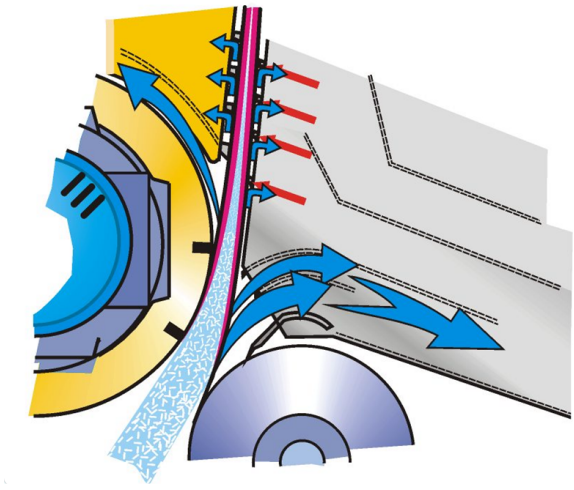

Figure 1.3: The structure of a modern gap former. By courtesy of Metso Paper, Inc.

1.2 On the modelling of fibre suspension flows

Despite of the strong two-phase nature of the fibre suspension, papermaking applications have traditionally been modelled with pure water. The main reason for this is that in all practical applications the amount of fibres exceeds the limit that can be modelled in detail: for a typical headbox fibre concentration of 1 %, a volume of one litre contains approximately 10^7 fibres*. Several academical studies including real, flexible fibres, have been made, but always with considerable simplifications: the model considers only a very small volume [68],[109] or the flow is Stokesian [111], for example. On the other hand, to model the whole headbox or even the flow phenomena on the meter-scale, a completely different type of simplifications have to be made: depth-averaging of equations, treatment of the tube banks as a porous medium etc. [33]. Although neglecting those phenomena might sound as a fatal error, useful results can be achieved, since the suspension behaviour is quite close to that of water, when the flow velocity is high enough. This characteristic is often called "fluidisation" [32] and it takes place even in suspensions having higher concentrations in the stock preparation unit processes, for example.

However, fibre suspensions cannot always be modelled as water, since its behaviour changes remarkably, if the concentration is increased and flow speed decreased. Different flow regimes have been widely studied by many researchers, since even though the simulations performed with water can provide good results from ovarall behaviour, more sophisticated models are needed when the small scale phenomena are investigated. It has been observed [66] that under certain conditions for turbulent flow, the drag reduction takes place, i.e. the friction loss for the fibre suspension is lower than for water at the same flow rate. This character is, nevertheless, rarely included in fibre suspension modelling, since most of the experiments are performed for simple pipe flow and the fundamental theory of the water-fibre interaction does not exist.

Two-phase characteristics of fibre suspension flows have been attempted to take into account by modelling the suspension as a generalised Newtonian liquid. This kind of rheological approach is suitable especially when higher concentrations are investigated, for example for pipe flows [39], refiners [46] and screens [114], but it does not characterise the phenomena in the wet end of the paper machine with enough accuracy. Another common approach is to model the special characteristics of fibre suspension flows as a passive scalar. Such simulations have have been performed for flocculation [108] and orientation [51], for instance. In these models, the flow field is computed as it were pure water, but the studied characteristic is described with its own conservation equation.

One way to avoid the modelling of individual fibres, but still take into account the existence of two separate phases having their own fluid dynamical properties, is to use an Euler-Euler approach instead of an Euler-Lagrange approach. Naturally two-fluid Eulerian approach is still a coarse simplification of the real suspension

*For a typical pine pulp presented in Table 4.1, the volume of one fibre is $7.6 \cdot 10^{-13}\mathrm{m}^3$. Assuming the density of the wet pulp to be 1100 kg/m^3 (see Section 3.5) and having 10 g of fibres in one litre of water, the number of fibres in one litre is $1.2 \cdot 10^7$.

flow, but at least it enables the variation in the local concentration and investigation of both of the phases separately. The separation of the phases is undoubtly important to include in modelling of certain unit-processes, e.g. web forming [40], since most of the phenomena depend greatly on local concentration.

This cut-through presented the simulation approaches very shortly, since the modelling of fibre suspension flows is such a wide research area. The themes more closer related to this thesis, fibre orientation, fibre flocculation and dewatering, are discussed more profoundly in Chapter 2.

1.3 Motivation and objectives for the thesis

The motivation for this thesis is derived from the real challenges to improve the understanding of the effect of headbox and forming section fluid dynamics on the paper sheet forming. In all simulated geometries, the focus has been on modelling real-life problems instead of making crucial simplifications of modelled mechanisms. Therefore, fibre orientation and fibre flocculation, as well as the free jet and dewatering are all included in this thesis, as together they determine the basic structure of the paper produced.

In addition, one goal has been the development of new tools for the fibre suspension flow simulations. These tools are based on a commercial CFD, where all the models used have been implemented in. Many special characteristics, such as orientation, have previously been modelled with in-house codes developed by researchers, since special models are often not easy to implement in commercial codes. These in-house codes are, however, usually imposible to use by any other than the developer himself, and they are rarely connectable to modelling of other phenomena. In addition, the two-way coupling is slow and complicated to perform, if the flow field is first solved in one software, and the resulting field is used in simulation of the orientation, for example, in the other software. Using a commercial CFD sofware, by contrast, offers the possibility to create dependencies between all the modelled mechanisms in one software, and it is relatively easy for others to continue the work of one reseacher.

Finally, the author has had in her mind the development of the new basis for fibre suspension flow research. This basis lies on the two-phase modelling, and including as much physics and real phenomena in the simulation as possible. As mentioned in the previous section, fibre suspension flows are rarely modelled with two-phase approach, as long as real unit-processes are investigated. This is, however, the future trend, since the computing capacity has been continuously increasing and the experiments provide more and more detailed information for the development of the fundamental theory and for the model validation. Moreover, very often the simulated situation is simplified so much that is has nearly nothing to do with the real-world phenomena. That kind of research is naturally valuable, when studying the micro-scale phenomena and developing new physical theories, but for the industrial challenges it does not have a lot to give. The purpose of this reseach has been to reveal the mechanisms - and challenges - related to flocculation and sheet forming, and create a novel modelling approach to be further developed

to describe the flocculation phenomena in more and more detail.

The concrete objectives of the thesis are

- to develop CFD tools suitable for industrial-scale simulations
- to develop fibre suspension flow modelling based on the Eulerian multi-phase approach instead of commonly used one-phase flow or rheological approximations
- to extend the solution of the fibre orientation probablity distribution (FOPD) model from mathematically one-dimensional form to two-dimensional one, and to predict fibre orientation in the headbox jet
- to bring new modelling approach to the pulp and paper industry for the mechanical fibre flocculation modelling to replace a more abstract flocculation index of the 20 years old Steen's model
- to predict concrete floc size distributions and evolution of the floc size by means of CFD
- to study the influence of the jet-to-wire speed ratio to resulting fibre floc evolution in the initial drainage zone

1.4 Related publications

Part of the research presented in this thesis has also been published in journal and conference papers. The following papers are directly related to this work:

- Hämäläinen, T., Hämäläinen, J., *Modelling of fibre orientation in the headbox jet*, Journal of Pulp and Paper Science, Vol. 33 (1), pp.49-53, 2007
- Hämäläinen, T., Hämäläinen, J., Salmela, J., *Evolution of Fibre Flocs in a Turbulent Pipe Expansion Flow*, in proceedings of 6th International Conference on Multiphase Flow, ICMF'07, Leipzig, Germany, 2007
- Hämäläinen, T., Hämäläinen, J., Korpijärvi, J., *Prediction of the Sheet Formation Using the Fibre Floc Evolution Model*, in proceedings of PaperCon '08 - TAPPI/PIMA/Coating Conference, 2008

In all the three papers mentioned above, the modelling and the implementation, as well as analysing the results, were carried out by the author of this thesis under the guidance of Jari Hämäläinen. For the second paper the experimental data was produced by Juha Salmela and for the third paper the simulated geometry was provided by Jarmo Korpijärvi, but all the theoretical and computational work was done by the author of this thesis.

In addition, the following publications has been refered to:

- Hämäläinen, J., Hämäläinen, T., Madetoja, E., Ruotsalainen, H., *CFD-based Optimization for a Complete Industrial Process: Papermaking*, in "Optimization based on Computational Fluid Dynamics", Eds. D. Thévenin and G. Janiga, Springer, 2008

- Niskanen, H., Hämäläinen, T., Eloranta, H., Vaittinen, J., Hämäläinen, J., *Dependence of fibre orientation on turbulence of the headbox flow*, 94th Annual Meeting of Pulp and Paper Technical Association of Canada, pp. B339-B342, 2008

The first mentioned does not directly relate to the subject of this thesis, but it provided a possibility for assuring the reliability of the CFD in the slice channel. The contribution of the author of this thesis in the mentioned book chapter consists of modelling the pilot-scale-sized slice channel for the comparison with HOCS Fibre simulator. The most of the simulations presented in, and also the ideas behind the chapter were contribution from Jari Hämäläinen. Elina Madetoja and Henri Ruotsalainen provided the examples for the optimisation and decission-support cases. For the second publication, that is, the conference paper by Niskanen et al., the author of this thesis has been a member of the supervising group. Although the paper has been referenced in this thesis, the results are not included, since they will be part of doctoral thesis of Heidi Niskanen.

Finally, there are two more papers, which are not referenced in this thesis, since they are to be submitted:

- Hämäläinen, T., Hämäläinen, J., *Modelling the Flocculation with Fibre Floc Evolution Model*, to be submitted

- Hämäläinen, T., Hämäläinen, J., *Modelling the Influence of the Jet-to-Wire Ratio to Resulting Fibre Floc Evolution in the Initial Drainage Zone*, to be submitted

The above papers contain mainly the same results presented in this thesis, and the contribution of the author of this thesis is the modelling and the implementation, as well as analysing the results under the guidance of Jari Hämäläinen.

Chapter 2

Special characteristics of fibre suspension flows

Since the detailed modelling of fibre suspensions is not possible in practical applications, suspensions are often tried to describe by simulating separately the special characteristic of intrest. Every special characteristic needs specified modelling method; orientation, flocculation and dewatering have to be connected to the local flow field and turbulence in different ways. The following three subsections give a brief view about the nature of the named characteristics, but firstly some common terms, which often cause confusion, are explained.

In this thesis, the terms formation and forming are used as definined also by Norman and Söderberg in their extensive review of forming literature [83]: the term *formation* exclusively refers to the small-scale basis weight variation of the ready paper sheet (or the paper web in the forming section) and the term *forming*, for one, covers the process of producing the paper web in the forming section. In addition, following the practise introduced in [83], the term "consistency" is avoided, and the use of term *concentration* is prefered. Although the term "consistency" is widely used in the pulp and paper industry for the pulp concentration, it may cause misunderstanding, since the word has also other meanings.

Nonetheless, regarding the terminology of fibre orientation, slightly different utilisation compared to [83] is applied. The term *orientation* is used both for the overall process of orientation of fibres and the orientated state of the suspension. In addition, the term *fibre orientation angle* is often employed for the *fibre orientation misalignment*. Similarly, the utilisation of the term flocculation differs from the one proposed in [83], where flocculation could mean both the aggregated state of the suspension and the process of fibres attaching into a floc. In this thesis, the term *flocculation* is exclusively reserved for the dynamic overall process, in which the flocs coalesce and break-up. As regards to the aggregated state of the suspension, it is chosen to use the term *flocculated state of the suspension*.

2.1 Fibre orientation

Fibre orientation is often considered simply as a misalignment angle with respect to the machine direction (MD), having a profile in the cross machine direction (CD). Modelling and optimization of the CD profile of the fibre orientation angle is presented in [36], where the orientation is modelled based on the MD/CD velocity ratio together with the jet-to-wire speed difference. The model gives surprisingly good results when applied to cross-directional fibre orientation profile control, but when investigating the forming of the paper structure, a more comprehensive approach is needed.

Large scale phenomena, such as curling of a paper sheet, can be predicted with acceptable accuracy using only the described simple model, but predicting small scale phenomena, such as cockling and fluting, requires information of local fibre orientation distribution. Simple models assume that there is only one fibre at each position, but to be precise, in any location (or, in a small volume) there are plenty of fibres oriented more or less randomly in different directions, thus forming a distribution of fibre orientation angles.

The fibre orientation probability distribution, ψ, can be presented as a statistical function or as a so-called "orientation ellipse" (see Fig. 2.1). The orientation ellipse provides the same information as the probability distribution, that is, the misalignment angle and the anisotropy. The angle θ shows the direction in which the most of the fibres are oriented and the anisotropy (i.e. the ratio between the axes of ellipse) describes the magnitude of unequal orientation, in other words, the variance.

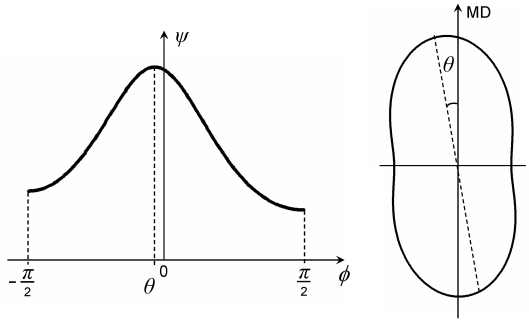

Figure 2.1: Correspondence of fibre orientation distribution and the orientation ellipse.

The importance of fibre orientation in the structure of the paper sheet has been extensively reviewed in [79] and the effects of its z-directional variation have been

studied in [67]. The measurement of the orientation is usually performed for the ready paper, and the most commonly used method is the tape splitting, in which the paper sample is splitted into several layers, see [24], for example. The online measurement techniques in papermachine are described in [101]. To enhance fundamental knowledge of the orientation in the wet end, several experimental studies have been made for the orientation in the flowing suspension, see for example [13], [23] and [112].

The mathematical model for the fibre orientation distribution was originally derived by Jeffery in early 1920's [53]. He studied an ellipsoidal particle moving in a Stokes flow, assuming an inertialess particle and a constant fluid velocity gradient. The theory is later extended to more complex shear flows; see for example [102]. During the recent years, the fibre orientation model has actively been studied for pulp and paper industrial applications by Olson and co-authors, for example, [84], [85], [86]. For an extended review of different geometries, see Hyensjö [48].

One disadvantage in the orientation distribution model is that it is quite difficult and costly to solve (more discussion can be found in Section 3.2). Hence, there exist other approaches to overcome these difficulties, and one of them is the orientation tensor approach, used by Advani and Tucker [2], among others. In the orientation tensor method the distribution is described with even-order tensors. However, this procedure leads to other problems: one has to define a closure equation to obtain resolvable system of equations.

The fibre orientation is mostly modelled as a passive scalar, since the detailed modelling would require the simulation of real, flexible fibres and their interactions, which cannot be afforded in the industrial scale. Therefore, a one-phase modelling approach is usually sufficient for orientation studies in practical applications. As a consequence, neglecting the fibre-fibre interactions signifies that the suspension is assumed very dilute. However, all the performed experiments for the fibre orientation are also made for dilute suspensions, since distinguishing a single fibre is not possible even for concentrations used typically in headboxes, see [12], [23] and [112], for example.

2.2 Fibre flocculation

The flocculation of a suspension is determined by its uniformity and mobility of fibres [60]. It has been suggested in [104], that the interfibre contact is a key factor in flocculation, since it has a straightforward effect on the two named properties. In papermaking process, plenty of chemicals are added in the fibre-water suspension in order to enhance and strenghten the interfibre contacts. However, fibre flocculation is known to occur primarily from mechanical interaction between fibres [72]. It has been shown also by simulations [100] that fibres flocculate without attractive forces and that the floc formation occurs through an elastic interlocking mechanism. Fibre-fibre interaction becomes important when a certain critical concentration is exceeded. Mason [72] suggested this condition to be as one in which there is less than one fibre in a volume having a diameter equal to the length of a single fibre. In practical papermaking concentrations this value is always sur-

passed, and hence, the interaction has to be taken into account. In addition, the behaviour of the fibrous phase depends significantly of the type of fibre contact. In order to characterise the behaviour of different pulps, Kerekes and Schell [60] have defined a parameter called crowding factor:

$$N_{cf} = \frac{2}{3} c_v \left(\frac{L_f}{D_f} \right)^2 \tag{2.1}$$

where c_v denotes volumetric fibre concentration, L_f average fibre length and D_f average fibre diameter. The crowding factor represents the number of fibres within the rotational sphere of influence of a single fibre, see illustration in Fig. 2.2, where the crowding factor is 6.

Figure 2.2: Schematic characterisation of the definition of crowding factor.

In many references, see e.g. [60], the crowding factor is represented by means of mass concentration of fibres, c_m, and fibre coarseness, ω_f, giving the form

$$N_{mf} \approx \frac{5 c_m L_f^2}{\omega_f} \tag{2.2}$$

It should be noted, however, that this notation is rather misleading, since it does not provide a dimensionless number like the Eq. (2.1), but has units of [m^3/kg], if the procedure recommended in [60] is used; to obtain the right order of magnitude, the value of concetration has to be expressed in %. If these inconveniences are excluded, the values of Eqs. (2.1) and (2.2) agree relatively well: for a given pulp used later in numerical examples N_{cf} gives the value of 116 and N_{mf} the value of 102. As a matter of fact, several corrections, e.g. [45] and [63], to the definition of crowding factor have been proposed, which indicates that the concept of the crowding factor has recieved considerable interest, but on the other hand, is not very well established. Therefore, the special attention has always to be paid when using this dimensionless number. In this thesis, the definition of Eq. (2.2) is exclusively used.

Kerekes and Schell suggested that crowding factor could be a useful tool for characterising the flocculation potential of different pulps [60]. They have used crowding factor to classify fibre suspensions into three different regimes perceived also by Soszynski [107], see Table 2.1. When the crowding factor is less than 1, fibre suspension is in dilute regime, which is characterised by chance of collision. Forced collisions appear when the crowding factor is between 1 and 60* ; this regime is called semi-concentrated. For values greater than 60, the fibre suspension is in concentrated regime, which is characterised by continuous contact between fibres.

Table 2.1: Characterisation of fibre suspension regimes by means of crowding factor

Regimes	Type of fibre contact	Crowding factor, N_f
Dilute	Chance collision	$N_f < 1$
Semi-concentrated	Forced collision	$1 < N_f < 60^*$
Concentrated	Continuous contact	$N_f > 60^*$

The crowding factor has been agreed to characterise the fibre flocculation phenomenon by several authors, Kerekes and Schell [61], among many others, but its utilisation in modelling has been limited to simple expressions for so-called flocculation index [45]. Or, the flocculation tendency of different pulps has been estimated by experimental methods in order to determine some guidelines for controlling the paper properties, see for example [20] or [21]. The approach is established on number of contacts per fibre and connected to flow conditions by simple equations. Although these approximations are still far from being able to predict the flocculated state of fibre suspension in real papermaking environment, they provide very useful knowledge of behaviour of fibre suspensions. Farnood et al. [26] have also presented a theoretical model for the intra-floc forces, but it is derived for simple model flocs containing only couples of fibres, and has not been used in any real-scale studies. Totally another type of approach is presented by Hourani [44], whose model is based on the mass-action law and the energy spectrum of turbulent flow. However, the model still contains parameters which determination is not straightforward, and hence, one cannot talk about an overall model to be used widely in industrial applications.

To the author's knowledge, the flocculation model the most used at the industrial scale applications is the one proposed by Steen [108]. Steen's model treats the fibre suspension as one-phase flow, and the flocculation phenomenon is described by the concentration variations solved as a passive scalar. He defined a concept called flocculation intensity, which describes the concentration fluctuation of the imagined fibrous phase. Steen's model has been compared to experimental results

*The upper value is defined by apparition of coherent flocs, which has been observed to occur for crowding factors between 60 and 130, depending on the local flow conditions. For more detailed discussion see [60].

by many researchers, Hyensjö among others [50], whose reference data was produced by Karema et al. [57]. It has been shown in [50] that Steen's model is able to capture the tendencies at some level, if the model parameters are adequately tuned, but it is still far away from predicting the flocculated state of the suspension. Kuhn and Sullivan [64] and Plikas et al. [90] used similar approach of scalar fluctuation as Steen has presented. However, the model parameters were calibrated with the experimental data obtained by Raghem-Moayed [94], and hence, the model is applicable only for flows where grid-generated turbulence dominates. In addition, no matter how well the model parameters are tuned, the scalar approach always neglects the real physical two phase nature of fibre suspensions, and for example, real concentration variations cannot be investigated. Moreover, the flocculation intensity is an intangible concept, which is difficult to connect to the real behaviour of flocs, especially to the incidence of different floc sizes.

Although the modelling of the flocculation has not been a very active area of research, there exists a great amount of experimental work. Floc formation and disruption in several kinds of flows has widely been studied by many authors: for floc formation in decaying turbulence, see [58] and [95], and for floc break-up in extensional flows, see [59] and [52], just to mention few. Based on these studies, one can define some geometry-dependent correlations, which may be very useful in improving certain unit-processes in papermaking, but still the fundamental knowledge of floc break-up and coalescence mechanisms is lacking. There is, thus, a real need for more detailed experiments, which could reveal the connection between flocculation and small-scale flow phenomena.

2.3 Dewatering and paper web forming

Although the fluid dynamics in the headbox affect greatly the quality of the paper produced, the basic structure is determined during the forming process. After the forming section, only fines and fillers can move towards the surfaces during pressing, but the fibres stay in positions they have taken during the forming.

The modelling of forming includes first of all the modelling of free jet, since the jet contraction and the jet angle depend on the slice opening and the bottom lip extension, for example. Söderberg carried out both experimental and theoretical studies of planar liquid jets [105]. He assumed incompressible Newtonian fluids and laminar flows, and derived the model to solve the jet position based on the force balance of the jet following general free-boundary theories. The jet shape was solved based on a potential flow model. The Reynolds numbers were 1000 and 10000, when for a typical jet it should be around 300000 (the slice opening $\approx$ 1 cm and the jet speed $\approx$ 1800 m/min). A more advanced approach is presented by Niemistö et al. in [76], where the flow is turbulent and modelled with the $k-\varepsilon$ model. In their work the position of the free surface was solved numerically without the surrounding gas, i.e. iterated with the help of the kinematic condition $u \cdot n = 0$, where u is velocity and n is the outward unit vector of the free surface. With today's commercial CFD softwares the modelling of free jet is, nevertheless, quite a routine task, but requires remarkable computer capacity, and is still fairly

challeging, if some special characters, such as flocculation, for exemple, is included in the model. In many practical applications, a simple, approximative solution is accurate enough, and hence, one can rely, for instance, on Tappi Technical Information Sheet (TIS), where the determination of the jet contraction and the angle is based on inviscid equations (potential flow). In addition, several authors, see e.g. [48], have studied different phenomena in the free jet by using a fixed jet, i.e. a straight channel with slip boundary conditions.

In order to predict the forming of the paper produced, one should include the effects of different dewatering components (forming roll, loadable blades, vacuum roll etc.) in the forming section, but also the dewatering and the consolidation phenomena. Modelling the jet impingement and the initial drainage zone has been the objective of many recent studies. Audenis and Dahkild examined the impingement of an inviscid jet on a single fabric [5], while Dalpke and her co-authors have published several studies for a twin-wire machine in order to enhance the knowledge on phenomena in the initial drainage and the fibre mat build-up, see e.g. [15] and [17]. In order to investigate the hydrodynamical forces and hydrodynamical shear at the vicinity of the forming fibre mat, Deng and Martinez have performed an experimental and theoretical study with a channel partially filled with the porous medium [18]. The pressure pulse on wires has been investigated computationally by Audenis [4], where also the wire porosity is included in the model. Experimental studies for the pressure pulsation have been carried out with KTH-former by Holm [42] and Bergström [10], who examined also the floc elongation and breakage during the roll forming for different jet-to-wire ratios. The wire position and pressure distribution due to the loadable blades have earlier been studied by Zhao and Kerekes [119] and by Zahrai [118].

The simulation of the fibre retention has not been such a popular area of research as the other phenomena on the drainage zone, but some studies on the initial fibre retention have been made, see for example [7]. In most of the studies, see e.g. [17], the retention has been assumed 100%, and the attention has been paid on other issues. Also, the dewatering process has widely been treated as a purely filtration process, and the web consolidation has been taken into account only in few studies, see for example Hiltunen [40].

As can be imagined based on the research briefly described above, the prediction of formation is highly complex issue, and it is not always straightforwardly connectable to flocculated state of a given suspension. The superposition of flocs and fibres upon one another on a moving wire may induce different level of uniformity on the web compared to the state in flowing suspension. It has been shown in [30], that superposition of flocs of low density improves the formation. On the other hand, the role of concentration is not that simple: Smith showed that the drainage conditions together with pulp concentration affect the resulting formation [104], and so does the fibre length as well [55]. Moreover, the mobility of fibres in a flowing suspension is an important property for the resulting formation, as shown by Martinez et al. [71]. They studied different suspensions in laboratory and papermachine scale and found a correlation between a critical crowding factor, yield stress and good formation.

Although several studies are entitled to give an impression that the formation is predicted based on the flocculated state of the suspension, the experimental and numerical studies really including that kind of investigation, are still rare. One such a study is presented by Dodson and Serafino [22], who attempted to model the formation resulting from a random distribution of flocs dispersed in the fibre suspension entering the wire section. Some other papers have been published as well, but usually the flocs are described with some idealistic configuration called "model flocs", meaning that a floc contains only few fibres and has a form of a star [19] or a disc [25] [27]. Therefore, these approaches are not utilisable in predicting the real formation based on the flocculated state, and they have been critisised also by producing unrealistic floc grammage levels [81].

One special property in web forming is the self-healing effect. It has been noticed that the fibre distribution in a ready paper sheet is more even than would be indicated by the flocculated state of the flowing suspension [80]. This is due to the fact that if there is a hole in the forming paper web during the dewatering process, the local dewatering resistance is lower than in other areas, and hence, the free suspension will be dewatered in that position and carry the free fibres there as well. This phenomenon is also called "hydrodynamic smoothing", and it has been noticed to vary depending on range of basis weight and crowding factor [98]. The results of Norman [80] confirmed that for small and medium floc sizes the real sheet is more even than the random sheet, but for larger flocs the sheet is, nevertheless, more uneven. Although the experimental work indicates that the effect of fibre mat resistance to the local forming is not always straightforward, it is, however, obvious, that the effect of already formed web should be included in simulations, such as Zahrai, for example, has done [118].

Chapter 3

Mathematical models

In the following sections the modelling approaches used in this thesis are presented. As already mentioned in Section 2.1, the fibre orientation can be modelled with one-phase flow approach, and hence, those equations are presented at first. The flocculation is modelled with a totally novel approach in pulp and paper industry, and therefore, the equations and theory behind them are comprehensively reported in Section 3.5. Since the modelling of flocculation requires the two-phase approach, the whole Eulerian two-phase equations are introduced in Section 3.3. In addition, the modelling of turbulence in fibre suspension flows is briefly reviewed in Section 3.4, since it has received a considerable attention during recent years, and is still a subject to debate. The last part of this chapter, Section 3.6, goes through the issues concerning the dewatering model used in this thesis.

3.1 Governing equations for one-phase flow

For the incompressible fluids, the stady-state continuity equation can be written as:

$$\frac{\partial}{\partial x_i}\left(\rho_c u_{c,i}\right) = 0 \tag{3.1}$$

where $u_{c,i}$ are time-averaged velocity components in cartesian coordinates x_i and ρ_c denotes the density of the fluid. The index c refers to continuous fluid, and is used also for the one-phase flow equations in order to have congruent notation throughout the thesis.

The momentum equation for the turbulent flow is:

$$\frac{\partial}{\partial x_j}\left(\rho_c u_{c,i} u_{c,j}\right) = -\frac{\partial}{\partial x_j}\left(p\delta_{ij}\right) + \frac{\partial}{\partial x_j}\left(\tau_{c,ij}\right) - \frac{\partial}{\partial x_j}\left(\rho_c \overline{u'_{c,i} u'_{c,j}}\right) + B_{c,i} \tag{3.2}$$

where p denotes pressure, δ_{ij} stands for Kronecker delta and $\rho_c \overline{u'_{ci} u'_{cj}}$ are Reynolds stresses, the modelling of which will be briefly reviewed in Section 3.4. B represents

body forces, such as gravity $\rho_c g_i$. The stress tensor, $\tau_{c,ij}$, can be written for incompressible fluid as

$$\tau_{c,ij} = \mu_c \left(\frac{\partial u_{c,i}}{\partial x_j} + \frac{\partial u_{c,j}}{\partial x_i} \right) \tag{3.3}$$

where μ_c is the dynamic viscosity of the fluid.

3.2 Modelling of fibre orientation - the FOPD model

In this thesis, the fibre orientation is modelled with the fibre orientation probability distribution model (FOPD model), used also by Olson, Hyensjö and their co-authors, see [48] and [86], for exemple. However, in several papers, e.g. [85], the fibre orientation has been studied in a simplified, one-dimensional (1D) headbox resulting in a reduced form of the FOPD model. In [51] the geometry was two-dimensional (2D), but still the orientation distribution was solved along a streamline, that is, in one-dimensional form. The simplified model is relatively easy to solve but, on the other hand, it looses the information perpendicular to the main flow direction by neglecting the other velocity components and their gradients.

The effect of the jet contraction has not been taken into account in the mentioned studies. Hyensjö modelled a straight channel to the extension of the slice channel in order to include the effects of jet in the FOPD modelling, but he did not have any jet contraction in his model [48]. It is, however, obvious that the sudden change in boundary conditions, from an accelerating channel flow to a free jet, has a strong influence on the flow, see for example [106]. Therefore, the initial fibre orientation depends strongly on the flow conditions in the slice jet; firstly, the jet contracts accelerating the flow speed, and secondly, all the velocity gradients and shear forces disappear after the jet contraction (*vena-contracta*). In this thesis the effect of the jet contraction is included in the model and the orientation distribution is modelled using the geometrically two-dimensional and mathematically three-dimensional form (see Eq. (3.10)), which includes all the relevant flow field information. Most of the results presented here are also reported in [37].

The distribution function (and the orientation ellipse) is determined in each position. Furthermore, there are two orientation angle distributions: one in the horizontal (MD,CD)-plane and another in the vertical (MD,z)-plane. In fact, the same mathematical model determines the both angles with minor changes in model parameters (see [85]). In this thesis, the simulations are performed for the orientation in the vertical plane, and hence, the model derivation is presented for that angle, see Fig. 3.1. Futher, the equation is given in the same form as it is implemented in the simulation software. Since the model equations, the model implementation and papermaker's coordinate system notations differ from each other, they are all represented in Fig. 3.1: the first symbol, e.g. x_1, is used in model equations, the second symbol, e.g. MD, is the papermaker's coordinate, and finally, the third one, e.g. x, is used in model implementation and when representing the results in Section 5.

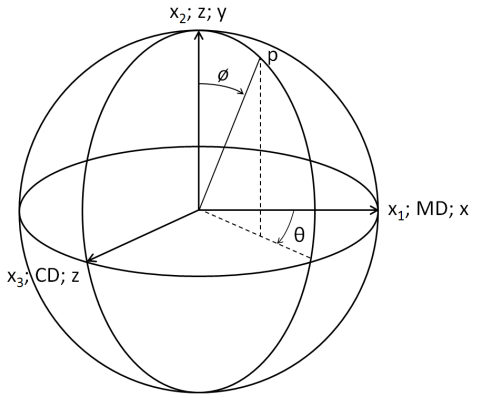

Figure 3.1: Orientation angles in spherical coordinates [77].

The FOPD equation is based on the planar approach of the Fokker-Planck equation:

$$\frac{D\psi}{Dt} - D_t \frac{\partial^2 \psi}{\partial x_i^2} = -\frac{\partial}{\partial \phi}\left(\psi \dot{\phi}\right) \tag{3.4}$$

where $\psi(t, x_i, \phi)$ denotes the fibre orientation probability distribution, ϕ is the fibre orientation angle in position x_i at time t, D_t the translational diffusion coefficient and $\dot{\phi}$ the time rate of change of the orientation vector of an ellipsoid of revolution [3]. Based on Jeffery [53] $\dot{\phi}$ can be written

$$\dot{\phi} = -\frac{D_r}{\psi}\frac{\partial \psi}{\partial \phi} - \frac{1}{2}\sin(2\phi)\frac{\partial u_1}{\partial x_1} - \sin^2\phi \frac{\partial u_1}{\partial x_2} + \cos^2\phi \frac{\partial u_2}{\partial x_1} + \frac{1}{2}\sin(2\phi)\frac{\partial u_2}{\partial x_2} \tag{3.5}$$

where D_r is the rotational diffusion coefficient. Eq. (3.5) is valid for fibres having infinite lenght-to-diameter aspect ratio, that is, for relatively long fibres, see Olson and Kerekes [86]. It has been numerically tested that for fibres used in pulp and paper industry, this simplification does not violate the results; the aspect ratio should be below 10 before any modification in the orientating behaviour could be seen, and thus, this simplification is justified.

Using Eq. (3.5) the right hand side of Eq. (3.4) can be written

$$\begin{aligned} -\frac{\partial}{\partial \phi}\left(\psi \dot{\phi}\right) = &-\frac{\partial}{\partial \phi}\left(-\psi \frac{D_r}{\psi}\frac{\partial \psi}{\partial \phi}\right) - \frac{\partial}{\partial \phi}\left(-\psi \frac{1}{2}\sin(2\phi)\frac{\partial u_1}{\partial x_1}\right) \\ &- \frac{\partial}{\partial \phi}\left(\left(-\psi \sin^2\phi\right)\frac{\partial u_1}{\partial x_2}\right) - \frac{\partial}{\partial \phi}\left(\left(\psi \cos^2\phi\right)\frac{\partial u_2}{\partial x_1}\right) \\ &- \frac{\partial}{\partial \phi}\left(\psi \frac{1}{2}\sin(2\phi)\frac{\partial u_2}{\partial x_2}\right) \end{aligned} \tag{3.6}$$

Since D_r and velocity gradients do not depend on ϕ, the equation can be reorganised as follows:

$$\begin{aligned}-\frac{\partial}{\partial\phi}\left(\psi\dot{\phi}\right) =& D_r\frac{\partial^2\psi}{\partial\phi^2} + \underbrace{\frac{\partial}{\partial\phi}\left(\psi\frac{1}{2}\sin\left(2\phi\right)\right)}_{(1)}\frac{\partial u_1}{\partial x_1} + \underbrace{\frac{\partial}{\partial\phi}\left(\psi\sin^2\phi\right)}_{(2)}\frac{\partial u_1}{\partial x_2} \\ &- \underbrace{\frac{\partial}{\partial\phi}\left(\psi\cos^2\phi\right)}_{(3)}\frac{\partial u_2}{\partial x_1} - \underbrace{\frac{\partial}{\partial\phi}\left(\psi\frac{1}{2}\sin\left(2\phi\right)\right)}_{(4)}\frac{\partial u_2}{\partial x_2}\end{aligned} \tag{3.7}$$

The derivatives for the terms denoted with (1), (2), (3) and (4) can be expressed

$$\begin{aligned}(1)\qquad \frac{\partial}{\partial\phi}\left(\psi\frac{1}{2}\sin\left(2\phi\right)\right) &= \frac{\partial\psi}{\partial\phi}\frac{1}{2}\sin\left(2\phi\right) + \psi\frac{\partial}{\partial\phi}\left(\frac{1}{2}\sin\left(2\phi\right)\right) \\ &= \left(\frac{1}{2}\sin\left(2\phi\right)\right)\frac{\partial\psi}{\partial\phi} + \left(\cos\left(2\phi\right)\right)\psi \\ (2)\qquad \frac{\partial}{\partial\phi}\left(\psi\sin^2\phi\right) &= \frac{\partial\psi}{\partial\phi}\sin^2\phi + \psi\frac{\partial}{\partial\phi}\left(\sin^2\phi\right) \\ &= \left(\sin^2\phi\right)\frac{\partial\psi}{\partial\phi} + \left(\sin\left(2\phi\right)\right)\psi \\ (3)\qquad -\frac{\partial}{\partial\phi}\left(\psi\cos^2\phi\right) &= -\frac{\partial\psi}{\partial\phi}\cos^2\phi - \psi\frac{\partial}{\partial\phi}\left(\cos^2\phi\right) \\ &= -\left(cos^2\phi\right)\frac{\partial\psi}{\partial\phi} + \left(\sin\left(2\phi\right)\right)\psi \\ (4)\qquad -\frac{\partial}{\partial\phi}\left(\psi\frac{1}{2}\sin\left(2\phi\right)\right) &= -\frac{\partial\psi}{\partial\phi}\frac{1}{2}\sin\left(2\phi\right) - \psi\frac{\partial}{\partial\phi}\left(\frac{1}{2}\sin\left(2\phi\right)\right) \\ &= \left(\frac{1}{2}\sin\left(2\phi\right)\right)\frac{\partial\psi}{\partial\phi} + \left(-\cos\left(2\phi\right)\right)\psi\end{aligned} \tag{3.8}$$

Substituting the derivatives in Eq. (3.6) gives:

$$\begin{aligned}-\frac{\partial}{\partial\phi}\left(\psi\dot{\phi}\right) =& D_r\frac{\partial^2\psi}{\partial\phi^2} \\ &+ \underbrace{\left[\frac{1}{2}\sin\left(2\phi\right)\left(\frac{\partial u_1}{\partial x_1} - \frac{\partial u_2}{\partial x_2}\right) + \sin^2\phi\frac{\partial u_1}{\partial x_2} - \cos^2\phi\frac{\partial u_2}{\partial x_1}\right]}_{C}\frac{\partial\psi}{\partial\phi} \\ &+ \underbrace{\left[\cos\left(2\phi\right)\left(\frac{\partial u_1}{\partial x_1} - \frac{\partial u_2}{\partial x_2}\right) + \sin\left(2\phi\right)\left(\frac{\partial u_1}{\partial x_2} - \frac{\partial u_2}{\partial x_1}\right)\right]}_{R}\psi\end{aligned} \tag{3.9}$$

Using the above notations C and R, and suppressing the time derivative, Eq. (3.4) becomes:

$$-D_t \frac{\partial^2 \psi}{\partial x_i \partial x_i} - D_r \frac{\partial^2 \psi}{\partial \phi^2} + \frac{\partial}{\partial x_i}\left(u_i \psi\right) = C \frac{\partial \psi}{\partial \phi} + R\psi \tag{3.10}$$

The unknown probability function $\psi(x_1, x_2, \phi)$ depends on the geometrical position (x_1, x_2) and on the angle ϕ. Hence, it leads to a non-standard geometrical modelling, that is, when geometry is two-dimensional, the FOPD model is three-dimensional. The section 4.1 introduces in more detail, how the dimensions are handled in the model, and describes also the boundary conditions used.

One shortcoming of the FOPD model is that it is derived for dilute suspensions. This means that fibre-fibre interactions are not taken into account. This is somehow quite a serious drawback, since, as mentioned before, in all practical papermaking applications, there are fibre-fibre connections. Krochak et al., for example, showed that flocculation occurs even at low concentrations [62]. In addition, in the current model, there is only one-way coupling between fluid dynamics and the FOPD model, that is, fluid dynamics affect to fibre orientation, but not vice versa. The turbulence modification in the presence of fibres is largely recognised phenomenon, and it could quite easily be added in the model by modifying the source terms of turbulence equations. However, this is not accomplished, since the fundamental theory of this phenomenon does not exist, see Section 3.4 for futher discussion. Despite of the mentioned deficiencies, the FOPD is, however, the best available model at present, and widely used by many reseaches, since it provides, after all, very useful knowledge of fibre suspensions. It is worth to keep in mind that also the experiments investigating the fibre orientation are made for dilute suspensions, the concentration being $\approx$0.01%, i.e. even less than in white water. In addition, the tissue headboxes are typically run with the concentration of $\approx$ 0.1%, and thus, in such applications the FOPD model might be able to fairly accurately predict the fibrous structure of the end product.

3.3 Eulerian two-fluid model

The Eulerian two-fluid model used in this thesis is based on the "traditional" two component forms of continuity and momentum equations, which can be found in any multiphase text book, see e.g. [14]. The equations presented here follow mainly [14] and are all formulated in the steady-state form. The two-fluid approach is commonly accepted modelling method, and used by several researhers for air-fibre flows, see eg. [69] and [73]. In the Eulerian approach, the prescence of particles in the flow is taken into account by modelling the particle phase as a separate, immiscible liquid, and the interactions between two phases are included in the momentum equations via drag and possible other forces. The governing equations are averaged, and in each computational cell there is a certain volume fraction (even an infinitely small) of both flowing media. In this thesis, the equations are formulated for water and flocs, and hence, the material properties for floc phase are

not the same as for fibres. Determining the floc phase properties is a complicated issue, and it will be more closely discussed in Section 3.5.

The continuity equation for two-fluid flow can be written

$$\frac{\partial}{\partial x_i}\left(\alpha_k \rho_k u_{k,i}\right) = S_k \tag{3.11}$$

where the index k is c for continuous phase (here water) and d for dispersed phase (flocs). α_k stands for the volume fraction, ρ_k for the density and u_k for the velocity. S_k is the source term, which is, naturally, equal to zero, if no mass transfer between the two fluids is present.

The momentum equation for the continuous phase can be written as:

$$\begin{aligned}\frac{\partial}{\partial x_j}\left(\alpha_c \rho_c u_{c,i} u_{c,j}\right) = &-\alpha_c \frac{\partial}{\partial x_j}\left(p\delta_{ij}\right) + \frac{\partial}{\partial x_j}\left(\alpha_c \tau_{c,ij}\right) + f_{cd}\left(u_{d,i} - u_{c,i}\right) \\ &- \frac{\partial}{\partial x_j}\left(\alpha_c \rho_c \overline{u'_{c,i} u'_{c,j}}\right) + B_{c,i}\end{aligned} \tag{3.12}$$

and for the fibrous phase:

$$\begin{aligned}\frac{\partial}{\partial x_j}\left(\alpha_d \rho_d u_{d,i} u_{d,j}\right) = &-\alpha_d \frac{\partial}{\partial x_j}\left(p\delta_{ij}\right) + \frac{\partial}{\partial x_j}\left(\alpha_d \tau_{d,ij}\right) + f_{cd}\left(u_{c,i} - u_{d,i}\right) \\ &- \frac{\partial}{\partial x_j}\left(\alpha_d \rho_d \overline{u'_{d,i} u'_{d,j}}\right) + B_{d,i} + F^{SP}_{d,i}\end{aligned} \tag{3.13}$$

where $B_{c,i}$ and $B_{d,i}$ are body forces, and $F^{SP}_{d,i}$ represents additional interphase momentum transfer to be added in certain circumstances, for example in the dewatering modelling, see Section 3.6. The terms $f_{cd}\left(u_{d,i} - u_{c,i}\right)$ and $f_{cd}\left(u_{c,i} - u_{d,i}\right)$ in Eqs. (3.12) and (3.13) represent the interphase drag between water and fibrous phase. The drag coefficient, f_{cd}, can be written as:

$$f_{cd} = \frac{C_{cd}}{8} A_{cd} \rho_c \left|u_{d,i} - u_{c,i}\right| \tag{3.14}$$

where A_{cd} is the interfacial area density defined as $A_{cd} = 6\alpha_d / d_{ave}$, where d_{ave} denotes the mean diameter of spherical particles. The dimensionless drag coefficient, C_{cd}, is modelled with the Schiller-Naumann [99] correlation, which is commonly used in dispersed particle flow simulations:

$$C_{cd} = \begin{cases} \frac{24}{Re_r}\left(1 + 0.15\left(Re_r\right)^{0.687}\right) & \text{if } Re_r < 1000 \\ 0.44 & \text{if } Re_r > 1000 \end{cases} \tag{3.15}$$

where Re_r is the relative Reynolds number based on the relative speed between continuous and dispersed phase, $Re_r = \rho_c d_{ave}\left|u_{c,i} - u_{d,i}\right| / \mu_c$. For single fibres, there exist models for drag coefficients, but they are not suitable for flocs, since

flocs can be assumed quasi-spherical, except in strogly elongational flows. In addition, there are no better assumptions available for the fibre floc drag, and hence, the Schiller-Naumann correlation is chosen.

3.4 Modelling of turbulence

Turbulence modification in presence of particles is well-recognised, but still inadequately known phenomenon. Several authors have used the modified $k-\varepsilon$ model based on [92]. The model includes the additional dissipation caused by the prescence of particles, but neglects the additional production due to the particles. Although in some fluid-particle flows the supplementary production is important [69], in the modelling of flocculation in fibre-water suspensions it can be neglected, since wake production does not occur. The dampening of turbulence is not, however, such straightforward phenomenon. It has been shown by many authors, e.g. [28] and [116], that fibres and flocs reduce turbulence intensity. For example, Norman and Söderberg suggested [83] that the prescence of fibres in a flow will suppress those scales of the flow which are smaller than the fibre size. Bennington and Thangavel [9] noticed that when fibre concentration is increased, more and more energy was removed from the turbulence cascade. In addition, it is suggested [83] that fibres and flocs modify also the turbulence spectrum in such a way that it is no longer continuous as it is for single-phase flows.

Nevertheless, the detailed measurement of turbulence in typical wet end concentrations is not yet possible, and hence, no reliable theory about the turbulence dampening in fibre-water suspension is available. Therefore, in this thesis, the simulations for the water phase are mostly performed with the standard $k-\varepsilon$ model, without any modification of the source terms. One exception of this procedure is done for the FOPD model in the slice channel, for which the Reynolds Stress Model is applied. The reason for this is that in the slice channel turbulence is not at all isotropic [88], and it might probably have an effect on orientation. Nevertheless, for flocculation modelling an isotropic turbulence model is used, since it has been thought that the uncertainty in the flocculation model does not specifically lie in turbulence modelling, but rather, in the definition of floc break-up and coalescence mechanisms.

In the $k-\varepsilon$ model for the continuous phase the Reynolds stresses, $\rho_c\overline{u_{c,i}^{'}u_{c,j}^{'}}$, in Eq. (3.2) are modelled using the Boussinesq hypothesis:

$$-\rho_c\overline{u_{c,i}^{'}u_{c,j}^{'}} = \mu_{tc}\left(\frac{\partial u_{c,i}}{\partial x_j}+\frac{\partial u_{c,j}}{\partial x_i}\right)-\frac{2}{3}\delta_{ij}\rho_c k_c \tag{3.16}$$

where k_c is the turbulent kinetic energy of the continuous phase given by

$$k_c = \frac{1}{2}\overline{u_{c,i}^{'}u_{c,i}^{'}} \tag{3.17}$$

and μ_{tc} is the turbulent (or eddy) viscosity for the carrier phase defined by

$$\mu_{tc} = \rho_c C_\mu \frac{k_c^2}{\varepsilon_c} \tag{3.18}$$

where C_μ =0.09 and ε_c is the turbulent kinetic energy dissipation. The transport equations for the turbulent kinetic energy, k_c, and for the dissipation, ε_c, of the continuous phase can be written:

$$u_{c,i}\frac{\partial(\alpha_c\rho_c k_c)}{\partial x_i} = \frac{\partial}{\partial x_i}\left(\left(\mu_c+\frac{\mu_{tc}}{\sigma_k}\right)\frac{\partial(\alpha_c k_c)}{\partial x_i}\right)+\alpha_c P_{kc}-\alpha_c\rho_c\varepsilon_c \tag{3.19}$$

$$\begin{aligned} u_{c,i}\frac{\partial(\alpha_c\rho_c\varepsilon_c)}{\partial x_i} &= \frac{\partial}{\partial x_i}\left(\left(\mu_c+\frac{\mu_{tc}}{\sigma_\varepsilon}\right)\frac{\partial(\alpha_c\varepsilon_c)}{\partial x_i}\right)+\alpha_c C_{\varepsilon 1}P_{kc}\frac{\varepsilon_c}{k_c} \\ &\quad -\alpha_c\rho_c C_{\varepsilon 2}\frac{\varepsilon_c^2}{k_c} \end{aligned} \tag{3.20}$$

where the model constants are: $C_{\varepsilon 1}$ =1.44, $C_{\varepsilon 2}$ =1.92, σ_k =1.0 and σ_ε =1.3 [65]. P_{kc} is the production of the turbulent kinetic energy by the mean velocity field given as

$$P_{kc}=\mu_{tc}\left(\frac{\partial u_i}{\partial x_j}+\frac{\partial u_j}{\partial x_i}\right)\frac{\partial u_i}{\partial x_j} \tag{3.21}$$

As stated above, the Reynolds Stress Model is used for the FOPD simulation. The transport equation for Reynolds stresses can be found in any turbulence text book, see e.g. [91], and is applied in the steady-state form [1]:

$$\begin{aligned} u_{c,l}\frac{\partial\left(\rho_c\overline{u_{c,i}^{'}u_{c,j}^{'}}\right)}{\partial x_l} &= \mathcal{P}_{ij}+\mathcal{R}_{ij}+\frac{\partial}{\partial x_l}\left(\left(\mu_c+\frac{2}{3}C_s\rho_c\frac{k_c^2}{\varepsilon_c}\right)\frac{\partial\overline{u_{c,i}^{'}u_{c,j}^{'}}}{\partial x_l}\right) \\ &\quad -\frac{2}{3}\delta_{ij}\rho_c\varepsilon_c \end{aligned} \tag{3.22}$$

where $\mathcal{P}_{ij}$ is the production tensor given by

$$\mathcal{P}_{ij}=-\rho_c\left(\overline{u_{c,i}^{'}u_{c,l}^{'}}\frac{\partial u_j}{\partial x_l}-\overline{u_{c,j}^{'}u_{c,l}^{'}}\frac{\partial u_i}{\partial x_l}\right) \tag{3.23}$$

and $\mathcal{R}_{ij}$ is the pressure-strain correlation, defined as

$$\mathcal{R}_{ij}=\mathcal{R}_{ij,1}+\mathcal{R}_{ij,2} \tag{3.24}$$

There exist several different propositions for $\mathcal{R}_{ij,1}$ and $\mathcal{R}_{ij,2}$, one of them being

$$\begin{aligned} \mathcal{R}_{ij,1} &= -\rho_c\varepsilon_c C_{s1}a_{ij} \\ \mathcal{R}_{ij,2} &= -\rho_c C_{r2}k_c S_{ij}+\rho_c C_{r4}k_c\left(a_{ij}S_{ij}+a_{ji}S_{ij}-\frac{2}{3}a_{ij}\cdot S_{ij}\delta_{ij}\right) \\ &\quad +C_{r5}\rho_c k_c\left(a_{ij}\Omega_{ji}+a_{ji}\Omega_{ij}\right) \end{aligned} \tag{3.25}$$

and the anisotropy, a_{ij}, the strain rate, S_{ij}, and the vorticity, Ω_{ij}, are written as

$$a_{ij} = \frac{\overline{u'_{c,i}u'_{c,j}}}{k_c} - \frac{2}{3}\delta_{ij} \tag{3.26}$$

$$S_{ij} = \frac{1}{2}\left(\frac{\partial u_i}{\partial x_j} + \frac{\partial u_j}{\partial x_i}\right) \tag{3.27}$$

$$\Omega_{ij} = \frac{1}{2}\left(\frac{\partial u_i}{\partial x_j} - \frac{\partial u_j}{\partial x_i}\right) \tag{3.28}$$

Finally, the coefficients in Eqs. (3.22) and (3.25) are: C_s =0.22, C_{s1} =1.8, C_{r2} =0.8, C_{r4} =0.6 and C_{r5} =0.6.

For the fibrous phase, one cannot really speak about turbulence, but rather some fluctuation. Therefore, only a simple algebraic model is applied, and it is given as follows [1]

$$\mu_{td} = \frac{\mu_{tc}}{Pr_t} \tag{3.29}$$

where Pr_t is the turbulent Prandtl number.

3.5 Modelling of fibre flocculation - the FFE model

The flocculation is modelled with a totally novel approach in pulp and paper industry, the Fibre Floc Evolution (FFE) model. The suspension is modelled as a turbulent two phase flow, with water being the carrier phase and the flocs as the dispersed phase. Since the modelling approach is Eulerian, the presence of single fibres is neglected, and the floc phase is treated as an immiscible liquid, having its own properties. Even though flocs are small fibre networks, which have a mechanical strength, they can be treated as a continuum, as far as the micro-scale phenomena are not taken into account. In addition, it must be emphasised that the properties of flocs are different from those of single fibres, and naturally, different from those of water.

In order to describe the physical behaviour of flocs, the fibrous phase is divided into several size groups, each of them representing different floc size. The model is based on the population balance method, and thus, it provides detailed information of the floc size evolution. Flocs can coalesce into larger flocs or break-up into smaller ones, which means that the basic flocculation dynamics is taken into account. It is recognised that in real processes fibres can detach from a floc by some kind of erosion mechanism, or, a single fibre can attach to a floc, and hence, modify the local floc size distribution. However, these mechanisms are not implemented into the FFE model, since any experimental data for such a validation does not exist, and modelling the effects mentioned would be very complicated.

The population balance method, as well as break-up and coalescence models used, are commonly known methods, and therefore, they are only briefly presented

in next three subsections. The break-up phenomenon is modelled using Luo and Svendsen model [70] and the coalescence with Prince and Blanch model [93]. Both models are based on the theories of isotropic turbulence and on the assumption that the particle size can be modified by eddies having length scale equal to or smaller than the particle. The mentioned models are derived for spherical particles, such as bubbles. It has also been assumed that particles do not consist of smaller components in the same way as flocs consist of fibres. Therefore, the smallest modelled unit refering to particle, is floc, in this thesis. Thus, it is worth to keep in mind that when presenting the break-up and coalescence models in Subsections 3.5.2 and 3.5.3 the word "particle" refers to floc.

Although the flocculation has been an active area of research for decades, it is still a matter of debate, which is the mechanism that causes the break-up and coalescence of flocs. As early as 1979, Wahren stated that floc dispersion and aggregation are competing effects both promoted by turbulence [113]. Also Yokogawa et al. found a direct relation between the increased turbulence intencity and more uniform suspension when studying the effects of various turbulence generators [117]. Nevertheless, some researches have disagreed with these observations and proposed that floc dispersion occurs due to the elongational flows, i.e. due to the strain [82]. However, it has been proven by pilot-scale tests that the flocs break up most efficiently in the tube expansion of the turbulence generator [57] where the increase of the turbulent kinetic energy can be observed, while the elongation due to contractions is often able only to stretch the floc, which recovers its quasi-spherical shape after the elongation ceases [59]. In addition, it is commonly known fact that the relatively calm flow in the slice channel is capable only to maintain the floc size obtained in the turbulence generator, not to further break up the flocs [103]. It is, therefore, an appropriate approach to use the Luo and Svendsen model for the break-up and the Prince and Blanch model for coalescence, since both are based on theories leaning on turbulence contribution in particle size modification.

In addition, the viscosity of fibre suspension flows has been the objective of many studies. Head loss (wall friction and apparent viscosity, as well) in long tubes of pulp-water mixture flows have been studied by Brecht and Heller [11], for example, and it is known to vary significantly depending on the pulp concentration, fibre properties etc. The viscosity has been modelled as a generalized Newtonian fluid following the Power-Law model by Myréen [75] or as a Bingham fluid by Wikström [114], for example. However, these studies are not directly applicable to two-phase flow modelling, since they are treating the flowing media as a one-phase flow. In other words, the suspension is assumed homogenious having one viscosity dependent on shear rate, but not on local concentration, for example. When modelling the suspension as a real two phase flow, the properties of different fluids have to be determined separately. This is to say, we need the viscosity of the fibrous phase, which can not be determined directly from measurements of the water-fibre mixture. To approximate the viscosity of the fibrous phase, the method used by Holmqvist, is applied [43]. He defined the viscosity of the suspension, μ_s, in the function of the volume fraction of fibrous phase, α_d, giving

$$\mu_s(\alpha_d) = \mu_c\left(1 + a\alpha_d^b\right) \tag{3.30}$$

where μ_c is the dynamic viscosity of the carrying phase, and a and b are empirical constants, $2.8 \cdot 10^5$ and 3.1, respectively. In order to ensure that the chosen approach is valid for the FFE model, several numerical tests using different values for fibrous phase viscosity is performed. It is noticed that the results remain the same even if the viscosity value is multiplied by factor of 10, and hence, it can be concluded that the approximation of the Eq. (3.30) is good enough for the concentrations used. In addition, it must be emphasised that only a constant value based on the average concentration is used, since also the experiments provide correlations based on the average concentration.

Another basic property of the fibrous phase to be determined is the density. Similarly as for the viscosity, there exists no experimental data for the density of the floc phase, since measurements provide only the properties of the mixture. The floc phase density can, however, be approximated by using the material properties of the dry pulp found in literature. The specific volume of the unbleached pine kraft is $\approx$0.0034 m^3/kg, which gives 294 kg/m^3 for the density of the dry pine pulp [31]. By assuming the fibre wall density to be 1520 kg/m^3, it results in that the dry pulp contains 19% of solids and 81% of air. Consequently, the wet pulp, where the air is replaced by water, has the density of 1100 kg/m^3. Naturally, the wall thickness within different pulps and even within spring and summer fibres vary remarkably, which affects the volume fraction of water in a pulp, which, in turn, has an influence in the pulp density. The above value is, however, an average approximation for the fibrous phase density, and it is used in the simulations presented in this thesis.

3.5.1 Population balance approach

The population balance method is widely used tool in engineering of dispersed phase systems. Applications include crystallisation, pharmaceutical manufacture, fluisized beds and microbial processes, for example. Whenever the interactions of particles of different sizes is studied, the population balance method provides a powerful approach in determining the properties of the resulting product and its dependence on processes such as coalescence, breakage and surface growth [96]. In the population balance approach one additional conservation equation is solved for each size group, and thus, in order to study ten different particle sizes, for example, ten complementary equations are needed.

Let $N = N(V_m, t)$ represent the number density of particles of size V_m at time t. The population balance equation for the size group V_m then is [1]:

$$\frac{\partial}{\partial t}N + \frac{\partial}{\partial x_i}(Nu_d) = B_B - D_B + B_C - D_C \tag{3.31}$$

where B_B, D_B, B_C and D_C represent the birth rate due to break-up of larger particles, the death rate due to break-up into smaller particles, the birth rate due

to coalescence of smaller particles, and the death rate due to coalescence with other particles, respectively. These rates may further be expressed as

$$B_B = \int_{V_m}^{\infty} g\left(V_n; V_m\right) N\left(V_n\right) dV_n \tag{3.32}$$

$$D_B = N\left(V_m\right) \int_0^{V_m} g\left(V_m; V_n\right) dV_n \tag{3.33}$$

$$B_C = \frac{1}{2} \int_0^{V_m} Q\left(V_m - V_n; V_n\right) N\left(V_m - V_n\right) N\left(V_m\right) dV_n \tag{3.34}$$

$$D_C = N\left(V_m\right) \int_0^{\infty} Q\left(V_m; V_n\right) N\left(V_n\right) dV_n \tag{3.35}$$

where $g\left(V_m; V_n\right)$ represents the specific break-up rate at which the particles of size V_m break into particles of size V_n and $(V_m - V_n)$. Similarly, $Q\left(V_m; V_n\right)$ represents the specific coalescence rate at which the particles of size V_m coalesce with particles V_n to form particles of size $(V_m + V_n)$. The population balance approach applied in this thesis is homogenous, that is, the density and the velocity are same for all size groups.

3.5.2 Break-up model

The floc break-up is modelled using the Luo and Svendsen model [70]. The model is originally developed for drops and bubbles in turbulent flows, and it is based on the theories of isotropic turbulence and probability. Although turbulence is not isotropic in all the papermaking applications, such as in the headbox slice channel [87], the fine-scale structure of most non-isotropic turbulent flows is locally nearly isotropic [41]. In addition, the actual challenges in the flocculation modelling lie in the description of the entire model, not in modelling turbulence. Another simplification in the model is made, when only the binary breakage of fluid particles is taken into account. This means that multiple breakages on the same particle do not occur simultanously, and hence, one parent particle is always divided into two daughter particles, if the breakage takes place. This is an acceptable assumption, since the likelihood of several breakages occuring precisely at the same time is very small. Further, the occurence of break-up is connected to the energy level and the length scale of the arriving eddy: Only eddies having length scale equal to or smaller than the particle diameter are able to induce the break-up. The derivation of turbulence interaction with particles is comprehensively presented in [110], and hence, only the main equations, following the work of Luo and Svendsen, are given here.

The model considers the break-up of particles of volume V_m into two daughter fractions, one of them having the volume V_n.

$$g(V_m;V_n) = C_B 0.923 N_m \left(1-\alpha_m\right)\left(\frac{\varepsilon_c}{d_m^2}\right)^{1/3}\int_{\xi_{min}}^{1}\frac{\left(1+\xi\right)^2}{\xi^{11/3}}e^{-\chi}d\xi \tag{3.36}$$

with

$$\chi = \frac{12\sigma\left[f_{BV}^{2/3}+\left(1-f_{BV}\right)^{2/3}-1\right]}{\beta\rho_c\varepsilon_c^{2/3}d_m^{5/3}\xi^{11/3}} \tag{3.37}$$

In Eqs. (3.36) and (3.37), N_m, α_m and d_m are the number density, volume fraction, and diameter of the parent particles, respectively. σ denotes the internal strength of a particle, ρ_c the continuous phase density, and ε_c the continuous phase turbulent kinetic energy dissipation. f_{BV} denotes the breakage volume fraction, the parameter β is a numerical constant equal to 2.0, and C_B is a supplemental break-up coefficient, and its role is to control the break-up rate. ξ is the dimensionless size of eddies in the inertial subrange of isotropic turbulence, i.e. the size ratio between an eddy and a particle. The lower limit of integration is given by

$$\xi_{min} = \frac{\lambda_{min}}{d_m} \tag{3.38}$$

To be exact, in Eq. (3.36) the microscale of eddies, λ_d, should be used as the lower limit, but it has been replaced by the minimum size of eddies in the inertial subrange of isotropic turbulence, λ_{min}, since the expressions for bombarding frequency of eddies and breakage probability are only valid for this subrange. This is, however, justified, since the very small eddies have very low energy, and thereby, have an negligible effect on the break-up process [70]. The minimun size of eddies in the inertial subrange has been given as $\lambda_{min}/\lambda_d \approx 11.4 - 31.4$ [110], where λ_d denotes Kolmogorov length scale, given as

$$\lambda_d = \left(\frac{\nu_c^3}{\varepsilon_c}\right)^{1/4} \tag{3.39}$$

where ν_c is the continuous phase kinematic viscosity. In this work, the value 11.4 is used for λ_{min}/λ_d.

3.5.3 Coalescence model

The coalescence phenomenon is described with the model of Prince and Blanch [93], which is originally developed for gas or liquid bubbles flowing in the liquid. This model is, however, suitable for fibre flocs, because fibre flocs may agglomerate, such as bubbles. The model assumes the particles to be spherical, which is evidently not true for flocs in all circumstances. However, it is commonly known that flocs do not coalesce in the areas, where there are strong shear or elongation forces present. It can, therefore, be assumed that the form of a floc is quasi spherical, if the flow conditions are favorable to coalescence, and hence, the chosen model can be applied.

In the model of Prince and Blanch it is assumed that the coalescence of two particles occurs in three steps. First, the particles collide trapping a small amount of liquid between them. This liquid film then drains until it reaches a critical thickness, which means that the film ruptures and the particles join together. It is, therefore, evident that coalescense rate is tightly connected to collision rate. Further, every collision does not lead to coalescense, and hence, it is necessary to determine the collision efficiency. Two particles will coalesce only, if they remain in contact for a period, which is sufficient to thin the liquid film between them down to the critical value of rupture.

There are several mechanisms, which may cause collisions of two particles: turbulence, buoyancy, laminar shear, difference in particle velocities etc. In [93] three first mentioned are considered, but in this work only the effects of turbulence are included. This is justified by assuming that in the practical papermaking applications, such as in the headbox, the flow conditions are dominated by turbulence, and including the other mechanisms would not give any further value for the flocculation model. If there was a need to add the other mechanisms, it could be done quite straightforwardly, since they are assumed cumulative.

In order to follow the depicted behaviour, coalescence of two particles of size m and n is modelled by the turbulent collision rate, θ_{mn}^{T}, and the collision efficiency, η_{mn},

$$Q\left(V_m; V_n\right) = \theta_{mn}^{T} \eta_{mn} \tag{3.40}$$

The collision efficiency, η_{mn}, is relating the time required for coalescence, t_{mn}, with the actual contact time during collision, ζ_{mn}, by

$$\eta_{mn} = e^{-t_{mn}/\zeta_{mn}} \tag{3.41}$$

The time required for coalescence is given as

$$t_{mn} = \left(\frac{\rho_c r_{mn}^3}{16\sigma}\right)^{1/2} \ln\left(\frac{h_{init}}{h_{crit}}\right) \tag{3.42}$$

where h_{init} is the initial film thickness, h_{crit} is the critical film thickness when rupture occurs, and r_{mn} is the equivalent radius taking into account that the radii of the coalescing particles may be different:

$$r_{mn} = \left[\frac{1}{2}\left(\frac{1}{r_m} + \frac{1}{r_n}\right)\right]^{-1} \tag{3.43}$$

The actual contact time of two particles is calculated using

$$\zeta_{mn} = \frac{r_{mn}^{2/3}}{\varepsilon_c^{1/3}} \tag{3.44}$$

The turbulent collision rate in Eq. (3.40) is given as follows

$$\theta_{mn}^{T} = C_{CT} A_{mn} \left(u_{tm}^2 + u_{tn}^2\right)^{1/2} \tag{3.45}$$

where C_{CT} is the turbulent coalescence coefficient used for defining different collision tendencies for particles of different substance. The collision cross-sectional area of the dispersed particles, A_{mn}, is defined by

$$A_{mn} = \frac{\pi}{4}\left(d_m + d_n\right)^2 \tag{3.46}$$

The velocity of particles is assumed to be the turbulent eddy velocity of the length scale of the particle. Thus, for the particle of size m the velocity is given by

$$u_{tm} = \sqrt{2}\varepsilon_c^{1/3} d_m^{1/3} \tag{3.47}$$

The model is, therefore, based on the assumption that eddy motion of the length scale of the particle is considered to be primarly responsible for the relative motion between two particles. In the other words, very small eddies no not contain sufficient energy to affect the particle motion. On the other hand, much larger eddies transport groups of particles without changing their relative positions. In addition, in the definition of the turbulent eddy velocity, Eq. (3.47), turbulence is assumed isotropic, and the particle size lies in the inertial subrange.

3.6 Modelling of dewatering

Modelling the forming of the paper web involves usually the modelling of the free jet, and thus, there are three phases present: water, flocs and the surrounding air. In this thesis the dewatering phenomena are described with a relatively simple model, although many researchers have performed much more detailed simulations. However, the purpose of this work is not to study the dewatering phenomena, but instead, to examine its effect on floc behaviour and on the forming of the paper web. In addition, the simulations are performed for a two-dimensional Fourdrinier-type of forming section, where the phenomena are simpler than in the gap former. It is then easier to assure that the complex flow field is adequately modelled, and also the results are easier to interpret.

The water removal through the wire is based on the analytical expression for the head loss, Δp, as a function of the fluid mass flux, $\dot{q}$, through the wire:

$$\Delta p = p - p_a = \frac{1}{2}\rho_c R_w \left(\frac{\dot{q}}{\rho_c A}\right)^2 \tag{3.48}$$

where p is the local static pressure above the wire, p_a is the atmospheric pressure under the wire (assumed zero), ρ_c is the density of water, A is the unit area and R_w stands for the fabric resistance (a dimensionless coefficient). The resistance coefficient takes into account the thickness and the porosity of the wire. The equation is valid for a relatively open wire when the Reynolds number based on the wire pore flow is high enough. If the resistance is high leading to a small water velocity, the Darcy law should be used in order to take into account the viscous permeability (see [17], for example). However, since the water velocity through the wire is relatively high, especially in the beginning of the forming section, it is

assumed that the viscous effects can be neglected. Hence, the mass flux, $\dot{q}$, per unit area, A, can be solved from the Eq. (3.48) leading to the expression:

$$\frac{\dot{q}}{A} = \sqrt{\frac{2p\rho_c}{R_w}} \tag{3.49}$$

which is used as a sink term on the wire to simulate the water removal. The simulated static pressure on the wire depends on the position in MD. Thus, the water removal varies in different positions and it is not known a-priori. The fibre retention is assumed to be 100%, but the effect of it could be easily added to the model in such a way, for example, that if flocs of the smallest size group collide with the moving fabric, certain percentage of them are drained through the wire with the water, if the flow conditions are favourable (i.e. pressure gradient strong enough). This feature is, however, left out in order to keep the model simple and easier to interpret.

In the forming section, when water is drained through the wire, the volume fraction of the fibrous phase increases and the collisions of flocs introduces additional force. These interactions can be taken into account by adding the solids pressure force, presented by Gidaspow [29], in the momentum equation of the dispersed phase (3.13):

$$F_{d,i}^{SP} = -G_0 e^{C_{SP}(\alpha_d - \alpha_{d,max})} \frac{\partial \alpha_d}{\partial x_i} \tag{3.50}$$

where G_0 is the reference elasticity modulus, C_{SP} stands for the compaction modulus, α_d represents the local volume fraction of the fibrous phase and $\alpha_{d,max}$ is the maximum packing parameter. The physical meaning of $\alpha_{d,max}$ is to restrict the maximun volume fraction of fibres into a reasonable level. Gidaspow's model has been used for modelling wood fibres in gas flows by Melander [73], who has proposed $G_0 = 1$ Pa, and the same value is used in this thesis as well. However, the maximum volume fraction of fibres is estimated higher than in Melander's work, since he had loosely packed fibres, which does not describe the situation in the forming section. It is assumed that the local volumetric concentration does not increase over 15%, which is more than double the value Melander had. Although the average concentration does not raise up to 15% during the first tens of centimetres, there may be remarkable concentration variations in the flowing suspension, since the water is removed through the wire. Hence, a sufficiently high value is chosen in order not to limit the solution too much.

The coefficient C_{SP} is chosen such that too strong gradients of the solids pressure force are avoided. As the mathematical representation of $F_{d,i}^{SP}$ reveals, bigger the coefficient C_{SP} is, more aggressive the effect of the force $F_{d,i}^{SP}$ is. Therefore, the value for C_{SP} is kept around 40, since it ensures the convergence in reasonable time, and still does not have influence in the areas of small volume fractions. In other words, the solids pressure gradient is only activated in regions close to the maximum packing, where its tendency is to prevent solid volume fractions from becoming too large. Two-phase models can be used without the solids pressure term

inside the headbox, for example, since the suspension is relatively homogeneous and dilute. However, neglecting the solids pressure force in the forming section would lead to unrealistic concentration levels, since flocs would pack extremely tightly onto the wire surface.

Chapter 4

Model setup

The simulations presented in this thesis are all done by the commercial CFD software ANSYS CFX. The implementation of each model, as well as model parameters and boundary conditions used, are explained in the following sections. Even though modelling of some special characteristics, such as FOPD, is more difficult with a commercial than with an in-house code in terms of convergence and boundary conditions, the same approach is applied for all the characteristics in order to create an approachable basis for simulating the forming of the paper structure. Certainly, choosing the modelling tool is always a compromise: with a commercial software, it is easy to program simple add-ons, but the whole complexity of the phenomena might not be implementable. On the other hand, if the simulation would be built on an in-house code the implementing of turbulence models, for example, would be a challenge itself. In addition, creating an in-house code including all the features presented below, would be extremely long work. Therefore, it is reasonable to start the development of totally new model, such as the FFE, with a commercial tool, since it offers many sub-models already implemented, but still enables the modification of model parameters or even the replacement of the sub-models with the own ones.

4.1 Model setup for the FOPD model

As stated earlier, the fibre orientation is studied in the headbox slice channel and in the jet. The situation can be assumed two-dimensional, if the effect of the slice channel edges and secondary flow disturbances can be neglected. Thus, the flow problem can be modelled with a 2D model consisting only of a vertical (x,y)-cross section, i.e, papermaker's (MD,z)-plane. However, including the FOPD model into a standard 2D CFD simulation increases dimensions of the model up to three. To be able to handle this in a commercial software, the model is made geometrically three dimensional such that the third coordinate axis stands for the angle ϕ belonging to $[-\pi/2, \pi/2]$, see Fig. 4.1, and it is discretised in elements such as the other directions. Since the FOPD is implemented in the software as a passive scalar,

it involves solving one complementary transport equation. The equation includes automatically three diffusion terms in each direction of cartesian (or cylindrical) coordinates, and in fact, the only way to include the physics of the phenomena, in addition to the source term, is via the diffusion coefficients. That is the main reason, why the FOPD equation is formulated as given by Eq. (3.10). Further, since the geometry is to be physically two-dimensional, but mathematically three-dimensional, the z-directional diffusion term represents the diffusion in angular coordinate, ϕ. The transport equation for the FOPD is implemented in ANSYS CFX with the cartesian notation as

$$-D_t\frac{\partial^2\psi}{\partial x^2} - D_t\frac{\partial^2\psi}{\partial y^2} - D_r\frac{\partial^2\psi}{\partial \phi^2} + \frac{\partial}{\partial x}\left(u_1\psi\right) + \frac{\partial}{\partial y}\left(u_2\psi\right) + \frac{\partial}{\partial z}\left(u_3\psi\right) = S_{FOPD} \quad (4.1)$$

from which the z-directional convection term has to be removed, since physically that dimension does not exist. Thus, the source term S_{FOPD} is given by:

$$S_{FOPD} = C\frac{\partial\psi}{\partial\phi} + R\psi + \frac{\partial}{\partial z}\left(u_3\psi\right) \quad (4.2)$$

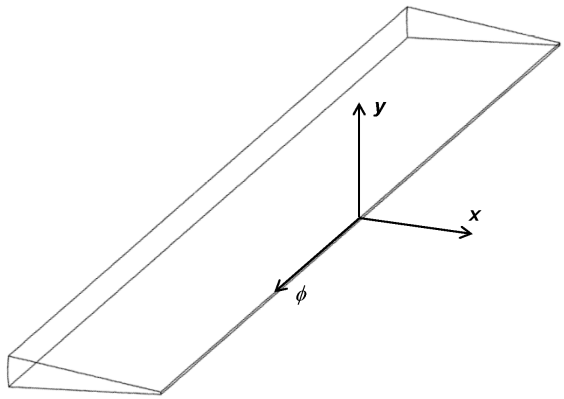

Figure 4.1: Coordinate system of the FOPD model.

As usual in free surface flows, also here the shape of the jet is not known *a-priori*, but instead solved by using a two-phase flow model. In other words, surrounding air above and below the jet is included in the CFD model as well. The jet is obtained as an area where the volume fraction of water is ≈1, while

in the surrounding air the volume fraction of water is ≈0. The jet can be solved independently from the FOPD model as the orientation does not affect the shape of the jet. In this study the slice channel has been modelled as symmetrical and without slice bar. It contracts from 100 mm to 8 mm and has the length of 500 mm. Numerical tests have attested that bigger the angle of the slice bar is, the more sensitive the geometry is for the convergence problems. This character is emphasised when using the geometrically two-dimensional form of the FOPD. With a 1D approach and using the streamline approach it is possible to model larger slice lip angles, but the simulations are not able to provide all the phenomena occuring at the slice opening. Thus, the mathematically two-dimensional form of the FOPD is used in this thesis.

The diffusion coefficients are estimated based on turbulent kinetic energy and on its dissipation rate, see [84]. Hyensjö has recently investigated deeply the determination of the rotational diffusion coefficient and presented three different hypotheses based on turbulence theories [48]. He also suggested some optimised values for parameters in the hypotheses. However, in this thesis, constant values, $D_t = 0.0001$ m^2/s and $D_r = 40$ m^2/s were used, since the anisotropic diffusion is a beta-feature of ANSYS CFX and the equations could not be implemented. The magnitude of the z-directional coefficient (corresponding the rotational diffusion) was found by comparing the results given in [51]. The value of the rotational diffusion coefficient is an active area of research, and in an on-going project, much more bigger values have been proposed by Niskanen et al. [78]. They based their suggestion on the experiments performed for flexible fibres in the slice channel with vanes. Those results differ remarkably from the ones presented by Ullmar [112], and the reason might be that Ullmar used flexible fibres in his experiments to create the pulp suspension-like conditions, but observed rigid tracer fibres. As a consequence, the results are not validated with experiments, but their reliability is assured by comparing them to previously reported studies, such as [51] and [85].

The FOPD model requires the boundary conditions like any typical CFD simulation. The fibre orientation distribution is assumed to be isotropic at the inlet. In fact, if the turbulence generator pipes had been included in the model as it is done in [78], there would be a profile with very small deviations from the isotropic distribution. Therefore, in practice, the profile is neglible, since the most dominating effect is the channel acceleration. The inlet velocity is assumed constant, which means that the effect of the turbulence generator pipes is not taken into account in the flow field simulation either.

At the edges, that is, $\phi = -\pi/2$ and $\phi = \pi/2$, periodic boundary conditions are applied. Boundary conditions on the bottom and top walls as well as on the surfaces of the jet are not trivial. In fact, the basic theory, how to implement the wall boundary conditions in the FOPD model, is missing, although some good experimental work on the boundary layer behaviour of the fibre orientation has been done [12]. The research is, however, rather fundamental, and according to its author, is not directly applicable in papermaking applications. Therefore, various boundary condition types were compared to get confidence that the chosen one does not disturb the solution. The zero-flux boundary condition, $\nabla\psi \cdot n = 0$,

where n is the normal of the wall, led to a nonrealistic solution, whereas the Dirichlet-type boundary conditions gave reasonable solutions. That is, the probability distribution was approximated using the analytic solution given in [85] and the mean orientation angle was set to a wall direction on the walls. An analogous approach was utilized for the jet as well.

The model provided similar results in the near-wall region as reported in the earlier study by Hyensjö [51], who avoided the determination of boundary conditions by choosing a model approach in which the FOPD is calculated postprocessed along streamlines and out of the CFD software. His approach, as well the one presented in this thesis, indicate that the head of the fibres tend to turn away from the wall. This proves that the chosen boundary condition does not disturb the solution due to a very small translational diffusion coefficient. This is also demonstrated within the results in Section 5.1, Figs. 5.4 and 5.7, for example.

4.2 Model setup for the FFE model

Since fibre flocculation is known to be strongly dependent on pulp properties, the simulations are performed for two different pulps; one consisting of pine fibres and the other of birch fibres (see Table 4.1). The mass concentration is converted to volume concentration used in multiphase flow equations by multiplying the value by 2, which is a commonly used rule of thumb. It is noteworthy, that the crowding factors of pine and birch differ significantly: according to definitions of Kerekes and Schell [60], the birch pulp is clearly in regime of forced collisions, while the pine pulp might already be dominated by continuous contact, see Table 2.1 in Section 2.2. Hence, the flocculation phenomena of these two pulps may obey different mechanisms.

Table 4.1: Characteristic properties of pulps used in simulations and experiments.

	Pine	Birch
Average fibre length [mm]	2.05	0.92
Average fibre diameter [μm]	22	16.7
Fibre coarseness [mg/m]	0.206	0.114
Mass concentration [%]	1	1
Crowding factor [ ]	116	40

Since the FFE model is totally novel approach in flocculation modelling, the model parameters need adjustment and validation. The results are validated with experimental studies carried out for a sudden expansion of a circular pipe, similar to the pipes in the headbox turbulence generator. The experiments are not part of this thesis, but performed earlier by Salmela and Kataja [97], and thus, the methods used are only briefly introduced in the following subsection.

To keep the modelling approach simple enough, only three model parameters are adjusted during the model validation phase, while the others are kept constant throughout the simulations. Until there is a good reason to believe that greater complexity provides more accurate information, it seems pointless to consider more parameters. Therefore, three "simpler" model parameters are chosen to be adjusted: the break-up coefficient, the coalescence coefficient and the internal strength of a floc. To give an insight of the model structure for future researchers, the parameters and variables of model equations are now briefly reviewed. It is emphasised that herein a parameter is given by the user, while a variable is solved by the CFD code. In other words, the parameters depend on the material properties, which have to be defined specifically for different flowing media, while variables are determined locally based on particular equations, and they are functions of simulated floc size, turbulence etc..

In the break-up model, that is, in Eqs. (3.36)...(3.39) the model variables, i.e. N_m, α_m, d_m, ε_c, and f_{BV}, are calculated based on the local flow conditions and the flocculated state of the suspension. They represent the number density of each floc size group, fibrous phase volume fraction, diameter of the parent particles, the continuous phase turbulent kinetic energy dissipation and the breakage volume fraction, respectively. The computation of the first four mentioned is straightforward, and the last one, f_{BV}, is based on the local kinetic energy of turbulent eddies (for more detailed explanation, see [70]). Hence, the only parameters to be determined for the break-up model are σ, which denotes the internal strength of a floc, and C_B, which is a supplemental break-up coefficient.

The variables in coalescence model, i.e. in Eqs. (3.40)...(3.47), are η_{mn}, t_{mn}, ζ_{mn}, r_{mn}, A_{mn} and u_{tm}, which denote the collision efficiency, the time required for coalescence, the actual contact time, the equivalent radius, the collision cross-sectional area and the turbulent eddy velocity of the length scale of the floc, respectively. The computation of these variables follow directly the equations presented in Section 3.5.3. The model parameters the user has to determine are h_{init}, h_{crit}, C_{CT} and σ, which denote the initial film thickness, the critical film thickness when rupture occurs, the turbulent coalescence coefficient and the internal strength of a floc, respectively. One can, thus, notice that the internal strength affects both the break-up and the coalescence mechanisms. Determination of the turbulent coalescence coefficient is discussed together with the internal strength of a floc and the break-up coefficient, since they are chosen to be the three model parameters used for adjusting the model for fibre flocs. Moreover, since there are no better assumptions, the values for h_{init} and h_{crit} are set to be the default values proposed by the software, that is, 0.1 mm and 10^{-5} mm, respectively. The values might be too small for flocs, since they are defined originally for bubbles, but a closer investigation is left for the future work.

The definition of the three chosen model parameters was quite a complex task, since their values are provided neither by experiments nor in the literature. The roles of break-up and coalescence coefficients are quite obvious when looking at Eqs. (3.36) and (3.45), since they appear only as dimensionless coefficients in the model equations. The parameter describing the internal strength of a floc is

analoguous to the surface tension, and hence, its adjustment for fibre suspension flows requires special attention, since one can assume that it is dependent on pulp properties. Several authors, Kerekes and Schell [60] and Huber et al. [45], for example, have reported that flocculated state of the measured suspensions correlated somehow with their crowding factors. In addition, since flocs are small coherent networks possessing measurable strength (at least to some extent), much of attention has been paid into the investigation of the yield stress of different suspensions.

Bennington et al. [8] performed extensive measurements for commercial wood fibre suspensions and synthetic fibre suspensions of low and medium consistency. They reported the yield stresses depending primarly on the local concentration of the suspension, but also fibre properties, such as aspect ratio and elastic modulus, was noticed to have an effect. The work was later extended by Dalpke and Kerekes, who proposed simple power-law type of correlations [16]. However, the most fundamental work is performed by Farnood et al. who presented an analytical equation describing the intra-floc forces [26] based on the model flocs. Farnood's model has the potential to model the internal strength of a floc, but since it is derived for a model floc having a form of "X-star", it unfortunately includes certain parameters that are not straightforwardly applicable to real flocs.

The numerical values for the three model parametres, namely, the break-up coefficient, the coalescence coefficient and the internal strength of a floc, were estimated by using a sensitivity analysis. In the gradient-based sensitivity analysis the model parameters were searched making a comparison between simulated and experimental average floc sizes (experiments were those performed by Salmela and Kataja [97]). First, the initial values for the model parameters were chosen, and the FFE model was solved using these specified values. Next, one of the parameters was varied a little, and the FFE model was solved again. This procedure was repeated for all the three parameters such that only one was modified at a time, while the others were kept constant.

An analysis was also required to formulate of a cost function to account for the goodness of the performed modification. Hence, the cost function was formulated such that it measured the difference between the simulated and measured average floc sizes at specified locations, and such that for a "perfect match" the value of the cost function would be zero. Next, the gradient of the cost function with respect to three model parameters was calculated by using the finite differences of the simulated cost function values. Finally, by advancing in the negative gradient direction with a chosen step length, better parameter values can be found. The procedure can be repeated until satisfactory model parameter values are found.

Since the saturation area is known to be very complex and at the same time important when predicting the flocculated state of the suspension, the measurement points at that area were given more weight in the cost function. The weighting of measurement points differently would, naturally, have provided slightly different values for the model parameters. In addition, it must be emphasised that if the parameters are strongly correlated, the gradient-based sensitivity analysis converges slowly and would require tens of iterations of the method. It is worth noticing

that one accurate CFD simulation of the FFE model in the turbulence generator pipe requires approximately 6 CPU hours, and hence, for one sensitivity analysis step, including three gradient component evaluations and at least two variations of the step length, would require at least $5 \times 6 = 30$ CPU hours.

Therefore, the algorithm was not repeated until the mathematically best possible fitting was found, but the final tuning was done manually. It was possible to see from the sensitivity analysis, that the break-up and coalescence coefficients settled around 15 to 25 and 5 to 10, respectively, for both of the tested pulps, but the internal strength of a floc depended on the pulp. The values giving the best fitting compared to the experimental results were 20 for the break-up coefficient and 7 for the coalescence coefficient. The values for the internal strength of a floc were 4 N/m and 1.46 N/m for pine and birch pulps, respectively. In comparison with the studies of Farnood [26] and Wahren [113] who obtained values of the order of 10^{-10} Nm for the stored energy per floc, the proposed values sound huge. In contrast, when comparing to results published by Bennington [8], Dalpke [16], Wikström [115] and their co-authors, the values 4 N/m and 1.46 N/m do not appear any unusual: for different pulps of 2 % mass concentration, they have all obtained yield stress values ranging from 10 to 180 Pa. Hence, the order of magnitude for the floc strength parameter is justified. In addition, it was found to fit with experimental data, as can be seen in the Section 5.2.2.

Once the parameters are adjusted in the turbulence generator pipe, the same values are applied also for other geometries for which no experimental data is available. Since the break-up and coalescence models take into account the accurately simulated local flow conditions and turbulence, it is assumed that there is no need for parameter tuning when studying different geometries. Naturally, due to the lack of experimental material, this has not been proven within this thesis. However, if it turns out that the model parameters have to be readjusted every time when the simulations are carried out for different geometries, then the whole break-up and coalescence model kernels should be revised. For further discussion, see Chapter 6.

Altogether, the flocculation is studied in three different geometries: in the turbulence generator pipe, in the slice channel and in the forming section. The details of the simulated geometries, as well as boundary conditions applied, are briefly introduced in Sections 4.2.2, 4.2.3 and 4.2.4.

4.2.1 On experimental reference material

The experiments used for validation of numerical results have been done earlier by Salmela and Kataja in the flow laboratory of VTT, and they are comprehensively reported in [97]. Part of the data set presented in this thesis is not fully included in [97], but has been considered in [38]. Hence, only a short description of methods used are given here. It is to be emphasised that the author of this thesis has not participated in experiments, but only used them as a reference for the model validation.

The flocculation has been measured downstream of a sudden backward facing step in 16 positions, and in one position upstream of the step. The diameter of

larger pipe was 26 mm and the diameter of the constriction 16 mm. The flow rates range between 0.5 l/s and 2.5 l/s.

The evolution of floc size has been measured optically using a back-light method. Typical image width was 30 mm and the height was the diameter of the pipe, i.e. 26 mm. Thus, the measured floc size is determined for this specified volume and it is an average over the whole pipe. Since the pipe is circular, vertically transmitted light integrates over smaller distance near the pipe walls than in the centre. Thus, the method may distort the data systematically depending on the radial position. Furthermore, the method cannot distinguish small overlapping flocs, but produces one large floc instead. However, the current experimental data is valuable for model validation as it can be assumed to be accurate enough, at least qualitatively, for the average floc size development in the axial direction. In addition, any other data including the floc size evolution was not available.

With regard to model validation, the data from simulations is taken in the same manner as in the experiments, i.e. averaging the floc size over 16 specified volumes. The FFE model would enable the investigation of the local floc size distribution, but unfortunately no data for such a comparison was available. Thus, in future work, this is an important issue to concentrate in.

4.2.2 FFE model in the turbulence generator

The turbulence generator pipe is modelled axisymmetrically in order to save the computational resources for accurate simulation of flocculation evolution. In addition, only the circular part of the pipe was considered, since the purpose in this simulation was to perform the model validation and adjust the required model parameters. Since the floc size distribution data was available only from 20 mm upstream of the expansion, the simulation is carried out in two steps; first, the flow and turbulence were solved in simple pipe having the same diameter as the first pipe in order to obtain appropriate inflow conditions. This was an obligatory step, because turbulence and velocity profiles had not been measured by Salmela and Kataja [97]. Second, the acquired profiles were given as an input to the actual model, as well as the floc size distribution provided by the experiments. The actual model consists of the 20 mm long constriction pipe and of the 1600 mm long expansion section, see Fig. 4.2.

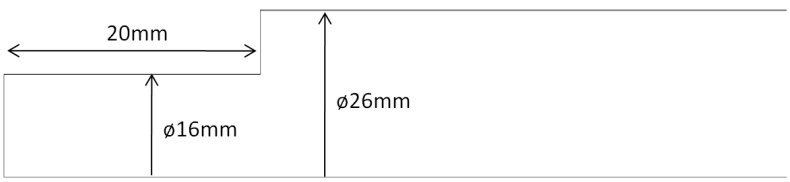

Figure 4.2: Axisymmetrical representation for the turbulence generator pipe used in model validation.

The effect of the number of size goups has been tested by performing the simulations with 5, 10 and 20 size groups. It was noticed that 10 and 20 size groups gave almost similar results everywhere, but 5 size groups was not enough to correctly predict the saturation area, see Fig. 4.3, and hence, 10 size groups was decided to use for all the simulations.

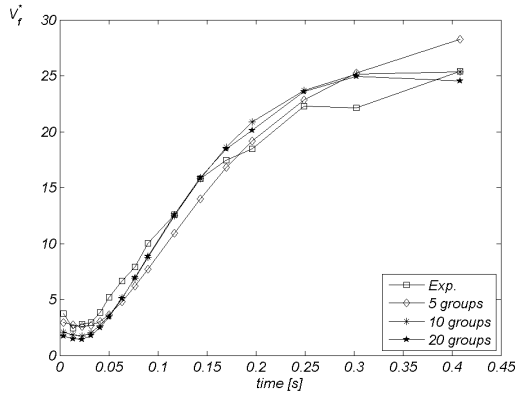

Figure 4.3: Comparison of the simulated dimensionless average floc volumes given by different number of size groups (5, 10 and 20) to the experimental results (experiments performed by Salmela and Kataja [97]).

4.2.3 FFE model in the slice channel

When the flocculation is studied in the slice channel, 60 mm wide model in the cross machine direction is used. The whole turbulence generator has not been modelled, but its effect on the CD-variation of the slice channel flow has been taken into account by modelling six inlets to the slice channel, see Fig. 4.4. The velocity profile of these inlets is assumed blunt, since it develops quite fast when entering in the channel. The floc size distribution is set based on the experience, but as will be demonstrated in Section 5.2.3, the FFE model posesses a "self-balancing" character, and hence, the minor deviances in the inlet boundary condition do not contort the solution. The slice channel is 600 mm long and includes two wedges (stiff, contracting lamellas), which end 120 mm before the slice opening.

The reliability of the carrying phase modelling has been assured (reported in [34]) by comparing the 3D simulations for the slice channel with the tailored slice channel model HOCS Fibre [36], which, in turn, has been validated with the pilot machine measurements in [35]. Both the MD velocity and pressure were measured by using a pitot tube along several CD lines inside the slice channel. It is also shown in [34], that both the HOCS Fibre and the 3D model used in this thesis, predict the CD velocities accurately enough. Hence, it can be assumed, that flow field simulations are accurate enough in order to give a reliable basis for the FFE

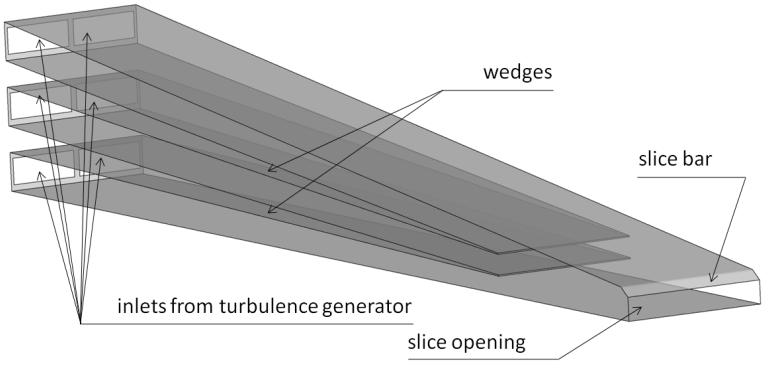

Figure 4.4: Slice channel with wedges.

modelling.

4.2.4 FFE model in the forming section

For the modelling of flocculation in the forming section, a 2D approach is used, since the system of equations for a three-phase flow including 10 conservation equations for different size groups would be extremely time consuming and challenging to solve in 3D. The forming is studied in the Fourdrinier-type of forming section including the free jet and the preceding slice channel with two wedges and the slice bar, see Fig. 4.5 for the overall view, and Fig. 4.6 for the detailed view. The fabric remains straight in the impingement area, i.e. the wire tension is assumed infinite. In other words, the wire is modelled as a flat moving wall the position of which is assumed known. In order to study the initial dewatering area, only the first 40 cm of the wire is included in the model.

The shape of the free jet, as well as the impingement of the jet, is not known *a-priori*, but they are solved with the free surface model. The flow is, therefore, modelled as a turbulent three-phase flow, including water, fibrous phase and the surrounding air. This approach reveals the natural physics of the phenomena, since any assumptions of the jet contraction after the slice opening or jet expansion after the impingement are not made. In several studies, [6] and [56], for example, the jet expansion has been neglected. Dalpke et al. [17] took the jet expansion into account, but in their simulation the flow was laminar and there were no concentration changes, since the suspension was modelled as pure water.

In the beginning of the slice channel the flow is assumed to have constant velocity and the floc size distribution has been set based on experience such as for the 3D slice channel. Outside the headbox, for the upper part of the air flow, the inlet boundary condition is set at constant velocity, and for the air inlet below the free jet, an opening condition with pressure level is used. This boundary condition lets the fluid flow in or out, and has, therefore, less effects to

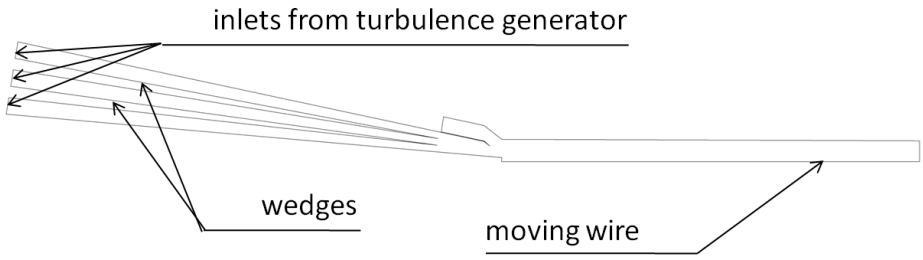

Figure 4.5: Geometry for the forming section simulation

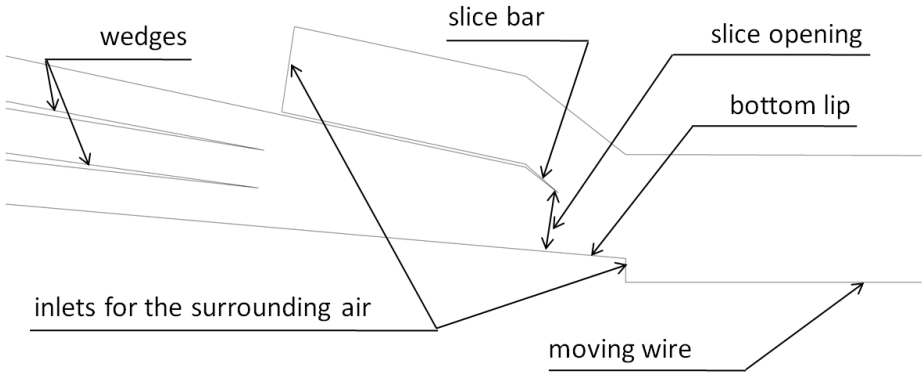

Figure 4.6: Detailed view of the slice opening area of the geometry for the forming section simulation

the overall flow conditions than other boundary condition types. This is the most convenient boundary condition type for the air below the jet, since it imitates the real conditions in the papermachine forming section. At the outlet of the domain there is naturally a pressure boundary condition, and the upper part of the surrounding air is restricted with a free slip wall.

The modelling of the moving wire requires special attention. The mass concentration of the suspension leaving the headbox is 1%, and during the dewatering the concentration increase is taken into account. The water removal and the solids pressure force have been programmed as add-ons in the commercial CFD code. The solids pressure force is present in all the domain, but it is activated only in areas where fibrous phase concentration approaches the maximum package, that is, in the water removal area. Further, in addition to the water removal, the moving wire must also be able to let the air pass through. This is accomplished by setting a similar sink term for air than for water, but naturally modifying the wire resistance such that a balanced solution is obtained.

The effect of the forming section on the floc size evolution is studied for three jet-to-wire ratios (J/W): J/W=0.9, J/W=1.0 and J/W=1.1, in order to demonstrate the effect of the shear on the development of the local floc size. The jet speed has been kept same for all the different simulations, 24 m/s, and the wire speed has been varied. The chosen jet-to-wire ratios give the wire velocity of ≈21.8 m/s for the drag mode (i.e. J/W=0.9) and ≈26.7 m/s for the rush mode (i.e. J/W=1.1). The computations are performed only for one web resistance, since the purpose of this work was not to study the dewatering phenomena in detail. In addition, the number of floc size groups is restricted to 10 also in this application, for keeping the needed computational resources reasonable.

Chapter 5

Numerical results and model validation

5.1 Fibre orientation in the slice channel and in the jet

5.1.1 On the representation of the FOPD results

When examining the numerical results, it is worth to keep in mind that the model is constructed in a way that the x-axis follows the centreline of the slice channel in MD. The position $x = 0$ lies at the slice opening, so the negative values of x situate inside the slice channel. The papermaker's z-direction is described with the vertical y-axis the origin being at the centreline (see Fig. 4.1).

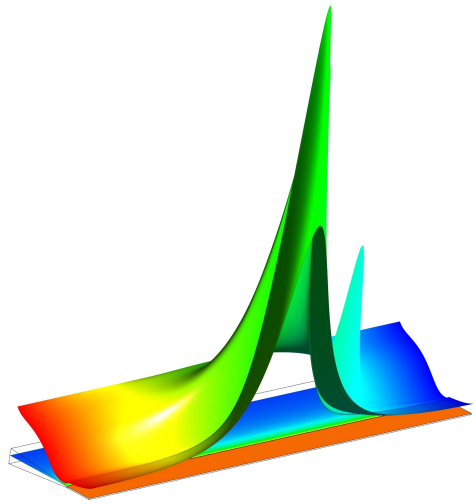

Figure 5.1: Visualisation of the orientation distribution 3 mm above the centre line throughout the slice channel and the jet.

The numerically solved FOPD model provides the whole probability distribution field. One example of a 2D field is presented in Fig. 5.1, which illustrates the orientation distribution 3 mm above the centre line throughout the slice channel and the jet. This kind of representation is not, nevertheless, very easy to interpret when printed out on a paper, and thus, the distributions are presented with customary graphs for different locations.

5.1.2 Development of fibre orientation in the slice channel and in the jet

At the beginning of the slice channel, $x = -500$ mm, the fibres are supposed to be isotropically oriented. Then, the acceleration of the flow starts to orient fibres in the main flow direction, which can be seen in Fig. 5.2, where the first three curves represent the situation inside the slice channel at the centreline. The fibres are most strongly oriented at the slice opening, $x = 0$ mm, but, in the jet ($x = 10$ mm, $x = 30$ mm, $x = 150$ mm), the orientation tends to randomize due to the absence of acceleration and shear forces. The results at the slice channel centreline agree well with the previous study reported in [85].

The change in the maximum probability peak along the centreline when the jet enters into free air can be seen even more clearly in Fig. 5.3. The peak decreases significantly during the first few centimetres, after which the role of convection in carrying the fibre orientation profile downstream in the jet can be seen. To the author's knowledge, the FOPD model has not been applied to the contracting jet before. Hyensjö had an extension after the slice channel imitating the jet, but it was not contracting [48]. Nevertheless, according to test performed with the same 1D solver that was used by Olson et al. [85], a 1D model presumes too slow dampening of the maximum value in the jet. This proves the importance of utilising the mathematically two-dimensional form of the FOPD model when desiring accurate results in the presence of strong velocity gradients.

To examine more closely what happens inside the slice channel, the fibre orientation distributions are illustrated at various vertical positions 150 mm upstream of the slice opening in Fig. 5.4. In the figure, the y-coordinate varies between -15 mm and 15 mm (y-15 and y15 in the graph) when the whole channel depth is from $y = -18$ mm to $y = 18$ mm, and y0 is in the middle. The orienting effect of the bottom and top walls can be seen clearly in Fig. 5.4. The peak is higher and the deviation narrower near the walls, that is, the fibres are more strongly oriented in the flow direction. Also, the fibres are not oriented in the paper plane direction (except at the centreline), but are shifted slightly due to the presence of the walls, which can be seen in the displacement of the distribution peak from zero. It is also noteworthy that the fibres in the region near the wall are inclined more than is the angle of the wall. This phenomenon has been reported already in the earlier study [49]. Since the geometry modelled and all boundary conditions are symmetrical, the numerical results are symmetrical too, as in Fig. 5.4. Therefore in the following figures, only the upper half of the slice channel is presented.

The jet contraction immediately after the slice opening affects the fibre orientation distribution strongly, as can be noticed in Fig. 5.5. (It is worth of noticing

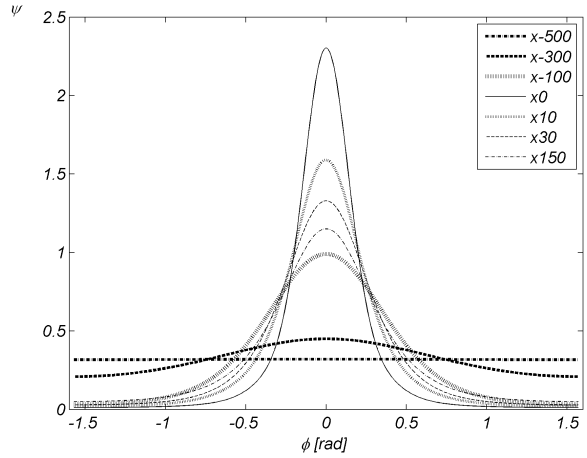

Figure 5.2: Development of the fibre orientation distribution along the centreline of the headbox slice channel and of the jet.

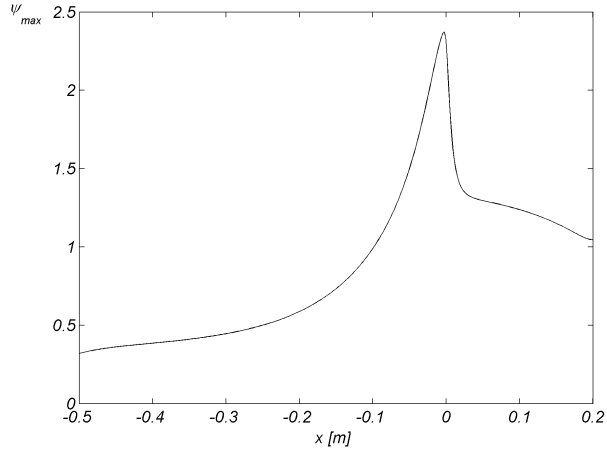

Figure 5.3: Development of the maximum value of the fibre orientation distribution along the centreline of the headbox slice channel and of the jet.

that the abscissa of the graph is different from the previous illustrations in order to be able to better examine the details.) As soon as the flow enters into free air, there are no solid walls restricting the flow direction, and the effects of friction and acceleration cease suddenly. The fibre orientation in the middle of the slice

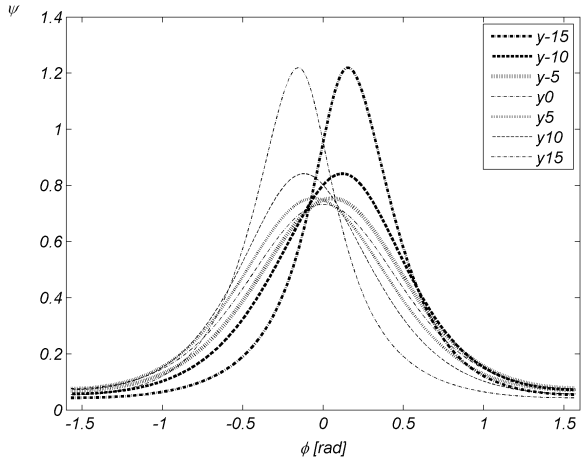

Figure 5.4: Fibre orientation distribution at various vertical positions inside the slice channel, 150 mm upstream of the slice opening.

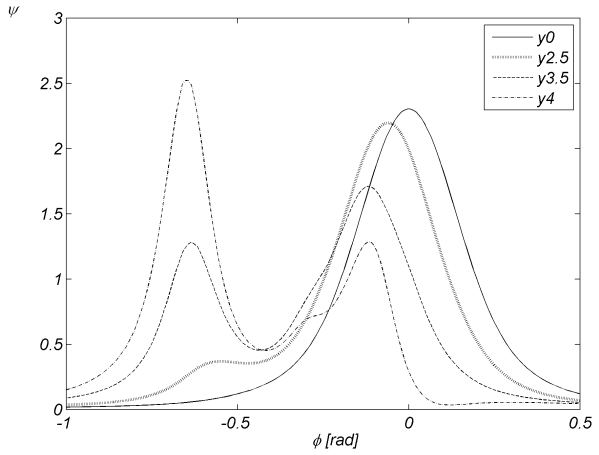

Figure 5.5: Fibre orientation distribution at various vertical positions at the slice opening.

opening is the customary Gaussian-like curve, but already 2.5 mm above the centreline there appears a secondary peak. When approaching the wall, the secondary peak increases while the main peak decreases such that, just near the wall, the secondary peak is notably higher than the main one. The main peak is due to

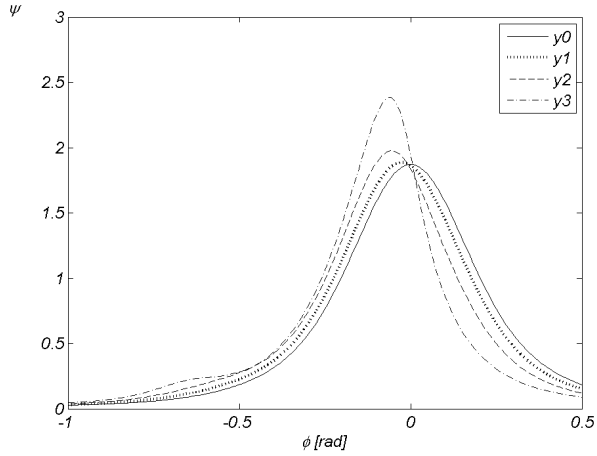

Figure 5.6: Fibre orientation distribution at various vertical positions 5 mm downstream of the slice opening.

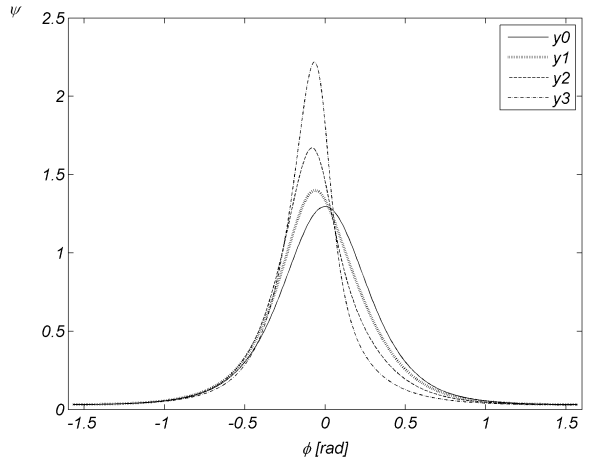

Figure 5.7: Fibre orientation distribution at various vertical positions in the headbox jet, 50 mm downstream of the slice opening.

the presence of the wall, such as inside the channel, whereas the secondary peak can be explained by the sudden contraction of the jet: the velocity gradients at the slice opening are steeper and therefore they orient the fibres more towards the centre of the jet than would be the effect of the wall only. Hence, at a narrow

area close to the slice lip, there are two almost equally probable orientation angles. This is the first demonstration of this kind of extraordinary phenomenon based on numerical simulations. The effect does not procede far in the jet; as a matter of fact, only 5 mm after of the slice opening it can barely be distinguished, as can be noticed in Fig. 5.6, and 10 mm downstream of the slice opening it has already faded out.

As stated before, fibre orientation tends to randomize in the slice jet. The orientation distribution changes rapidly from the strongly oriented towards the more random one during the first few centimetres. After that, it develops more slowly (shown in Fig. 5.3). To study the vertical variation of the fibre orientation distribution inside the jet, the distributions are illustrated in Fig. 5.7 at the position $x = 50$ mm downstream of the slice opening at the centreline ($y0$), 1 mm, 2 mm and 3 mm above it. It can be seen that fibres are more randomly oriented at the centreline than near the jet surfaces, so the effect of the slice channel walls and especially of the jet contraction is visible further in the jet, too.

5.2 Fibre flocculation inside the headbox

5.2.1 On the representation of the FFE results

The experimental data by Salmela and Kataja [97] used for the validation of the FFE model is presented with certain procedure, and therefore, it is wise to go through the methods before looking deeper to the results. Already in earlier studies of flocculation phenomena, Karema et al. [57] have mostly presented their results using the dimensionless floc volume:

$$V_f^* = \frac{< L_x >< L_y >^2}{l_f^3} \tag{5.1}$$

where l_f is the length-weighted mean fibre length, L_x and L_y are the length-weighted mean floc dimensions in flow direction and cross direction, respectively, and $<>$ denotes average over the image area and over the 200 exposures taken at each imaging position. Using the dimensionless floc volume is justified in certain occasions, since it facilitates the comparison of different pulps within a same graph, but on the other hand, this procedure conceals the physical phenomenon, because one cannot straightforwardly see the real floc sizes. As can be noticed in Fig. 5.8, for different pulps the same dimensionless volume (*top*) may signify remarkably different real floc volumes (*bottom*).

In addition, Karema et al. have presented the evolution of floc size as a function of mean residence time instead of the axial distance. This is a very suitable method, because it facilitates the comparison between different flow rates and enables the determination of accepted residence time, when designing a new turbulence generator, for example. The time $t = 0$ is set at the beginning of the sudden expansion and the spatial position is converted in temporal position using simply the mean flow velocity. However, when investigating a specified process in

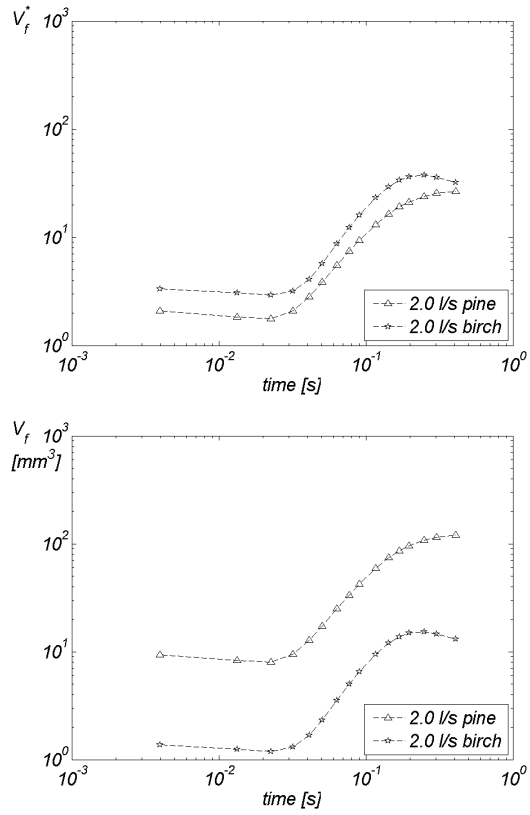

Figure 5.8: Comparison between the dimensionless (*top*) and real floc size (*bottom*) for two simulated data sets.

the wet end, it is also very informative to plot the data with the real dimensions, as done below for the results of slice channel and forming section.

Further, it has been a common procedure to illustrate the results using a logarithmic scale for both the abscissa and the ordinate. This might be quite misleading, as can be noticed when comparing Fig. 5.9 (*top*) to the Fig. 5.8 (*bottom*). A logarithmic scale may be useful in examining the gereral trends, as shown in next subsection, but when validating the CFD model, it accentuates too much the differencies within the small size groups and fades out the variations in bigger size groups. Further, when plotting the same situation using the floc diameter as an ordinate, one gets an illustration which is perhaps easier to connect to the flocculated state of the suspension or even to the resulting formation, see Fig. 5.9 (*bottom*). On the other hand, Fig. 5.9 (*top*) may be useful when turning the attention to the resulting local basis weight.

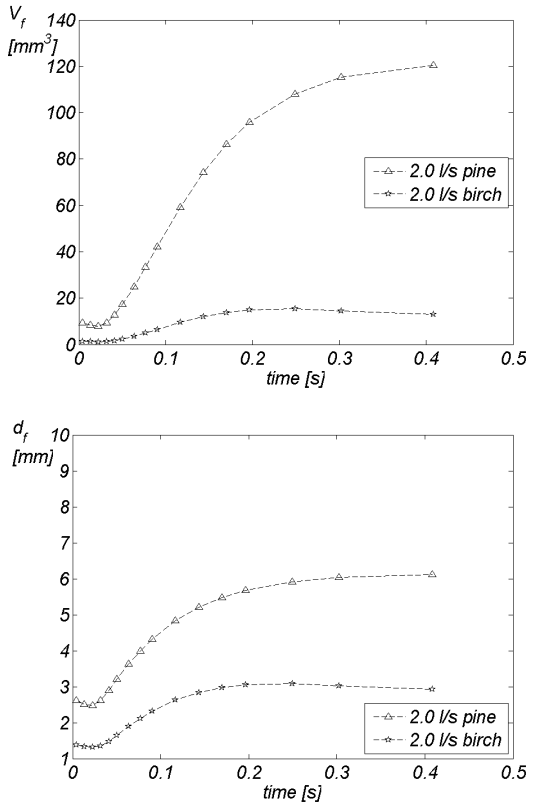

Figure 5.9: Comparison between the floc volume (*top*) and floc diameter (*bottom*) for two simulated data sets.

5.2.2 Model validation - flocculation in the turbulence generator pipe

Salmela and Kataja permormed a comprehensive set of experiments for the turbulence generator pipes [97], and their measurements are used for the model validation. The model parameters have assumed to depend on the flowing medium, but not on the geometry or flow rate, since the break-up and coalescence models already include the physics of the flow. Once the parameters have been determined in the turbulence generator pipe, the FFE model is used to investigate what happens to the floc size in the different parts of the headbox and in the forming section.

The model validation was carried out for three different flow rates: 1.5 l/s, 2.0 l/s and 2.5 l/s, and for two different pulps, pine and birch, presented in Table 4.1 in Section 4.2. The simulated flow rates correspond the average flow speeds of 2.8 m/s, 3.8 m/s and 4.7 m/s, respectively, in the turbulence generator pipe.

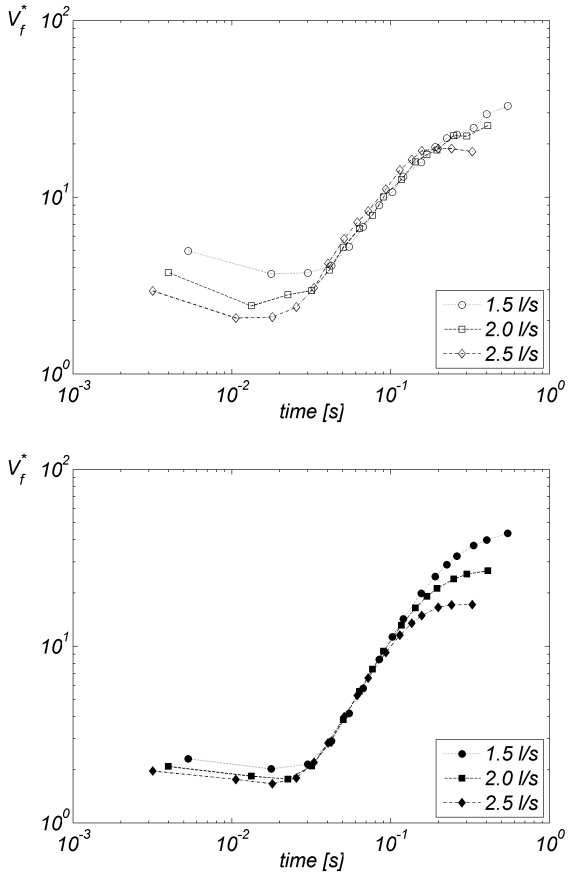

Figure 5.10: Measured (*top*) and simulated (*bottom*) floc size evolution of pine pulp as a function of the mean residence time for the flow rates of 1.5 l/s, 2.0 l/s and 2.5 l/s (experiments performed by Salmela and Kataja [97]).

In order to examine the general trends of the floc size evolution, it is useful to compare Fig. 5.10 (*top*) and (*bottom*), where the floc size evolution of pine pulp has been illustrated for the whole set of different flow rates for experimental and simulated results, respectively. Similar investigation is performed for birch pulp in Fig. 5.11. For the trend comparison, the logarithmic scale is useful. The simulated curves representing different flow rates overlap on the regrowth area, the minimum floc size being dependent on the flow rate. This is consistent with the experiments. Further, when reaching the saturation area, the simulated curves separate in a similar way as the measured ones, and hence, the general trends are well captured. In contrast, the minimum floc size appears to differ more than

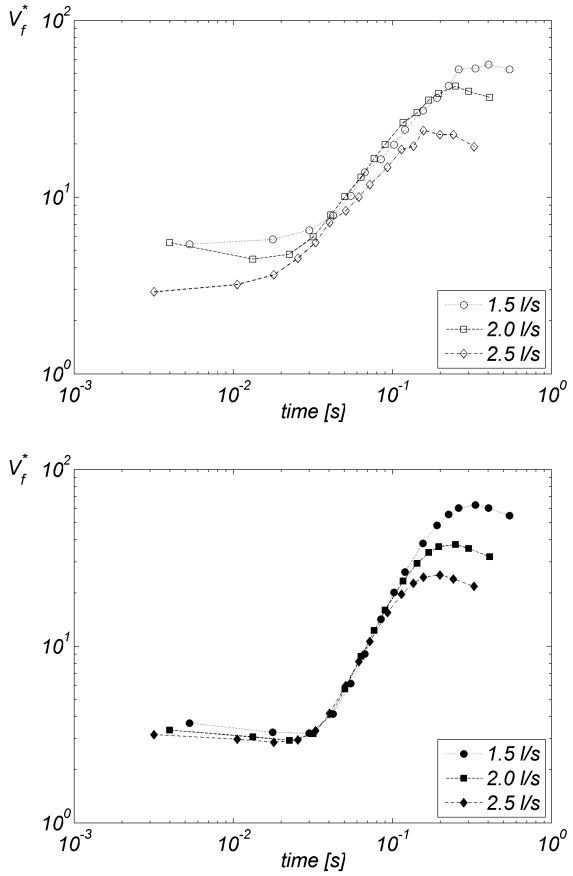

Figure 5.11: Measured (*top*) and simulated (*bottom*) floc size evolution of birch pulp as a function of the mean residence time for the flow rates of 1.5 l/s, 2.0 l/s and 2.5 l/s (experiments performed by Salmela and Kataja [97]).

other areas. The model seems too insensitive to predict correctly the effect of the increased turbulence and shear stress just after the expansion: the modelled curves differ only slightly from each other, while there are larger differences in the experimental ones. However, it has to be kept in mind that the logarithmic representation accentuates the differencies in small floc volumes, and as can be seen below in Figs. 5.12 and 5.13, the model predictions are not that inaccurate at all.

Next, it is worth to take a closer look and compare the simulated pine pulp results to experimental ones flow rate by flow rate; see Fig. 5.12, where "Exp." refers to experimental data and "CFD" to simulations. It can be noticed that the shapes

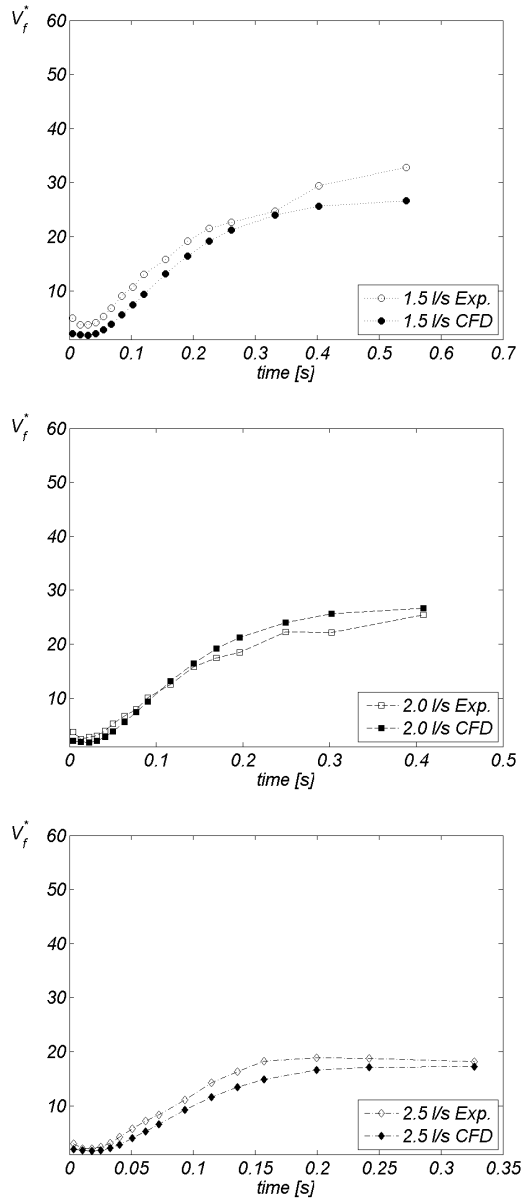

Figure 5.12: Simulated and measured floc size evolution of pine pulp as a function of the mean residence time for the flow rate of 1.5 l/s.(*top*), 2.0 l/s (*middle*) and 2.5 l/s (*bottom*) (experiments by Salmela and Kataja [97]).

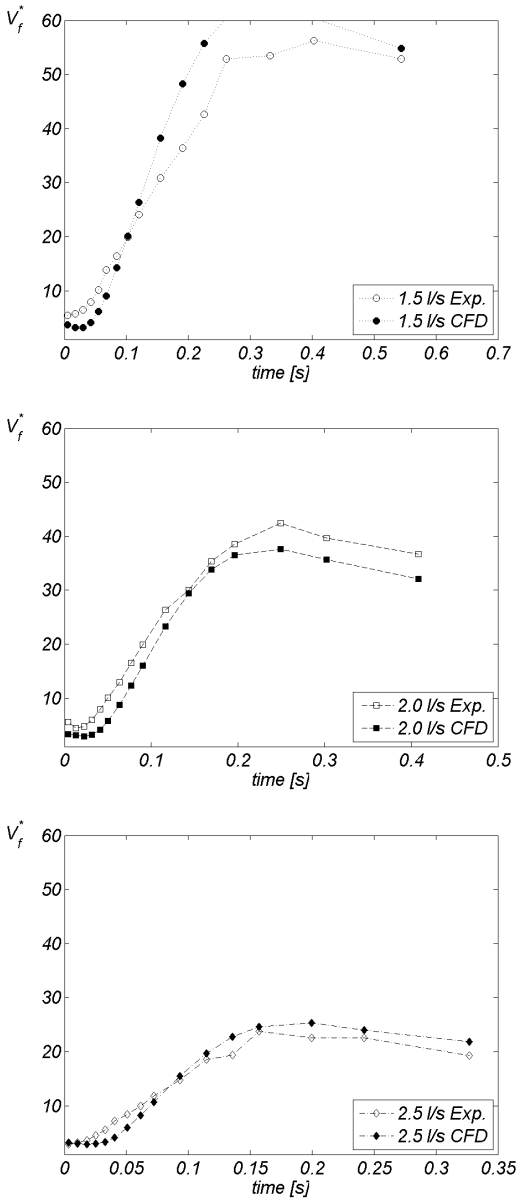

Figure 5.13: Simulated and measured floc size evolution of birch pulp as a function of the mean residence time for the flow rate of 1.5 l/s.(*top*), 2.0 l/s (*middle*) and 2.5 l/s (*bottom*) (experiments by Salmela and Kataja [97]).

of the simulated curves are similar to the experimental ones, which means that the general behaviour of both the floc break-up and the coalescence phenomena are well captured. The model slightly underestimates the minimum floc size occurring immediately after the sudden expansion, especially for the lowest flow rate. In contrast, the further growth of flocs is well predicted, the deviation between the simulated and experimental results being only about 10 % for the two highest flow rates. This result is of great value; this is the first occasion where fibre flocculation has been predicted quantitatively (and even with the acceptable accuracy), while previous researches have provided only some approximative information of the flocculation phenomenon, such as flocculation index or flocculation tendency. The new model has also demonstrated its suitability for the saturation area, which is known to be very complex. In fact, the percentual errors at the named area are smaller than in any other location, less than 10 % for two highest flow rates. Given that the saturation phenomenon is the most difficult from the modelling point of view, the results can be considered quite impressive.

As mentioned earlier in Section 4.2, the internal floc strength for the birch pulp was found to be 1.46 N/m, while the value for pine was 4 N/m. Hence, the relation between the internal floc strengths of the pine and the birch pulps is $\sim$ 2.7. This was found to be exactly the same as the relation between the crowding factors of the two named pulps:

$$\frac{N_{mf,pine}}{N_{mf,birch}} = \frac{\sigma_{pine}}{\sigma_{birch}} \tag{5.2}$$

where N_{mf} stands for the crowding factor and σ for the internal strength. To the author's knowledge, this is the first demonstration of this kind of dependency between floc strength and crowding factor. The finding is supported by the results of Huber et al. [45]; they reported the effect of the crowding factor and flow speed on the flocculation index, and proposed a simple correlation model based on experimental data. Also Kerekes and Schell [60] have reported that flocculated state of the measured suspensions correlated somehow with their crowding factors, as already mentioned.

As can be seen in Fig. 5.13, the beginning of the regrowth area is not as well predicted for birch as it is for pine. The slope of the simulated curve is steeper, and the simulations also predict that coalescence occurs later than in measurements. However, at the end of the regrowth, as well as in the saturation area, the agreement between simulations and experiments is very good. The reason, why the simulations of the birch pulp in the regrowth area do not agree with measurements as well as pine, might be that the mentioned pulps are in different regimes. Consequently, their flocculation may occur differently, and the model parameters should be adjusted in order to take this behaviour into account. However, the FFE model works acceptably for both of the pulps used in the simulations, and hence, the presented parameter values are used for all the other geometries.

5.2.3 Flocculation in the turbulence generator

The available experimental data provides information only about the evolution of the dimensionless mean floc size, but with CFD simulations many other intresting aspects can be studied. Although all the presented phenomena might not be absolutely correctly predicted, they give, nevertheless, relevant information of the local phenomena and can be used to determine, wheather the simulation is reliable or not. Therefore, some intresting findings are presented and discussed below. When investigating the countour plots, it is worth to keep in mind that the simulations are performed axisymmetrically, and hence, only the half of the pipe is presented.

The evolution of the different size groups can be examined by representing the size fractions as a function of the residence time, see Fig. 5.14. The data is taken in the same manner as for the model validation and for the experiment, that is, averaging over a volume covering the whole pipe diameter and having the length of 30 mm in the flow direction. It can be observed that immediately after the expansion, the number of the smallest flocs (group 1) is very high and there are practically no large flocs. However, the coalescence process starts to dominate very shortly, and hence, the number of the smallest flocs drops dramatically, while the amount of the medium size flocs starts to increase. The size fraction of the biggest flocs begins to grow later. This indicates that the coalescence phenomenon occurs sequentially; first, small flocs agglomerate together to form medium size flocs, which, in turn, coalesce into larger flocs.

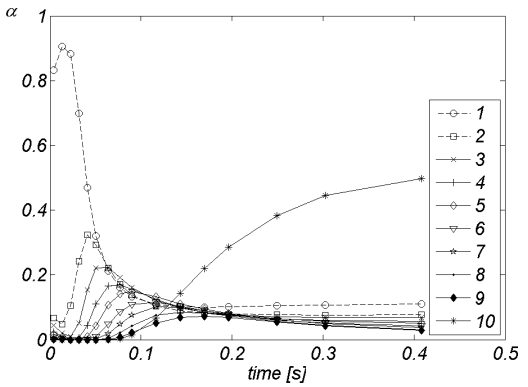

Figure 5.14: Simulated evolution of the different size groups of the pine pulp as a function of the mean residence time for the flow rate of 2.0 l/s.

The Fig. 5.14 reveals that there is a remarkable difference in the volume fractions of two smallest size groups in the beginning of the expansion, and the similar effect can be seen at the end of the pipe between two largest size groups. This indicates that higher number of size groups would be needed to more accurately predict the size group distribution. However, as seen in Fig. 4.3 in Section 4.2,

the increase of size groups did not affect the mean floc size. As a consequence, the chosen number of size groups is justified, until more accurate experimental data on different floc sizes for the model validation is available.

Since the FFE is a real two-fluid model, one can also examine such phenomena and flow characteristics which would remain completely unknown with one-phase approach. Fig. 5.16 illustrates the variations in the local concentration of the fibrous phase right after the expansion. It can be noticed that the FFE correctly predicts that there are practically no fibres in the backflow eddy. In addition, the mean floc diameter, for example, can be studied elaborately in different positions. The local mean floc size right after the sudden expansion is presented in Fig. 5.17. The flocs are clearly smaller near the pipe wall region than in the middle. This is caused by turbulence, which occurs due to the expansion, as can be seen in Fig. 5.18. The floc size decreases quickly right after the sudden expansion as the break-up forces dominate. It is worth to keep in mind that in the area presented in Figs. 5.16...5.18 the reflocculation has not been started yet.

One interesting finding is also the "self-balancing" effect of the FFE model. A pipe geometry with different contraction diameter was modelled, and since any experimental data for fibre floc size distribution at the inlet was not available, two different distributions were tested. One distribution was chosen to represent the situation where there would be plenty of small flocs and the other distribution was weighted for the medium-sized flocs. The distributions are given in Table 5.1. As can be seen in Fig. 5.15, the mean floc size curves differ only in the very beginning of the pipe expansion. This means that the mechanisms of the phenomena "take care" that the floc size evolution is strongly controlled by the local flow field and turbulence. Therefore, it enables the simulation of such geometries for which the experimental data does not exist, since even though the initial guess for the inlet boundary condition would be somewhat wrong, the model still predicts correctly the floc size evolution.

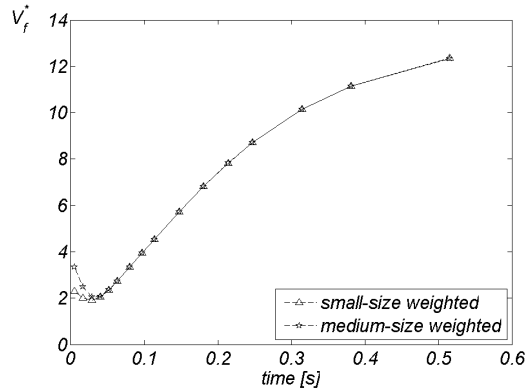

Figure 5.15: Selfbalancing character of FFE model.

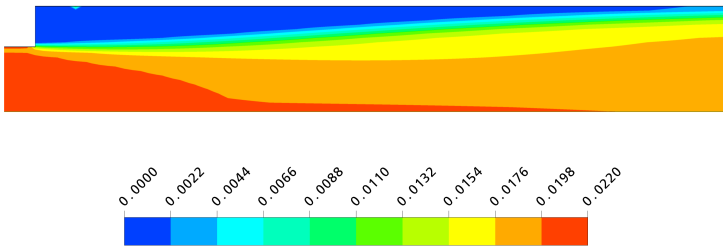

Figure 5.16: Simulated volume fraction of fibrous phase after the sudden pipe expansion. The height of the step is 5 mm.

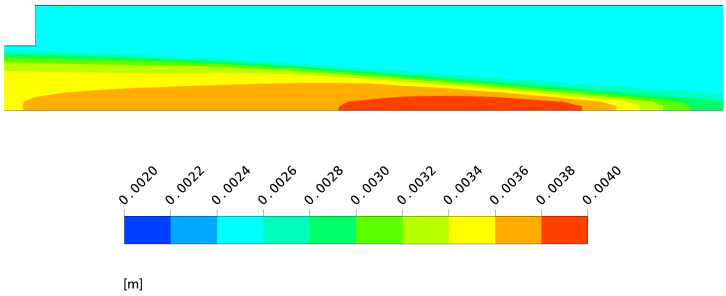

Figure 5.17: Simulated mean floc diameter after the sudden pipe expansion.

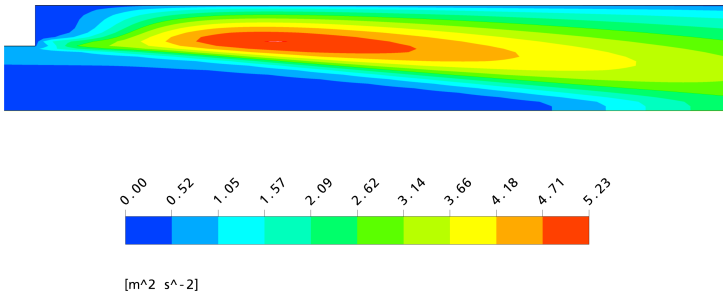

Figure 5.18: Simulated turbulent kinetic energy after the sudden pipe expansion.

Table 5.1: Volume fractions of two different fibre floc size distributions for the self-balancing test.

Size group number	Small-size weighted	Medium-size weighted
1	0.3	0.03
2	0.2	0.05
3	0.15	0.1
4	0.1	0.15
5	0.1	0.3
6	0.05	0.2
7	0.05	0.1
8	0.03	0.05
9	0.02	0.02
10	0	0

5.2.4 Flocculation in the slice channel

The floc size evolution in the slice channel is an intresting subject to investigate, since in modern headboxes, the design of the slice channel has recieved a lot of attention. Unfortunately, no experimental data for comparison is available. Nevertheless, the fibre floc size seems to behave quite reasonably, as can be seen in Fig. 5.19, where the mean floc size is plotted along the line going through the slice channel in MD. (The line is situated in the middle of the two wedges in z-direction and in the middle of the outlet of turbulence generator pipe in CD-direction.) When entering into the slice channel, the mean floc diameter is about 3 mm, but near the slice opening the small flocs have coalesced and formed bigger ones. It is worth of pointing out that the graphs in Figs. 5.19 and 5.20 are not plotted till the end of the slice channel, since the examination of a single line would provide misleading results: In Fig. 5.26 it can be noticed that floc size evolution follows streamlines, and hence, a straight line would present results the interpretation of which would be somewhat difficult.

Investigation of evolution of the different size groups in Fig. 5.20 reveals that contrary to the situation in the turbulence generator pipe expansion in Fig. 5.14, ten size groups is sufficient to reliably predict the floc size distribution in the slice channel, since the differencies in the volume fraction between two smallest and two largest size groups are relatively small. Flocs of all sizes start to coalesce right after the beginning of the slice channel, but the process remains quite calm, and the overall floc size grows relatively slowly. This is due to flow velocity, which is kept quite high with the wedges, and naturally the shear induced by walls that breaks up the flocs. The simulated floc size development in the slice channel is congruent with the "real-life" findings. Also, the recent headbox development is focusing in avoiding the re-flocculation by minimizing the suspension residence

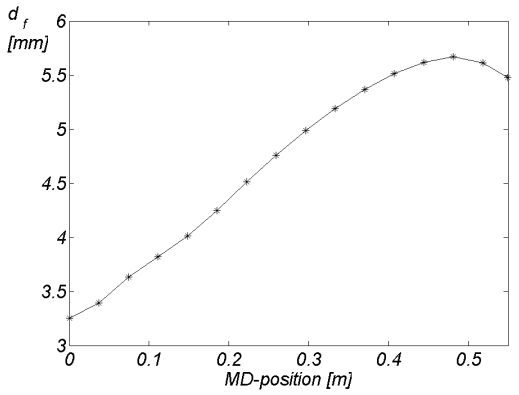

Figure 5.19: The evolution of the mean floc diameter inside the slice channel, along the line at the middle of the turbulence generator pipe.

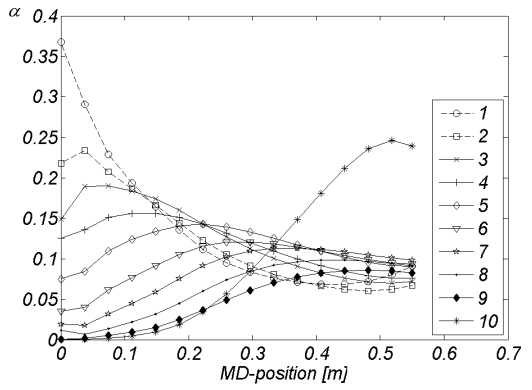

Figure 5.20: The evolution of different floc size groups inside the slice channel, along the line at the middle of the turbulence generator pipe.

time from the turbulence generator to the forming zone, and also by using wegdes instead of lamellae.

The overall development of the flocculated state of the suspension can be studied with Figs. 5.21 and 5.22 where the local mean floc size and the local velocity, respectively, are presented at the centre plane between two wedges. The mean floc size is not even in the cross machine direction, since there is velocity and turbulence profile due to the turbulence generator, which was modelled by 2x3 tube entries. The effect of turbulence generator proceeds far downstream and remains visible at the slice opening as well. The floc size near the slice opening may by

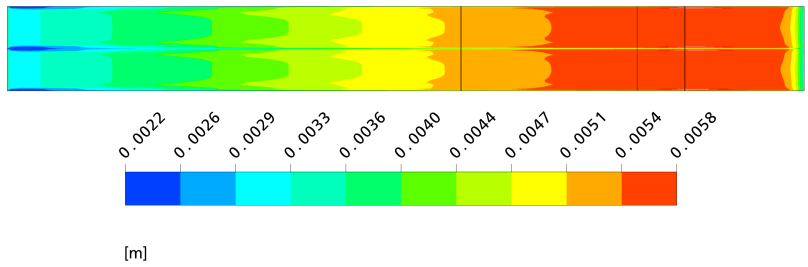

Figure 5.21: The local mean floc diameter inside the slice channel at the centre plane between two wedges.

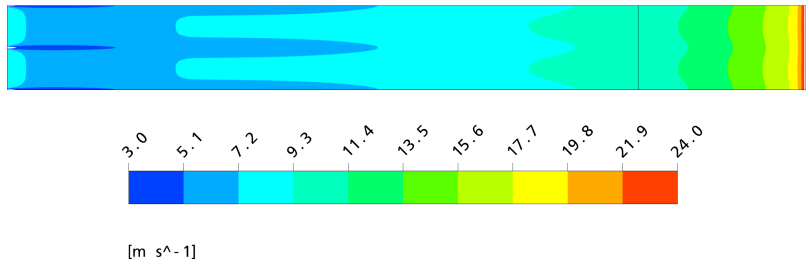

Figure 5.22: The local velocity profile inside the slice channel at the centre plane between two wedges.

slightly mispredicted due to the vicinity of the outlet boundary, but still it can be concluded that strong velocity gradients and turbulence created by the slice lip reduce the mean floc size significantly at the end of the slice channel.

One extraordinary detail is the prediction that the floc size would remain significantly smaller in the middle of the figure, at the wake of turbulence generator pipe walls. (Same effect occurs also at the top and bottom of the figure, where symmetric boundary conditions are applied, even though it is not very clearly visible.) This effect can be closer examined with the Fig. 5.23, which represents the detailed view of the slice channel. (The black lines in Fig. 5.21 indicate the location of the detailed view.) Smaller mean floc size cannot directly be explained by any single property of the flow field, but it must be somehow connected to turbulence and strong velocity gradients occuring in the wake. The turbulence kinetic energy is presented in Fig. 5.24 for the comparison.

It is also intresting to examine the mean floc size evolution between the wedges. It can be seen in Fig. 5.25 that floc size is smaller near the walls, which is naturally, caused by the shear layer near the wall. The distance between the wedges is not

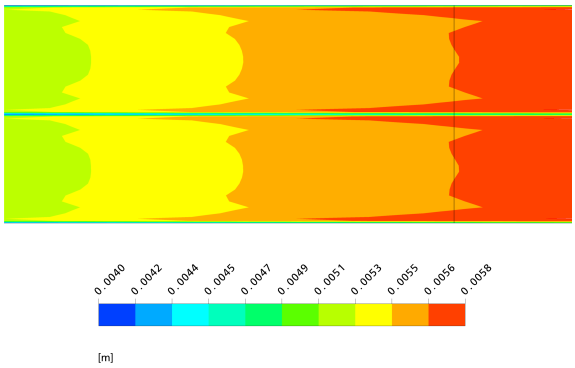

Figure 5.23: Detailed view of the local mean floc diameter inside the slice channel at the centre plane of turbulence generator pipe.

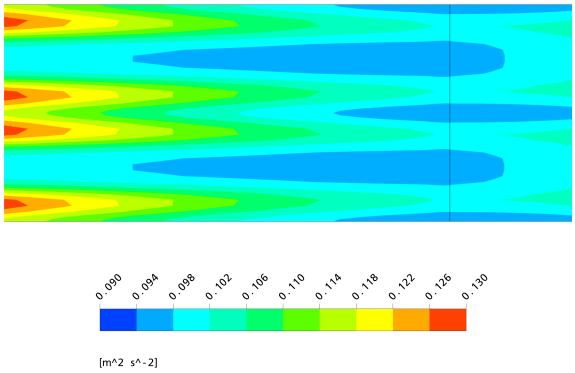

Figure 5.24: Detailed view of the turbulent kinetic energy inside the slice channel at the centre plane of turbulence generator pipe.

exatly the same, which causes the differencies in the countour: the floc size is big at larger area in the middle gap than in the top and the bottom gaps. Also the effect of the slice bar is visible in the upstream, which can be concluded in the asymmetry of the contour of the middle gap, see Fig. 5.26. The end of the wedges is 0.5 mm thick, and obviously, no deattachment of the flow occurs, since the mean floc size profile remains stable.

As mentioned earlier in the Section 3.5, it is still a matter of debate, which mechanism breaks up the flocs. Some researchers claim that it is the elongation, while the others say it is turbulence. In the slice channel there is a continuous acceleration of the flow, i.e. elongation, but as seen with the results presented

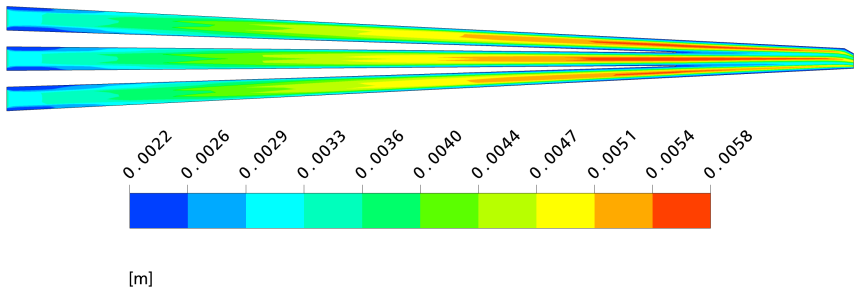

Figure 5.25: The local mean floc diameter inside the slice channel at the centre plane of turbulence generator pipe.

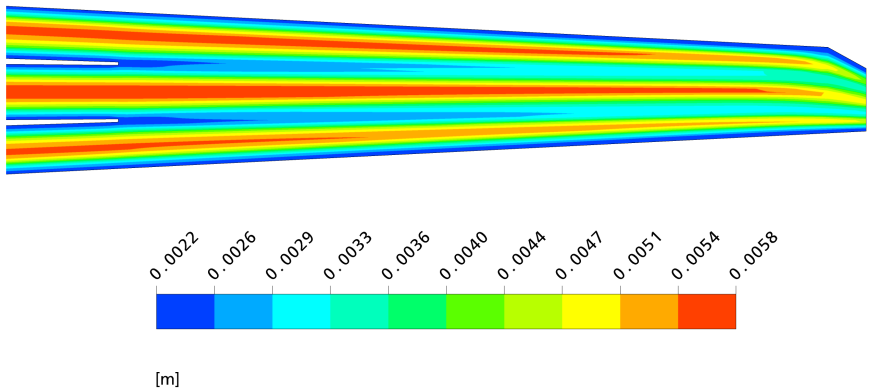

Figure 5.26: The local mean floc diameter inside the slice channel at the centre plane of turbulence generator pipe; the detail at the end of the channel.

above, the floc size is not decreasing, but increasing in the slice channel. This is consistent with the experimental findings of Karema et al. [57] presented also by Hyensjö [47]. Karema et al. pointed out that the floc size, in fact, increases also in the slice channel, although there are strong elongation forces present. Comparing the FFE model predictions to their experiments it can be concluded that the FFE model predicts correctly the floc size evolution in the slice channel at least qualitatively. This example shows that the model is applicable for different geometries without any parameter tuning.

5.3 Fibre flocculation in the forming section

Since there is no experimental data available for the validation of the floc size evolution in the forming section, it is worth to start to examine the results by looking the flow field in detail in order to ensure that the simulation of the complex flow field is adequately performed. The complicated phenomena of the flow field determine the flocculation process, and therefore, the reliability of the flow field modelling is one of the key issues.

In Fig. 5.27 it can be seen, how the velocity profile of water develops downstream of the wedges (far left in the illustration). The slice bar modifies the flow profile by inducing a low velocity area at the top of the channel just before the end, and accelerates the upper part of the jet faster than the rest of the jet. It is also worth of noticing that the velocity profile created by wedges is present in the jet after the *vena-contracta*, as well. The jet contraction coefficient predicted by simulations is ≈0.83, which is very typical value for this kind of construction.

The most critical area from the modelling point of view is the jet impingement on the moving wire. At the location where the jet hits the wire, an abrupt decrease in flow speed occurs above the fabric, and the jet expansion can be noticed when looking carefully the upper surface of the jet. This gives rise to a momentary decrease in the whole jet speed at this position, and it occurs for all jet-to-wire ratios as will be shown below. However, very quickly the speed of the jet increases again, but the streaks in the velocity profile are not present any more. The development of the velocity profiles at the impingement area gives valuable information of the flow phenomena, and hence it is worth to look at them more closely.

The velocity profiles over the whole thickness of the jet are presented in Fig. 5.28 for the J/W=1.0, and thus, both the jet and wire velocity were 24 m/s. The jet hits the wire ≈27 mm after the bottom lip, where $x = 0$, and the first velocity profile in the illustration (denoted with $x30$) is then right after the impingement. (The positions $x30$, $x50$, $x70$, $x100$, $x150$, $x200$, $x250$ and $x300$ in following illustrations refer to distance from the bottom lip in millimeters.) The strong decrease in the flow speed presented in Fig. 5.27, can also be seen when looking at the curve of $x30$ in Fig. 5.28: at the wire surface the water flows naturally at the wire speed, but right above, it has remarkably lower velocity due to the impact caused by the impingement. Also the overall speed is less than 24 m/s at the impingement zone, but the profile starts to develop quite quickly, as seen with curves $x50$ and $x70$, for example. When looking carefully the upper ends of the curves at different positions, it can also be noticed that the jet thickess is decreasing when suspension is moving downstream in the forming section. This is, naturally, due to the water removal.

When comparing the velocity profiles for three different jet-to-wire ratios, J/W=0.9, J/W=1.0 and J/W=1.1, (Fig. 5.29) it can be noticed that the phenomena at the impingement area are very similar and independent of the speed difference between the jet and the wire. For all the three simulations the flow velocity right above the wire is ≈18 m/s, and thus, only the velocity gradient at the impingement is higher, if the wire speed is higher. Also the profiles of tur-

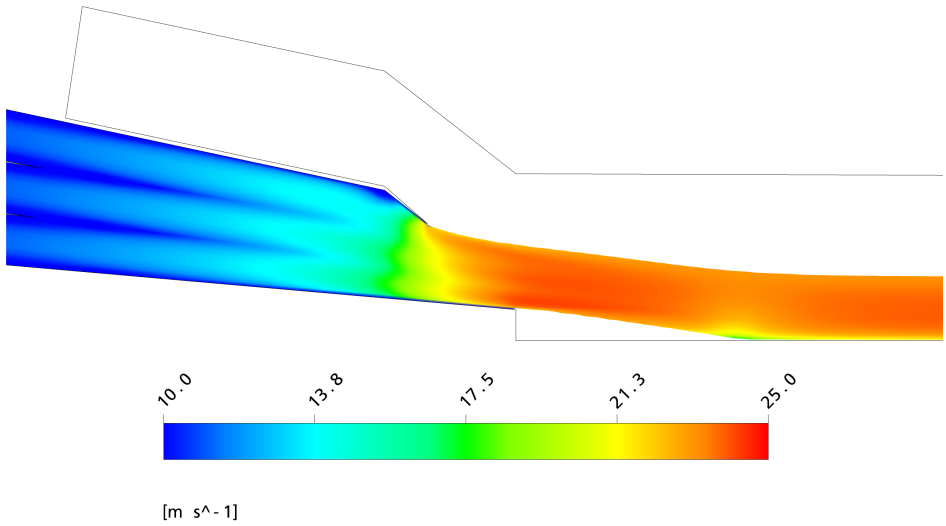

Figure 5.27: The impingement of the jet for J/W=1.0. The color represents the speed of the water.

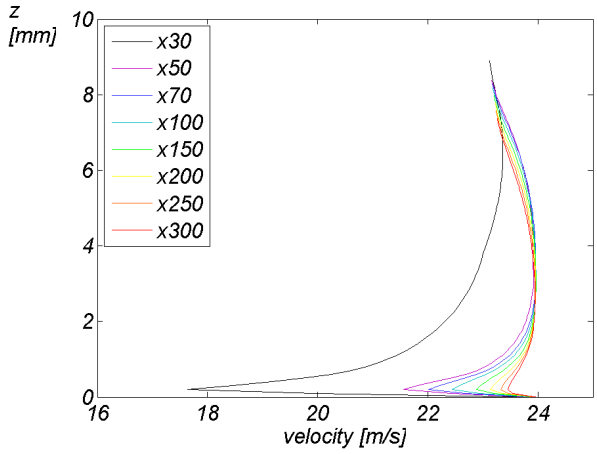

Figure 5.28: Water velocity profiles above the wire surface at 8 different MD positions for J/W=1.0. $x30$ denotes the MD location 30 mm downstream of the bottom lip, etc.

bulent kinetic energy (Fig. 5.30) attest that the jet impingement dominates the situation in the beginning, since the kinetic energy at $x30$ is very similar in all the illustrations, and hence, independent on the jet-to-wire ratio. A closer look into the turbulent kinetic energy profiles reveals that they are very similar for the J/W=1.0 and J/W=1.1, while J/W=0.9 differs from them significantly. Also, the velocity profiles indicate that for the drag mode there is a remarkable shear above the moving wire from the beginning of the forming section, while for the rush mode the drag forces do not to become important until the position $x150$.

The two-fluid simulation enables the inspection of the flow field separately for both of the phases. The Fig. 5.31 reveals that the velocity profiles of the floc phase are not as smooth as those of water, but the speed differences induced by the wedges in the slice channel are still present in the forming section. In addition, the decrease of velocity is not as dramatical for flocs as it is for water: when the flow velocity right above the wire is ≈20 m/s for flocs, for water it was only ≈18 m/s. Moreover, for the floc phase it takes longer to be accelerated again at the velocity of the free jet: the overall velocity does not reach 24 m/s until $x150$ for J/W=0.9 and J/W=1.0. These events are probably due to the bigger viscosity of the floc phase.

Since the purpose of this work is not to study the dewatering phenomena in detail, computations were performed only for one web resistance. Hence, the dewatering is similar for all three jet-to-wire ratios, since the water removal depends on pressure, which does not change, when the wire velocity is modified. As can be seen in Fig. 5.32, the dewatering is very strong at the location, where the free jet impinges the moving wire, which is ≈27 mm downstream of the bottom lip ($x = 0$ at the end of the bottom lip). Downstream of this point the dewatering is rather gentle, and it remains quite stable at the initial dewatering zone. The pressure field at the beginning of the forming section is illustrated in Fig. 5.34, where the scale is chosen such that the phenomena at the impingement zone are clearly visible, and hence, the white areas have the pressure level higher than the scale can represent. When the suspension enters in the surrounding air, the pressure level inside the jet drops significantly. It is also worth noticing that the pressure decreases faster at the top surface of the jet. The pressure level is lowest at the *vena-contracta* and it increases dramatically at the proximity of the impingement zone. The increase of the pressure covers practically whole the jet thickness. Very soon after the hitting point, the pressure decreases at the level where it was before the impingement, and this explains the high but narrow peak in the dewatering, presented in Fig. 5.32.

When examining the Fig. 5.33, it can be noticed that the floc size at the wire surface is at its minimum level at the impingement zone. The floc size is same for all the jet-to-wire ratios, which is very probable, since the dominating effect at the impingement is the sudden change in flow conditions, not the wire speed. In addition, the simulations predict that the local floc size increases at the beginning of the dewatering zone very similarly for all three jet-to-wire ratios. After the jet has "calmed down" the shear and turbulence start to decrease the floc size on the wire again, and this occurs fastest in the drag mode. This is most likely due

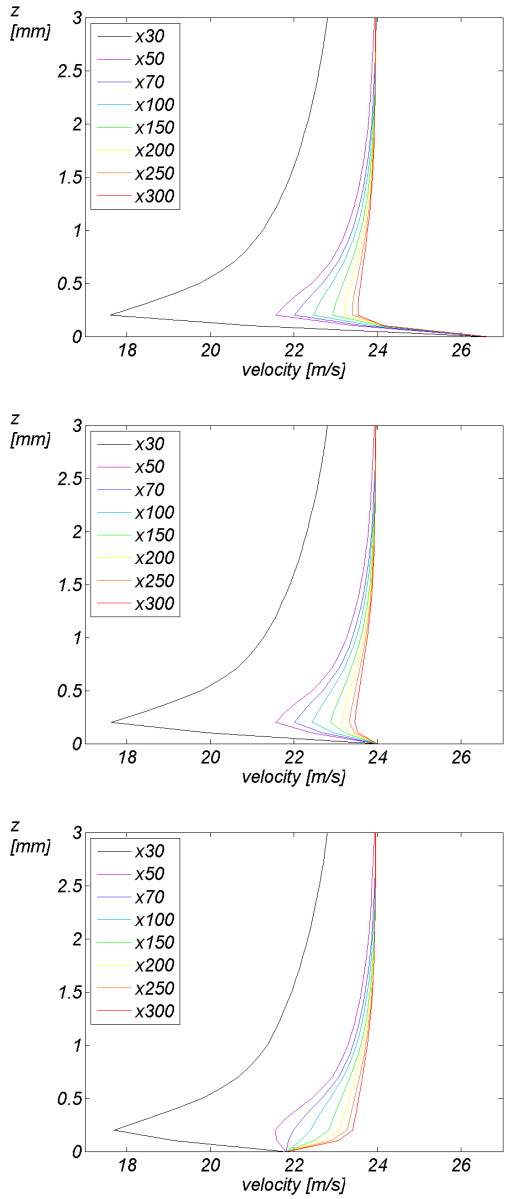

Figure 5.29: Water velocity profiles above the wire surface at 8 different MD positions for three different jet-to-wire ratios; J/W=0.9 (*top*), J/W=1.0 (*middle*) and J/W=1.1 (*bottom*).

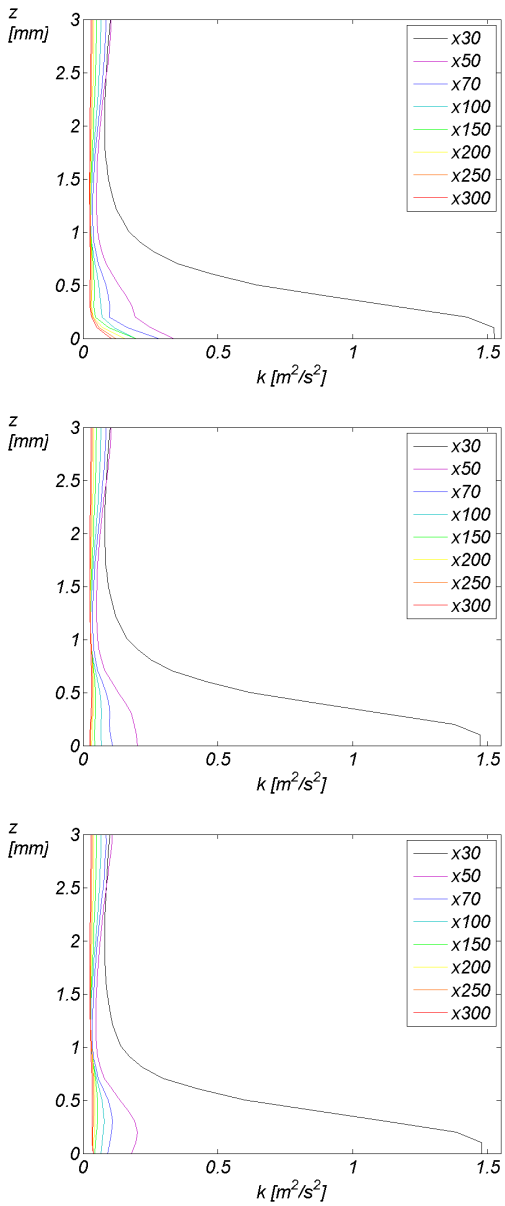

Figure 5.30: Turbulent kinetic energy profiles above the wire surface at 8 different MD positions for three different jet-to-wire ratios; J/W=0.9 (*top*), J/W=1.0 (*middle*) and J/W=1.1 (*bottom*).

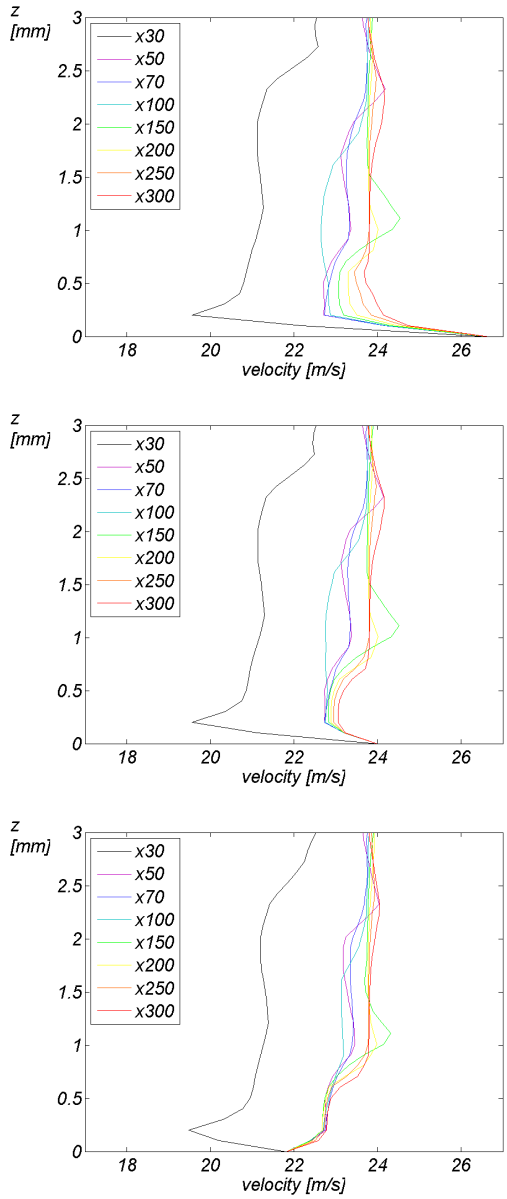

Figure 5.31: Floc phase velocity profiles above the wire surface at 8 different MD positions for three different jet-to-wire ratios; J/W=0.9 (*top*), J/W=1.0 (*middle*) and J/W=1.1 (*bottom*).

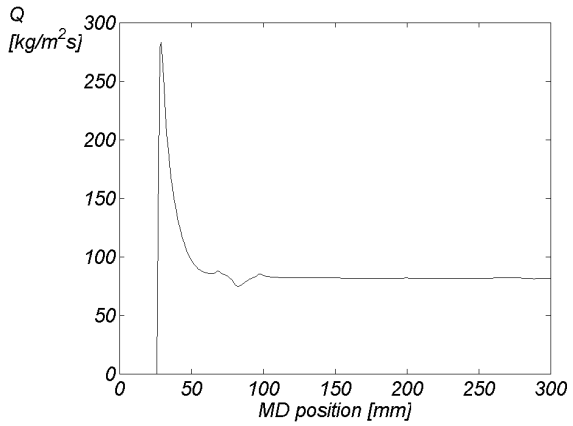

Figure 5.32: The initial dewatering occuring on the wire surface.

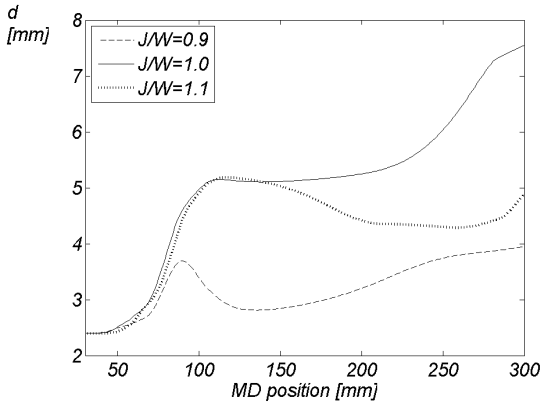

Figure 5.33: The mean floc diameter on the wire surface for three different jet-to-wire ratios.

to the higher turbulent kinetic energy and higher shear. In Fig. 5.33 it can be seen that for the rush mode, the floc size on wire does not turn down before the position $x150$ where the shear becomes important. However, the floc size does not diminish significantly, but rather stays at the same level. For J/W=1.0 the floc size increases continuously, since after the impingement there are no shear forces or increase in the turbulent kinetic energy to break up the flocs. Further in the downstream, i.e. at $x250$, the predicted floc size for J/W=1.0 seems somewhat too big compared to the jet thickness. However, the model still correctly predicts the fact that drag and rush modes are more efficient in the floc break up.

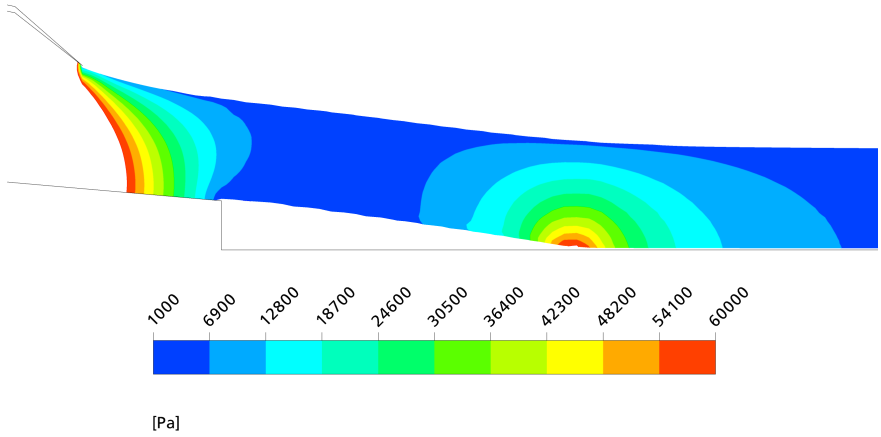

Figure 5.34: The impingement of the jet. The color represents the static pressure.

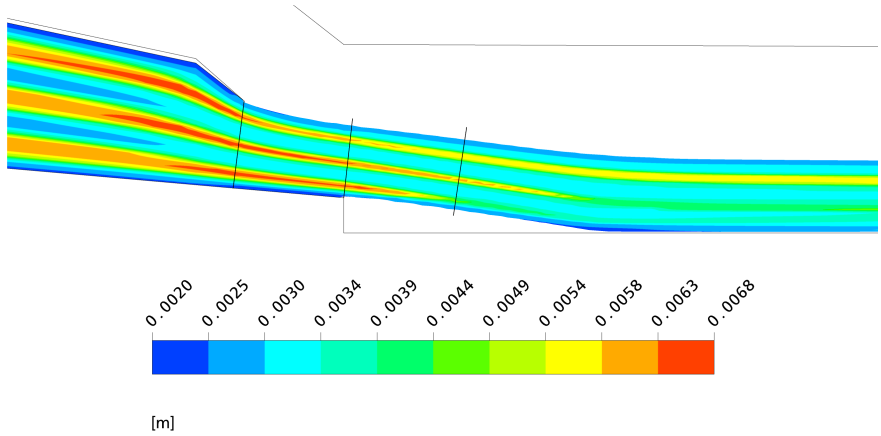

Figure 5.35: The mean floc diameter inside the slice channel, in the free jet and in the forming section, J/W=1.0.

The Fig. 5.33 gives only the information of the floc diameter on the wire surface, but it is interesting to look what happens in the jet thickness direction, and also before the jet hits the moving wire. The Fig. 5.35 presents the countour plot of the development of the mean floc size in the slice channel, in the free jet and in the very beginning of the forming section. The floc diameter is bigger between the wedges than in their wakes as seen already when investigating the phenomena in the slice channel in Section 5.2.4. The z-directional difference in the local floc

size is carried far downstream in the jet, but it can be seen that the impingement zone has a remarkable effect on the local floc size: the mean floc size reduces instantaneously at the proximity of the wire surface, while it remains practically untouched at the upper surface of the jet.

In order to get more exact values of the floc diameters at different locations over the jet thickness, the mean floc size is plotted along the black lines presented in Fig. 5.35, that is, at the slice opening, at the end of the bottom lip and in the free jet before it hits the wire surface. The profiles are depicted in Fig. 5.36, where the δ^* represents the distance from the middle of the jet ($\delta^* = 0$ at the middle). The mean floc diameter is almost symmetrical at the slice opening; only the slight deviation due to the slice bar can be distinguished. At the end of the bottom lip the jet has already visibly contracted and the reduce in the mean floc size occured due to the slice bar (at the top edge of the jet) can more clearly be seen. In the free jet, a little bit after the *vena-contracta*, the profile is not symmetrical anymore; the peak at the bottom lip side has significantly decreased, while the other peaks are only slightly smaller than before. However, based on the three graphs in Fig. 5.36, it can be concluded that the contraction of the jet reduces the floc size due to the velocity gradients and increased turbulent kinetic energy.

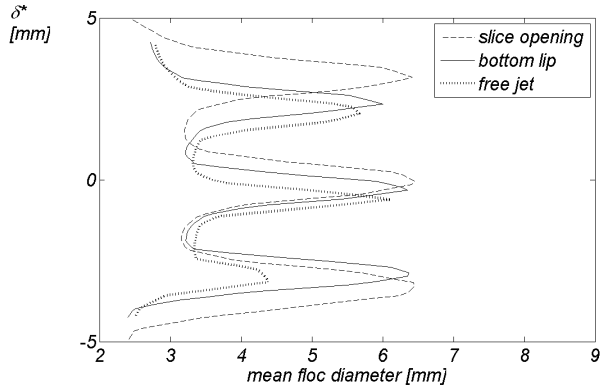

Figure 5.36: The mean floc diameter over the jet thickness at three different MD positions: at the slice opening, at the end of the bottom lip and in the free jet (The locations are illustrated in Fig. 5.35).

One drawback in the results in the forming section is that the local mean floc diameter is 1 mm bigger at the end of the slice channel than observed in the Section 5.2.4, even though the slice channel is exactly the same. This is due to 2D simplification: the model including the forming section assumes the even flow profile in the CD direction, while in reality there is always a profile due to the turbulence generator. The 3D model used in the Section 5.2.4 takes this into account, and hence, the floc size remains smaller. This inconvenience cannot be

avoided when using a 2D approach, and it may also explain too big floc size further in the forming section (Fig. 5.33).

Next, it is intresting to take a look at the development of the local mean floc diameter at the forming section, where the phenomena are highly complex, Figs. 5.37...5.40. At the impingement zone (Fig. 5.37) the profiles for all jet-to-wire ratios are quite similar, only the middle peak seems higher for the rush mode. When proceeding further downstream, the simulations predict that the floc size near the free surface remains bigger for the rush case. This is quite interesting suggestion, but due to the lack of the validation experiments, it is impossible to judge the validity of that prediction. In addition, it has to be kept in mind that predicted floc sizes are too big because of the 2D simplification, and hence, it is better to concentrate in the local differencies occuring at different positions over jet thickness and in MD, and in comparison between the jet-to-wire ratios.

When investigating the near wire area in Fig. 5.38, it can be noticed that shear and turbulence start to break up flocs more efficiently for the drag mode than for other cases already at $x100$. For the rush mode, the effect of velocity gradients can not be seen before $x200$ (Fig. 5.39), but when the effect takes place, it is quite strong. The model suggests that the increase in the floc size occurs in the streaks formed already inside the slice channel, while in the wakes due to the wedge walls, the floc size would remain significantly smaller during the initial forming. In other words, the wedge walls cause turbulence and shear, which break up the flocs inside the slice channel, and this effect is visible still in the initial dewatering zone. As a consequence, the model suggests that the floc size, and the resulting formation, are different in separate layers in the forming paper.

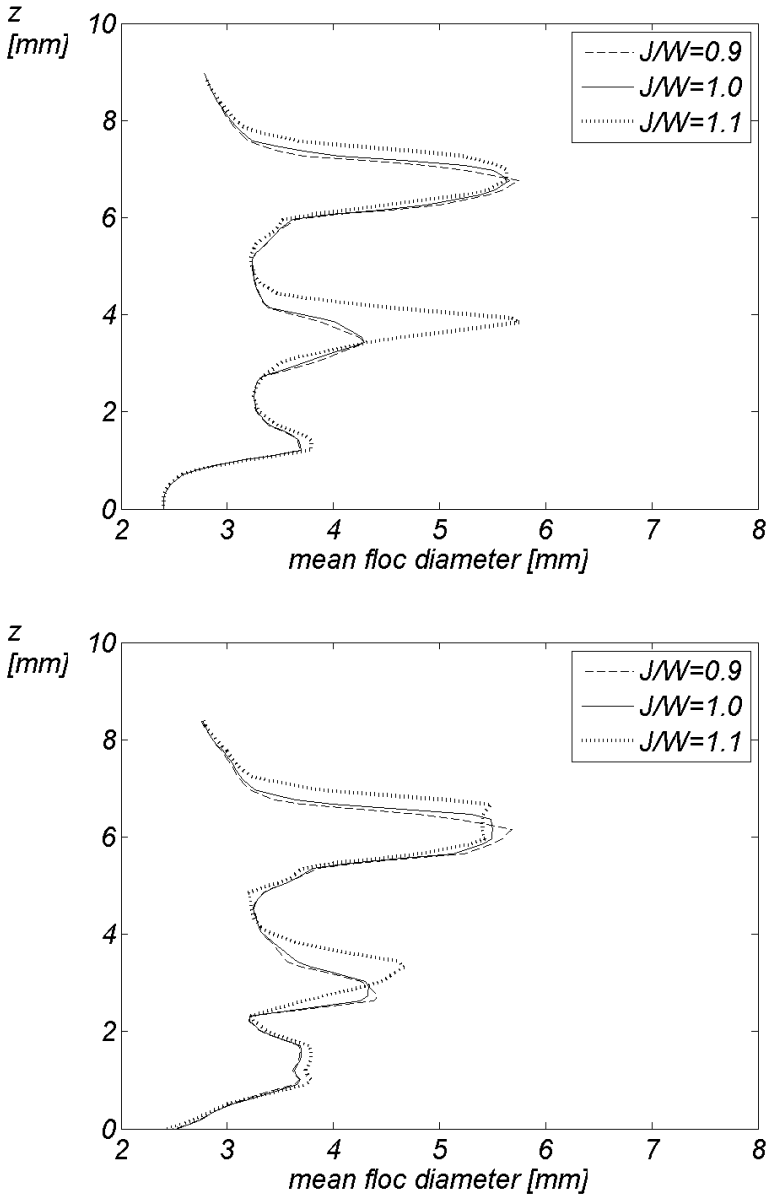

Figure 5.37: The floc diameter on the wire surface through the jet thickness at two different MD positions, $x30$ (*top*) and $x50$ (*bottom*), for three different jet-to-wire ratios.

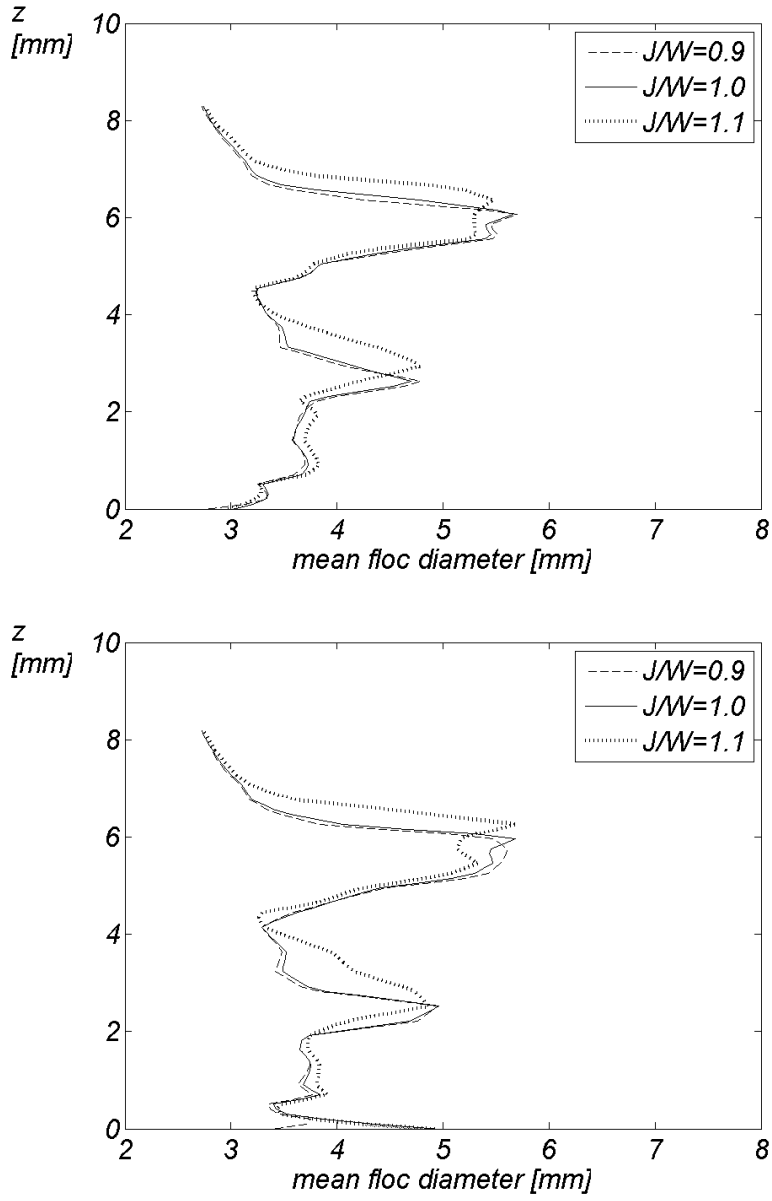

Figure 5.38: The floc diameter on the wire surface through the jet thickness at two different MD positions, $x70$ (*top*) and $x100$ (*bottom*), for three different jet-to-wire ratios.

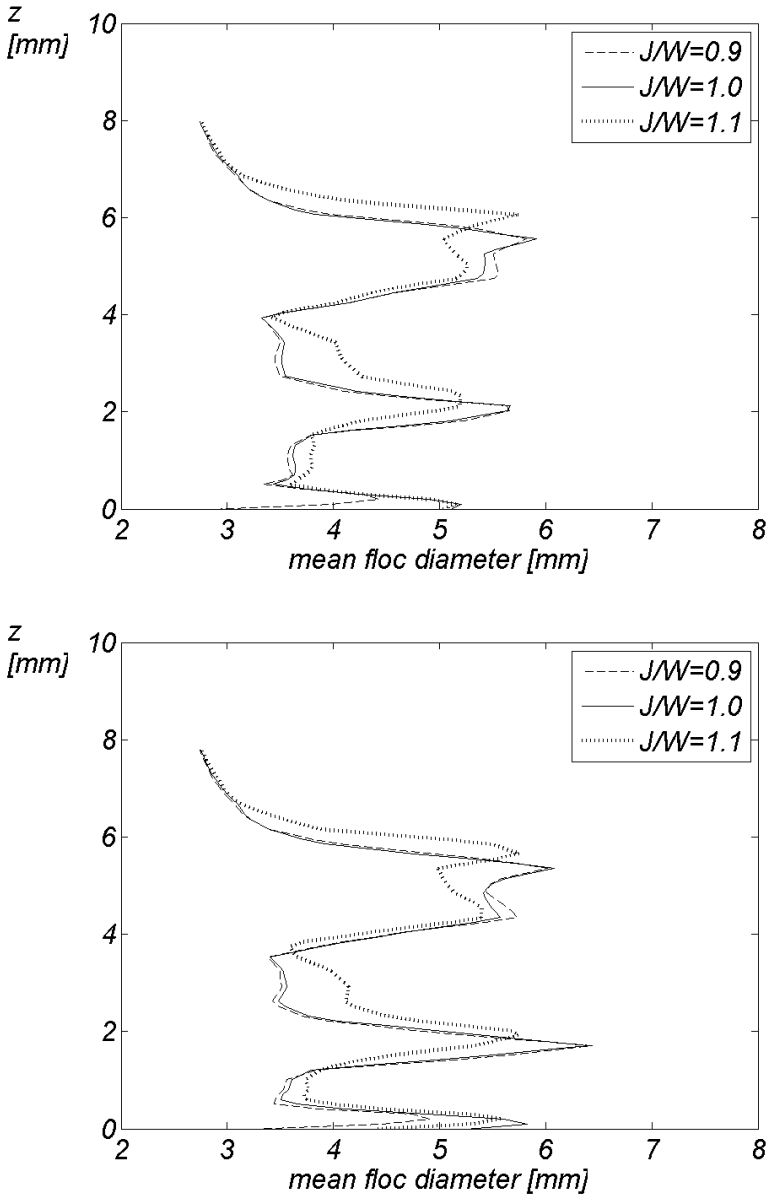

Figure 5.39: The floc diameter on the wire surface through the jet thickness at two different MD positions, $x150$ (*top*) and $x200$ (*bottom*), for three different jet-to-wire ratios.

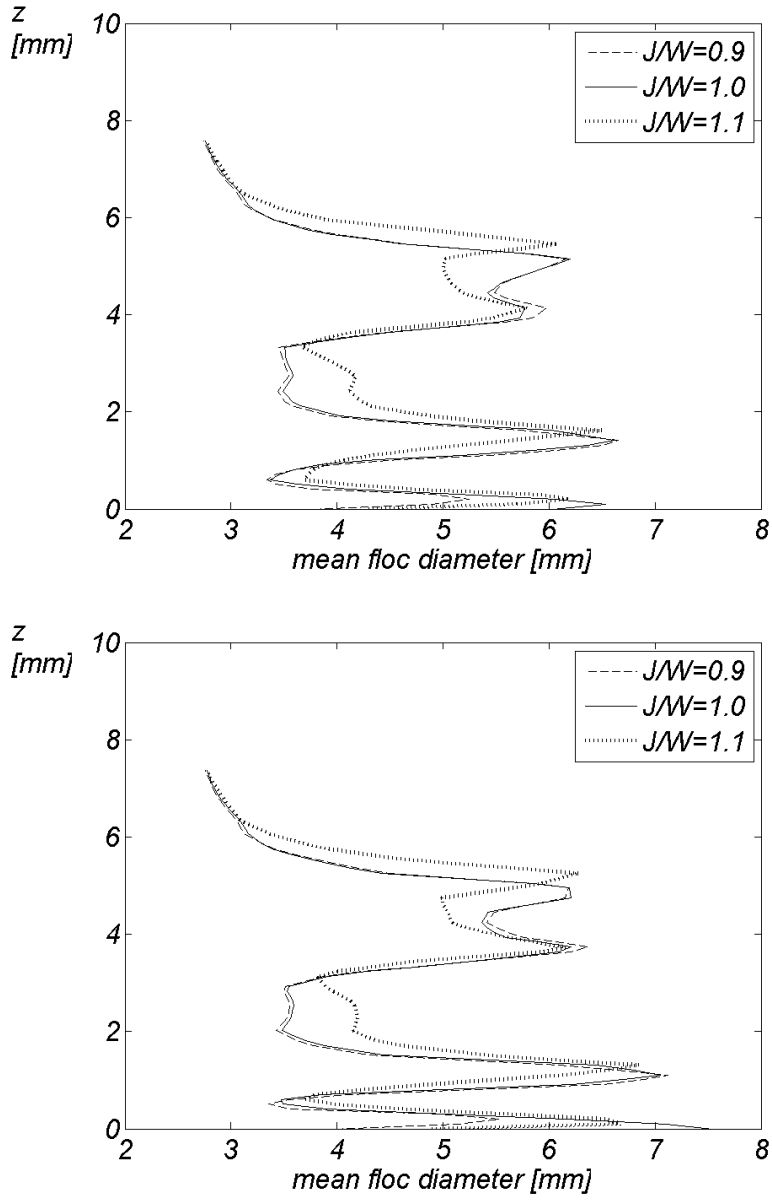

Figure 5.40: The floc diameter on the wire surface through the jet thickness at two different MD positions, $x250$ (*top*) and $x300$ (*bottom*), for three different jet-to-wire ratios.

Chapter 6

Future work and recommendations

Since a mathematical model is very seldom complete, some development ideas and remarks of current model assumptions are now summarised in this chapter. Hence, the purpose of this chapter is to provide insight into the strengths and the weaknesses of the models used.

As stated before, one common deficiency for both of the presented models, the FOPD and the FFE, is the modelling of the carrier phase turbulence. In principle, the turbulence could be accurately simulated for a one-phase Newtonian fluid, such as water, by using Direct Numerical Simulation (DNS), but it is too costly CPU time-wise, and not capable to resolve industrial-scale geometries. Moreover, the presence of fibres makes the situation even more complex, since the fibrous phase affects turbulence by dampening certain scales - and it is not even known which of them.

In addition, the drag forces between water and the fibrous phase determine velocity differences between the phases. Traditionally, the drag force is accounted for in the momentum equation of each phase by the drag coefficient, but reliable definitions for the coefficients of single fibres or non-spherical, deformable flocs do not exist.

Furthermore, as the concentration increases, fibre-fibre collisions take place and should be included in the models. Here, we collide once again with this trade-off between Lagrangian and Eulerian modelling approaches: modelling the effects of fibre-fibre, or floc-floc, collisions with Eulerian approach requires always considerable simplifications and assumptions. Therefore, the basic Eulerian two-phase flow modelling including four-way couplings (water-fibre and fibre-fibre, or water-floc and floc-floc) should be further developed to carefully account for the interactions.

Since the FOPD and FFE models are based on different assumptions, their limitations are separately presented in the following sections. Although they are both used for describing the headbox and forming section phenomena in this thesis, their direct combining in the same model would not be recommended until further development is considered.

6.1 Limitations and possibilities of the FOPD model

In the FOPD model the fibre suspension is considered so dilute that the fibre-fibre interactions can be ignored. Naturally, this is not true for typical wet end processes, which are aimed to be described in this, and many other, studies. One way to address this problem would be to perform micro-level simulations and derive the macro-level interaction terms to Eulerian multi-phase flow models. Mortensen et al., for example, have studied the orientation of a single fibre in a turbulent flow by using DNS [74]. In their work, the flow of the carrying phase was fully resolved and the fibre was assumed inflexible. In addition, in the recent doctoral thesis by Lindström, the fibre-level simulations were performed taking into account the fibre-fibre interactions [68]. Based on this kind of basic research, the macroscopic industrial-level CFD modelling tools can be further developed.

One of the weak points of the FOPD model is the definition of the translational and rotational diffusion coefficients. Some correlations based on the turbulent kinetic energy and dissipation are proposed in [84], but even the magnitude of the coefficient is still a matter of debate, see eg. [51] and [78]. Thus, futher studies are needed before the coefficients can be reliably determined.

Another serious drawback of the FOPD model is that it is derived for rigid fibres, or to be more accurate, for ellipsoidal particles. Wood fibres used in pulp and paper industry are, nevertheless, rather flexible, and their tendency to be aligned with the mean flow is not as strong as that of rigid fibres like seen in [78]. In addition, the determination of the experimental orientation of a curly fibre is not that unambiguous, and hence, the distributions can have quite a different form depending on the method used.

For the sake of simplicity, the FOPD model is practically always used only to simulate the projections of the fibre orientation angle; the one in (MD,CD)-plane or the one in (MD,z)-plane (see Fig. 3.1 for the clarification). However, the orientation of a fibre can, naturally, be the combination of these two angles, ϕ and θ. In order to study the resulting stratified orientation in a paper produced, one would need to model the whole three-dimensional distribution. This would, however, lead to a five-dimensional modelling problem, and thus, some dimensional reduction technique need to be applied to make the problem solvable for commercial CFD software.

The increasing pulp concentration involves the flocculation of fibres, which occurs even at relatively low concentrations [62]. Once the fibres are attached to a floc, their freedom to orient is strongly restricted, and after quick physical reasoning, the FOPD should not provide any reliable information about the resulting orientation. However, it has been shown in [36] that even a much more simple model, basing on the MD and CD velocity components, produces results accurate enough for the paper machine control purposes. Thus, it can be summarised that the mean angle of fibre orientation is accurately predicted by relatively simple tools, but when needing the information about local variations, for example to study cockling, a more accurate model, such as the FOPD is required.

6.2 Limitations and possibilities of the FFE model

The basic population balance method is a solid basis for the flocculation modelling assuming that there are clearly higher and lower concentration regimes, i.e. fibre flocs and voids, in the flow. However, if all the fibres were part of one large fibre network, (as can probably occur for high concenrations) the whole concept would be questionable. On the other hand, for that kind of situation one does not usually even talk about flocs. However, experiments have revealed the dynamics of the floc evolution for typical headbox concentrations [57], [97], and thus, the Fibre Floc Evolution (FFE) can be considered reasonable starting point for the flocculation modelling.

As mentioned before, the break-up and coalescence models are originally developed for gas-liquid flows. It was shown within the results of this thesis that those models offer an appropriate basis for the fibre flocculation modelling, but the model parameters, and possibly whole the model kernels, need to be revised in order to better describe the fibre suspension flows. The simulated results revealed that the internal strength of a floc and the crowding factor of the pulp are correlated, and that further studies are needed to determine the physical dependencies. In this thesis the pulps differed by length, diameter and coarseness, but they were of the same concentration. In addition, the floc strength was same for all different floc sizes, which may not be true. Since the strength of a floc is somehow correlated with the number of fibre-fibre bonds, it can be assumed that the internal floc strength varies depending, at least, on the fibre properties, floc size and local floc density. Hence, more simulations and experiments would be needed to properly define the internal strength of a floc.

In regard to other modified model parameters, the break-up and the coalescence coefficients, further research would be needed as well. In the model validation, they were kept constant, but it might occur that they should depend on pulp properties, turbulence or other flow field properties. It is accentuated that the mentioned parameters, if they turn out not to be constants, should be determined such that the model is applicable to different geometries without any parameter tuning, i.e. the parameters can depend on strain rate or turbulent kinetic energy, for instance, but not on the pipe diameter. As regards the other parameters, namely, the initial and the critical film thickness, they should also be determined specifically for fibre flocs.

The FFE model presented in this thesis has been validated only with one series of experiments including two different pulps, three different flow rates, but only with one type of geometry, namely the turbulence generator pipe. It is obvious that the model should be validated in different geometries and for different pulps and concentrations. It might occur that model parameters have to be completely revised in the future. However, the model provided at least qualitatively correct results in the slice channel, which is the first indication that the FFE model is a suitable approach for the fibre flocculation modelling. To more reliably validate the model parameters, more detailed experimental data is needed. For, now the measurements have provided information of the floc size averaged over the whole

pipe diameter, but in the future, data of the local floc size is required, since the flocculated state of the suspension varies considerably depending on the radial location, for example. This is most propably connected to the local properties of the flow field and turbulence.

In the current model, the turbulent conditions affect the break-up and coalescence mechanisms, but not vice versa. To more realisticly describe the fibre suspension flow, the turbulence modification due the prescence of flocs should be added in the model, as discussed above. In addition, a number of other mechanisms, such as the erosion or attachement of a single fibre into a floc, have not been added in the FFE model.

The interactions between water and fibrous phase have been modelled with standard type of drag laws developed for smooth, spherical and incompressible particles. The form of the floc is, nevertheless, far from those assumptions, and therefore, fibre-water interactions are not correctly simulated. The form of a floc can change significantly depending on local flow conditions, and the compressibility effects take place especially in the forming section. The consolidation process is not accounted for in this thesis, since it would require the definition of the fibrous phase as a totally different type of material. The phenomena in the forming section are, nonetheless, important when studying the forming of the fibrous structure of paper, and the effects of real porous wire as well as more detailed modelling of dewatering and retention would give valuable information of the phenomena.

Finally, when looking at the flowing fibre suspension, one can notice that its flocculated state is a sum of several factors, starting from the nature of the flow field, ending to the influence of chemistry. Without no doubt, also the fibre orientation affects the flocculation, since more isotropically oriented fibres have more possibilities to form bonds with neighbouring fibres. Consequently, the FOPD and the FFE models - or some of their more sophisticated descendants - should be combined one day . This goal might seem distant and unattainable today, but will most probably be achieved faster than we dare to believe.

Chapter 7

Conclusions

Ambitious goals to model the forming of the paper sheet by means of computational fluid dynamics were stated in a research proposal filed to Finnish Academy in 2005. At that time fibre orientation modelling was under active research by several authors, but the fibre flocculation modelling had remained practically unchanged since the pioneering work of Steen in 1990's. Both fibre orientation and flocculation were desired to be solved with a CFD tool available to industrial R&D. In other words, the research approach was to model complex phenomena such that it would be of intrest - and of use - in the industrial point of view. Thus, a commercial CFD software was chosen as a basis for the modelling work, and the simulations were performed in geometries as close to real ones as possible.

Now, in this light, the thesis in your hands shows that the challenging objectives have been reached. The fibre orientation modelling has been performed in the geometrically two-dimensional form in a headbox contraction, and the fibre flocculation modelling has been advanced to a completely new level, from Steen's flocculation index to the concrete measurable floc sizes. This thesis is the first proof that fibre flocculation can be studied by using the developed Fibre Floc Evolution (FFE) model based on the population balance of different floc sizes. Moreover, the FFE model creates a new basis to develop fibre suspension flow models in future, since the existence of two phases, water and fibrous phase, can be taken into account, and also the local variation of flocculated state of suspension can be studied.

Furthermore, simulations were extended outside of the headbox, to the free jet and to the forming section, in order to predict paper sheet properties to some extent. The whole forming section was not studied in detail, but the effect of initial dewatering zone to the floc behaviour was inspected. The aim of the thesis was not to make any "virtual paper sheet" by numerical simulations including billions of fibres, or have an accurate estimation of the basis weight, but instead to give fluid dynamical insight in understanding how the paper sheet is formed.

Fibre orientation was studied in geometrically two-dimensional form, and including the slice channel and the contracting jet in simulations. The numerical

results revealed new phenomena, such as quick decrease of anisotropy in the free jet and two equally probable orientation angles at the slice opening. The fast drop of anisotropy right after the slice opening proves the importance of including the free jet in the simulations, since the state of the orientation inside the slice channel does not characterise the situation in the jet with enough reliability. Further, even though the secondary peak appearing at the slice opening fades out very quickly, the existence of the peak proves that the FOPD model is capable to predict even very complicated phenomena. This would not be possible, if the one-dimensional formulation of the equation was used. Moreover, when investigating the orientation in the forming section one day, it is of utmost importance to have a model which is capable to simulate the behaviour of fibres submitted to complex phenomena at the jet impingement and during water removal.

Fibre flocculation was studied with a novel approach, the FFE model, which is capable to predict real floc sizes. The model developed within this thesis gives intresting possibilities when developing further the theory of the behaviour of the flocculated state of the suspension. It enables also the comparison of geometrically different constructions when designing parts of the headbox, since the model is relatively easy to use, and hence, applicable in every-day R&D work.

The FFE model was validated in the turbulence generator, and it was then used in investigation of the floc size behaviour in the slice channel and in the forming section. The floc size evolution in the slice channel was consistent with experimental findings and common knowledge, and furthermore, the FFE model offered more detailed information than previous studies. It was noticed that the effect of the turbulence generator pipe walls is visible far downstream, and also that the floc size is bigger in the middle of two wedges than near the wedge surface. The effect is inherited in the free jet and perceivable after the jet impingement as well. The finding attests the importance of the design of the slice channel, since the small floc size due to the wedge wall generated turbulence remains in the jet and leads to better formation. Variation of the jet-to-wire speed ratio was also shown to modify the development of the mean floc size, which is consistent with common knowledge: the drag mode was predicted to most efficiently break up the flocs, while J/W=1.0 had the least effect.

A mathematical model is very seldom perfect, and thus, also in the FOPD and FFE models, many details are left for further investigations. It is worthwhile to remember that there are still unsolved problems in modelling turbulence even in one-phase flow situations, and the presence of fibres does certainly not make it any simpler. Concerning particularly turbulence in fibre suspension flows, the modelling - as well as experiments - have barely taken the first steps; clearly the fibre concentration affects turbulence, but the interactions should be studied in more detail. It is known that the prescence of fibres dampens certain scales of turbulent fluctuations, but does the dampening occur similarly for different fibre orientation distributions, or for different floc sizes? And further, fibre-fibre interactions modify certainly the phenomena, especially, when going to higher concentrations, but how?

The FFE model is a good basis to study the flocculation, but there is still

room for further development. For example, the erosion of flocs by separation of single fibres as well as attachment of single fibres to flocs have been left out of the current FFE model. In principle, the Eulerian multi-phase flow approach makes it possible to include the erosion and attachment, but it means that the carrying phase is not any more pure water, but a mixture of water and single fibres. In addition, different floc sizes might have different strength properties, which affects the floc break-up mechanisms. Further, the chemistry; one essential part in the control of fluid mechanical phenomena in real papermaking process, and completely left away from the model. It is well recognised that retention chemicals have a remarkable role in the paper sheet forming and in development of fibre-fibre bonds, but they are not tried to be included in the models of this thesis.

In general, mathematical modelling and experimental measurements should be developed hand in hand. Now the modelling has been advanced to a new level and next step waits for new experiments. Fibre orientation distributions should be measured in higher concentrations in order to validate and develop the FOPD model to better describe the practical applications. Also, fibre floc size distributions should be measured instead of the average floc sizes in order to validate the FFE model more accurately, and to obtain valuable knowledge of the phenomenon itself.

The forming section modelling was simplified and only the initial dewatering of a Fourdrinier-type of former was studied. It would be intresting to extend the simulations further in the forming section, and to model also a modern gap former to see, how does the flocculation phenomenon differ in these two cases. Modelling the moving wire as a real porous medium would give more accurate information of the floc size behaviour during the water removal, as well as including the blades, vacuum rolls and other dewatering components in simulations. Thus, there is an obvious demand for further modelling work, what comes to the floc size and basis weight development in the whole forming section. And finally, the wet end fluid dynamical models could be linked to solid mechanical simulations in order to really predict the strength properties and dimensional stability, and even final end-use properties like printability of the paper sheet. Despite of the described potential development scenarios, already the current FFE model makes it possible to perform accurate and detailed investigations of flocculation phenomena and its dependency on different headbox and forming section design and running parameters with utilising a commercial CFD tool available as well for academical researchers as for industrial R&D.

REFERENCES

[1] *ANSYS CFX-11.0 electronical manual.*

[2] Advani S and Tucker C. The use of tensors to describe and predict fiber orientation in short fiber composites. *Journal of Rheology*, 31:751–784, 1997.

[3] Altan MC and Tang L. Orientation tensors in simple flows of dilute suspensions of non-brownian rigid ellipsoids, comparison of analytical and approximate solutions. *Rheologica acta*, 32(3):227–244, 1993.

[4] Audenis G. On the impingement of a plane liquid jet on the wires of a paper machine. Licentiate thesis, Royal Institute of Technology, Stockholm, Sweden, 1999.

[5] Audenis G and Dahlkild AA. Impingement of an inviscid plane liquid jet on a porous wall: A fixed domain method. *Nordic Pulp and Paper Research Journal*, 16(4):274–283, 2001.

[6] Baines WD. The papriformer Part II. flow in the formation zone of a two-wire machine. *Pulp & Paper Canada*, 68(10):T497–T505, 1967.

[7] Barratte C, Roux JC, Voillot C, Le Nest JF, Lonjont JC, and Mangin P. Simulation of initial fibre retention by forming fabric. In *54th Appita Annual Conference*, pages 415–420, Melbourne, Australia, 2000.

[8] Bennington CPJ, Kerekes RJ, and Grace JR. The yield stress of fibre suspensions. *Canadian Journal of Chemical Engineering*, 68:748–757, 1990.

[9] Bennington CPJ and Thangavel VK. The use of a mixing-sensitive chemical reaction for the study of pulp fibre suspension mixing. *Canadian Journal of Chemical Engineering*, 71:667–675, 1993.

[10] Bergström R. Fibre flocculation during twin-wire roll forming. Licentiate thesis, Royal Institute of Technology, Stockholm, Sweden, 2003.

[11] Brecht W and Heller H. A study of the friction losses of paper stock suspensions. *TAPPI Journal*, 33(9):14A, 1950.

[12] Carlsson A. Orientation of fibres in suspensions flowing over a solid surface. Licentiate thesis, Royal Institute of Technology, Stockholm, Sweden, 2007.

[13] Carlsson A, Lundell F, and Söderberg D. Fibre orientation control related to papermaking. *Journal of Fluids Engineering*, 129:457–465, 2007.

[14] Crowe C, Sommerfeld M, and Tsuji Y. *Multiphase Flows with Droplets and Par-*

ticles. CRC Press LLC, 1998.

[15] Dalpke B, Green SI, and Kerekes RJ. Influence of machine variables on fibre mat buildup at jet impingement. *Journal of Pulp and Paper Science*, 29(3):90–94, 2003.

[16] Dalpke B and Kerekes RJ. The influence of fibre properties on the apparent yield stress of flocculated pulp suspensions. *Journal of Pulp and Paper Science*, 31(1):39–43, 2005.

[17] Dalpke B, Kerekes RJ, and Green SI. Modelling jet impingement and the initial drainage zone in roll forming. *Journal of Pulp and Paper Science*, 30(3):65–70, 2004.

[18] Deng C and Martinez DM. Towards an understanding of the flow at the egde of a porous medium. *Journal of Pulp and Paper Science*, 32(4):1–6, 2006.

[19] Deng M and Dodson CTJ. Random star patterns and paper formation. *TAPPI Journal*, 77(3):195–199, 1994.

[20] Dodson CTJ. Fibre crowding, fibre contacts and fibre flocculation. *TAPPI Journal*, 79(9):211–216, 1996.

[21] Dodson CTJ and Kerekes RJ. On the structure of fibre flocs. Technical report, Presented at the COST Meeting on Multi-Phase Flows in Papermaking, Grenoble, 1997.

[22] Dodson CTJ and Serafino L. Flocculation, dispersion and dynamic scenarios for formation. *Nordic Pulp and Paper Research Journal*, 8(2):264–272, 1993.

[23] Eloranta H. Estimation of fiber orientation in pulp-suspension flow. In *3rd International Symposium on Two-Phase Flow Modelling and Experimentation*, Pisa, 2004.

[24] Erkkilä AL, Pakarinen P, and Odell M. Sheet forming studies using layered orientation analysis. *Pulp Paper Canada*, 99(1):81–85, 1998.

[25] Farnood RR, Dodson CTJ, and Loewen SR. Modelling flocculation. part i: Random disc model. *Journal of Pulp and Paper Science*, 21(10):J348–355, 1995.

[26] Farnood RR, Loewen SR, and Dodson CTJ. Estimation of intra-floc forces. *APPITA Journal*, 47(5):391–396, 1994.

[27] Farnood RR, Yan N, Kortschot MT, and Dodson CTJ. Modelling flocculation: A gallery of simulated flocculated papers. *Nordic Pulp and Paper Research Journal*, 12(2):86–89, 1997.

[28] Garner RG and Kerekes RJ. Measurement of turbulence in pulp suspension by laser anemometry. *Trans. Tech. Sect. CPPA*, 8(3):TR53–69, 1982.

[29] Gidaspow D. *Multiphase Flow and Fluidization*. Academic Press, 1994.

[30] Gorres J, Cresson T, and Luner P. Sheet formation from flocculated structures. *Journal of Pulp and Paper Science*, 15(2):55–59, 1989.

[31] Gullichsen J. Chemical engineering principles of fiber line operations. In Gullichsen J and Fogelholm CJ, editors, *Chemical Pulping*, **volume** 6A of *Papermaking Science and Technology*, pages A245–A327. Fapet Oy, Helsinki, Finland, 1999.

[32] Gullichsen J and Härkonen E. Medium consistency technology. II. storage dischargers and centrifugal pumps. *TAPPI Journal*, 64:113–116, 1981.

[33] Hämäläinen J. *Mathematical Modeling and Simulation of Fluid Flows in the Headbox of Paper Machines*. PhD thesis, University of Jyväskylä, 1993.

[34] Hämäläinen J, Hämäläinen T, Madetoja E, and Ruotsalainen H. CFD-based optimization for complete industrial process: Papermaking. In Thévenin D and Janiga G, editors, *Optimization and Computational Fluid Dynamics*. Springer, 2008.

[35] Hämäläinen J and Tarvainen P. CFD-based shape and control optimization applied

to a paper machine headbox. In *86th ann. meeting of PAPTAC*, pages A99–A102, 2000.

[36] Hämäläinen J, Tarvainen P, and Aspholm P. HOCS FIBRE – new tool for optimized fibre orientation angles. In *91st ann. meeting of PAPTAC, CD-proceedings*, 2005.

[37] Hämäläinen T and Hämäläinen J. Modelling of fibre orientation in the headbox jet. *Journal of Pulp and Paper Science*, 33(1):49–53, 2007.

[38] Hämäläinen T, Hämäläinen J, and Salmela J. Evolution of fibre flocs in a turbulent pipe expansion flow. In *6th International Conference on Multiphase Flow (CD-proceedings)*, 2007.

[39] Hammarström D. A model for simulation of fiber suspension flows. Licentiate thesis, Royal Institute of Technology, Stockholm, Sweden, 2004.

[40] Hiltunen K. *Mathematical and numerical modelling of consolidation processes in paper machines*. PhD thesis, University of Jyväskylä, Finland, 1995.

[41] Hinze JO. *Turbulence*. McGraw-Hill, New York, 1959.

[42] Holm R. *Fluid Mechiancs of Fibre Suspensions Related to Papermaking*. PhD thesis, Royal Institute of Technology, Stockholm, Sweden, 2005.

[43] Holmqvist C. *Mechanical Modelling of Blade Forming and Drainage of Flocculated Suspensions*. PhD thesis, Royal Institute of Technology, Stockholm, Sweden, 2005.

[44] Hourani MJ. Fiber flocculation in pulp suspension: Part 1: Theoretical model. *TAPPI Journal*, 71(5):115–118, 1988.

[45] Huber P, Roux JC, Mauret E, Belgacem N, and Pierre C. Suspension crowding for a general fibre-length distribution: Application to flocculation of mixtures of short and long papermaking fibres. *Journal of Pulp and Paper Science*, 29(3):77–85, 2003.

[46] Huhtanen JP. *Modeling of Fiber Suspension Flows in Refiner and other Papermaking Processes by Combining Non-Newtonian Fluid Dynamics and Turbulence*. PhD thesis, Tampere University of Technology, Finland, 2004.

[47] Hyensjö M. On fibre suspension flow modelling: Mechanical fibre flocculation and fibre orientation. Licentiate thesis, Royal Institute of Technology, Stockholm, Sweden, 2005.

[48] Hyensjö M. *Fibre Orientation Modelling Applied to Contracting Flows Related to Papermaking*. PhD thesis, Royal Institute of Technology, Stockholm, Sweden, 2008.

[49] Hyensjö M, Dahlkild A, Krochak P, Olson J, and Hämäläinen J. Modelling the effect of shear flow on fibre orientation anisotropy in a planar contraction. *Nordic Pulp and Paper Research Journal*, 22(3):376–382, 2007.

[50] Hyensjö M, Hämäläinen J, and Dahlkild A. Turbulent dilute fibre suspension flow modelling in a sudden circular pipe enlargement. In *89th annual meeting of Pulp and Paper Technical Association of Canada (CD proceedings)*. Springer, 2003.

[51] Hyensjö M, Krochak P, Olson J, Hämäläinen J, and Dahlkild A. Modelling a turbulent dilute fibre suspension in a planar contraction: Effect of vane types, vane position and wall boundary layer on fibre orientation distribution. In *5th Int. Conf. on Multiphase Flow, ICMF'04*, Yokohama, Japan, 2004.

[52] James DF, Yogachandran N, Loewen MR, Liu H, and Davis AMJ. Floc rupture in extensional flow. *Journal of Pulp and Paper Science*, 29(11):377–382, 2003.

[53] Jeffery GB. The motion of ellipsoidal particles immersed in a viscous fluid. *Proc. Royal Soc.*, A102:161–179, 1923.

[54] Jetsu P, Kellomäki M, Karema H, Salmela J, Lappalainen T, and Piirto M. Co-

herent structures of suspension flow and their inheritance in paper. In *12th Fundamental Research Symposium, Oxford*, September 2001.

[55] Jokinen O and Ebeling K. Flocculation tendency of papermaking fibers. *Paperi ja Puu*, 67(5):317–325, 1985.

[56] Jong JH. *Characteristics of Jet Impingement, Drainage and Compression in a Forming Roll of a Twin-Wire Machine*. PhD thesis, University of Toronto, Canada, 1998.

[57] Karema H, Salmela J, Tukiainen M, and Lepomäki H. Prediction of paper formation by fluidisation and reflocculation experiments. In *12th Fundamental Research Symposium*, pages 559–589, 2001.

[58] Kerekes RJ. Flocculation in decaying turbulence: A literature review. *Journal of Pulp and Paper Science*, 9(3):TR86–91, 1983.

[59] Kerekes RJ. Pulp floc behavior in entry flow to constrictions. *TAPPI Journal*, 66(1):88–91, 1983.

[60] Kerekes RJ and Schell CJ. Characterization of fibre flocculation regimes by a crowding factor. *Journal of Pulp and Paper Science*, 18(1):32–38, 1992.

[61] Kerekes RJ and Schell CJ. Effects of fibre length and coarseness on pulp flocculation. *TAPPI Journal*, 78(2):133–139, 1995.

[62] Krochak PJ, Olson J, and Martinez DM. The orientation of semidilute rigid fiber suspensions in a linearly contracting channel. *Physics of Fluids*, 20(7):DOI:10.1063/1.2949277, 2008.

[63] Kropholler HW and Sampson WW. The effect of fibre length distribution on suspension crowding. *Journal of Pulp and Paper Science*, 27(9):301–305, 2001.

[64] Kuhn DCS and P. Sullivan PE. Analysis and measurement of the flocculation intensity of flowing pulp suspensions. In *TAPPI Papermakers Conference (CD proceedings)*, Cincinnati, OH, USA, 2001.

[65] Launder BE and Sharma BI. Application of the energy-dissipation model of turbulence to the calculation of flow near a spinning disc. *Letters in Heat and Mass Transfer*, 1(2):131–138, 1974.

[66] Lee PFW and Duffy GG. Analysis of the drag reducing regime of pulp suspension. *TAPPI Journal*, 59:119–122, 1976.

[67] Leppänen T. *Effect of Fiber Orientation on Cockling of Paper*. PhD thesis, University of Kuopio, Finland, 2007.

[68] Lindström SB. *Modelling and Simulation of Paper Structure Development*. PhD thesis, Mid Sweden University, Sundsvall, Sweden, 2008.

[69] Ljus C. *On Particle transport and turbulence modification in air particle flows*. PhD thesis, Chalmers University of Technology, Sweden, 2000.

[70] Luo H and Svendsen HF. Theoretical model for drop and bubble breakup in turbulent dispersions. *AIChE Journal*, 42(5):1225–1233, 1996.

[71] Martinez DM, Kiiskinen H, Ahlman AK, and Kerekes RJ. On the mobility of flowing papermaking suspensions and its relationship to formation. *Journal of Pulp and Paper Science*, 20(10):341–347, 2003.

[72] Mason SG. Fibre motion and floccation. *Pulp and Paper Magazine of Canada*, 55(13):96–102, 1954.

[73] Melander O. *Fluid dynamics and flow structures of wood fibres suspended in gas flows*. PhD thesis, Chalmers University of Technology, Sweden, 2006.

[74] Mortensen PH, Andersson HI, Gillissen JJJ, and Boersma BJ. On the orientation of ellipsoidal particles in a turbulent shear flow. *International Journal of Multiphase Flow*, 34(7):678–683, 2008.

[75] Myréen B. Modeling the flow of pulp suspensions in pipes, part i. *Paperi ja Puu*, 5:497–504, 1989.

[76] Niemistö A, Hiltunen K, and Hämäläinen J. Fluid-structure interaction and free surface problems in papermaking process. In *ECCOMAS 2000 conference*, Barcelona, Spain, 2000.

[77] Niskanen H and Hämäläinen J. Modelling of fibre orientation in a paper machine headbox geometry. In *21st Nordic Seminar on Computational Mechanics*, pages 139–142, 2008.

[78] Niskanen H, Hämäläinen T, Eloranta H, Vaittinen J, and Hämäläinen J. Dependence of fibre orientation on turbulence of the headbox flow. In *94th Annual Meeting of PAPTAC, CD-proceedings*, pages B339–B342, 2008.

[79] Niskanen K, Kajanto I, and Pakarinen P. Fibre orientation. In Niskanen K, editor, *Paper Physics*, **volume** 16 of *Papermaking Science and Technology*, pages 37–50. Fapet Oy, Helsinki, Finland, 1998.

[80] Norman B. Overview of the physics of forming. In *9th Fundamental Research Symposium*, pages 73–149, Cambridge, 1989.

[81] Norman B. Letter to the editor. *Nordic Pulp and Paper Research Journal*, 12(3):210, 1997.

[82] Norman B, Moller K, Ek R, and Duffy G. Hydrodynamics of papermaking fibres in water suspension. In *Fibre-Water Interactions in Paper-Making*, pages 195–250, Oxford, 1977.

[83] Norman B and Söderberg D. Overview of forming literature: 1990-2000. In *12th Fundamental Research Symposium*, pages 431–558, Oxford, 2001.

[84] Olson JA. The motion of fibres in turbulent flow, stochastic simulation of isotropic homogeneous turbulence. *International Journal of Multiphase Flow*, 27:2083–2103, 2001.

[85] Olson JA, Frigaard I, Chan C, and Hämäläinen J. Modeling a turbulent fibre suspension flowing in a planar contraction: The one-dimensional headbox. *International Journal of Multiphase Flow*, 30:51–56, 2004.

[86] Olson JA and Kerekes RJ. The motion of fibres in turbulent flow. *International Journal of Multiphase Flow*, 377:47–64, 1998.

[87] Parsheh M. *Flow in Contractions with Applications to Headboxes.* PhD thesis, Royal Institute of Technology, Stockholm, Sweden, 2001.

[88] Parsheh M and Dahlkild A. Modelling the flow around elastic guiding vanes in the converging zone of a headbox. In *TAPPI Engineering/Process and Product Quality Conference*, pages 1433–1452, Anaheim, USA, 1999.

[89] Paulapuro H, editor. *Papermaking, Part 1, Stock Preparation and Wet End.* Number 8 in Papermaking Science and Technology. Fapet, Helsinki, 2000.

[90] Plikas A, Kuhn DCS, and P. Sullivan PE. A numerical model of fibre suspensions in a grid generated turbulent flow. In *ASME 2000 Fluids Engineering Division Summer Meeting: Proceedings of ASME FEDSM'00*, pages 991–996, Boston, Massachusetts, USA, 2000.

[91] Pope SB. *Turbulent Flows.* Cambridge University Press, Cambridge, 2000.

[92] Pourahmadi F and Humphrey JAC. Modeling solid-fluid turbulent flows with application to predicting erosive wear. *PhysicoChemical Hydrodynamics*, 4:191–219, 1983.

[93] Prince MJ and Blanch HW. Bubble coalescence and break-up in air-sparged bubble columns. *AIChE Journal*, 36(10):1485–1499, 1990.

[94] Raghem-Moayed A. *Characterisation of Fibre Suspension Flows at Papermaking*

Consistencies. PhD thesis, University of Toronto, Canada, 1999.

[95] Raghem-Moayed A and Kuhn D. Turbulent flocculation measurement. *Journal of Pulp and Paper Science*, 26(4):163–165, 2000.

[96] Ramkrishna D. *Population Balances - Theory and Applications to Particulate Systems in Engineering*. Academic Press, San Diego, 2000.

[97] Salmela J and Kataja M. Floc rupture and re-flocculation in turbulent shear flow. In *13th Fundamental Research Symposium*, pages 35–50, 2005.

[98] Sampson WW, McAlpin J, Kropholler HW, and Dodson CTJ. Hydrodynamic smoothing in the sheet forming process. *Journal of Pulp and Paper Science*, 21(12):J422–426, 1995.

[99] Schiller L and Naumann Z. A drag coefficient correlation. *Z. Ver. Deutsch. Ing.*, 77:318, 1935.

[100] Schmid CF, Switzer LH, and Klingenberg D. Simulation of fiber flocculation: Effect of fiber properties and interfiber friction. *Journal of Rheology*, 44(4):781–809, 2000.

[101] Shakespeare J. Tutorial: Fibre orientation angle profiles - process principles and cross machine control. In *TAPPI-proceedings, Process Contol, Electrical & Information Conference*, pages 593–636, 1998.

[102] Shanker R, Gillespie Jr. JW, and Güçeri SI. On the effect of nonhomogenous flow fields on the orientation distribution and rheology of fiber suspensions. *Polym. Eng. Sci.*, 31:161–171, 1991.

[103] Shimizu T, Yokogawa A, Suzuki M, and Nakamura I. Study on flow characteristics of pulp suspension: 2nd report - flocculation measurements of a thick fiber suspension. *Bulletin JSME*, 29:1487–1493, 1986.

[104] Smith MK. Formation potential of west coast kraft pulps. *Pulp & Paper Canada*, 87(10):69–76, 1986.

[105] Söderberg D. Experimental and theoretical studies of plane liquid jets. Licentiate thesis, Royal Institute of Technology, Stockholm, Sweden, 1997.

[106] Söderberg D. *Hydrodynamics of a plane liquid jet aimed at applications in papermanufacturing*. PhD thesis, Royal Institute of Technology, Stockholm, Sweden, 1999.

[107] Soszynski RM. *The Formation and Properties of Coherent Flocs in Fibre Suspensions*. PhD thesis, University of British Columbia, Canada, 1987.

[108] Steen M. *Turbulence and Flocculation in Fibre Suspensions*. PhD thesis, University of Trondheim, 1990.

[109] Switzer LH and Klingenberg DJ. Flocculation in simulations of sheared fiber suspensions. *International Journal of Multiphase Flow*, 30:67–87, 2004.

[110] Tennekes H and Lumley JL. *A First Course in Turbulence*. The MIT Press, Cambridge, MA, 1972.

[111] Tornberg A and Shelley MJ. Simulating the dynamics and interactions of flexible fibers in Stokes flows. *J. Comput. Phys.*, 196:8–40, 2004.

[112] Ullmar M. On fibre alignment mechanics in a headbox nozzle. Licentiate thesis, Royal Institute of Technology, Stockholm, Sweden, 1998.

[113] Wahren D. Fiber network structures in papermaking operations. In *Institute of Paper Chemistry Symposium 'Paper Science and Technology - The Cutting Edge'*, pages 112–129, Appleton, WI, 1977.

[114] Wikström T. *Flow and Rheology of Pulp Suspensions at Medium Consistency*. PhD thesis, Chalmer's University of Technology, Sweden, 2002.

[115] Wikström T and Rasmuson A. Yield stress of pulp suspensions: The influence of fibre properties and processing conditions. *Nordic Pulp and Paper Research*

Journal, 13(3):243–250, 1998.

[116] Xu HJ and Aidun CK. Characteristics of fiber suspension flow in a rectangular channel. *International Journal of Multiphase Flow*, 31:318–336, 2005.

[117] Yokogawa A, Suzuki M, and Shimizu T. Study on flow characteristics of pulp suspension flow - measurement of turbulence intensity and fiber concentration unevenness. *Bulletin JSME*, 28:846–853, 1985.

[118] Zahrai S. *On the Fluid Mechanics of Twin-Wire Formers*. PhD thesis, Royal Institute of Technology, Stockholm, Sweden, 1997.

[119] Zhao R and Kerekes RJ. Pressure distribution between forming fabrics in blade gap formers: Thin blades. *Journal of Pulp and Paper Science*, 21(3):97–103, 1995.